Jül-4336

Jülich Center for Hadron Physics (JCHP)
Institut für Kernphysik (IKP)
COSY

πN scattering lengths from pionic atoms

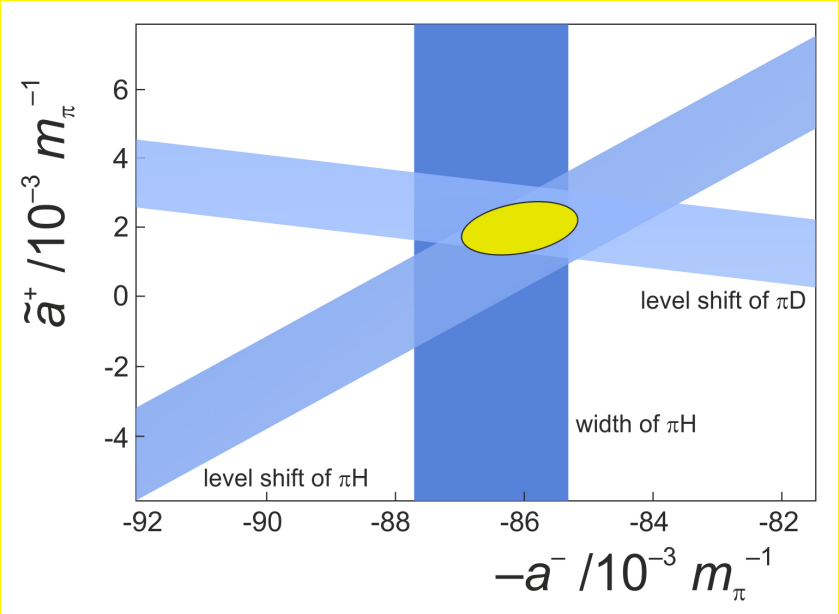

ANNUAL REPORT 2010
Articles

JÜLICH
FORSCHUNGSZENTRUM

K Further Contributions

1. Experimental Hadron Physics
   - 1.1 Study of the $pn \to pp_s\pi$ reaction near the threshold at ANKE
   - 1.2 Analyzing power of $\vec{p}d \to {}^3\mathrm{H}\pi^+$ and $\vec{p}d \to {}^3\mathrm{He}\pi^0$ $T_p = 353$ MeV measured at ANKE-COSY
   - 1.3 Double π^0 production in pp collisions at $T_p = 1.4$ GeV
   - 1.4 Coherent production of pion pairs in the reaction $pd \to pd\pi\pi$
   - 1.5 The η meson mass determination with ANKE at COSY
   - 1.6 The $pp \to pp\eta$ Reaction Dynamic Studies at 3.35 GeV/c Beam Momentum with WASA-at-COSY
   - 1.7 Study of the η meson production with the polarised proton beam
   - 1.8 Investigation of the ${}^3\mathrm{He}\eta$-final state in dp-collisions
   - 1.9 Status of the search for ^{4}He-η bound state by means of the WASA-at-COSY facility
   - 1.10 Measurement of Angular Distribution for $pd \to {}^3\mathrm{He}\eta(\to \gamma\gamma)$ reaction at $Q = 61$ MeV with WASA-at-COSY
   - 1.11 Preliminary analysis of the $\eta \to \pi^+\pi^-\pi^0$ decay
   - 1.12 Feasibility of the $\pi^0 \to e^+e^-$ measurement in the $pp \to pp\pi^0$ reaction at $T_{\mathrm{beam}} = 550$ MeV
   - 1.13 Measurement of $\eta \to \pi^+\pi^-e^+e^-$
   - 1.14 The $\eta \to \gamma e^+e^-$ Decay from pd Reactions with WASA-at-COSY
   - 1.15 Analysis of the $\eta \to e^+e^-e^+e^-$ double Dalitz decay
   - 1.16 Identification of the $pn \to d\omega$ reaction at ANKE
   - 1.17 Recent results from the charge-exchange breakup reaction $dp \to pp_sn$ study at ANKE
   - 1.18 Vector analyzing power of the $pp \to pp_s\pi^0$ reaction at intermediate energies at ANKE/COSY
   - 1.19 Analysis of the $pd \to pp_{(\mathrm{STT})} + X$ reaction at 353 MeV using ANKE STTs
   - 1.20 Neural network application for proton kinetic energy reconstruction in ANKE STT
   - 1.21 Formation of the ${}^1\mathrm{S}_0$ diproton in the reaction $pp \to pp_s\pi^0$ in the Δ isobar region
   - 1.22 Acceptance studies for the $pp \to nK^+\Sigma^+$ reaction at COSY-TOF
   - 1.23 Multifragmentation of Aluminium Nuclei by GeV Protons
   - 1.24 Double-polarized fusion
2. Developments for the Experimental Facilities
   - 2.1 Development of a Pellet Tracking System for PANDA and WASA
   - 2.2 Time calibration of the Forward Detector for use of the Time-of-Flight method with WASA-at-COSY
   - 2.3 Online control and data visualisation system for the COSY-TOF experiment
   - 2.4 Feasibility study of ^{3}H-η bound states production by means of the COSY-TOF facility
3. Theoretical Physics (see Highlights Sect.B for links to published papers)
4. Accelerator Division
   - 4.1 Status of COSY Injector Cyclotron, Ion Sources and Polarimeter
   - 4.2 Progress with the Scintillation Profile Monitor at COSY
   - 4.3 New PLC for Vacuum Bake Out System
   - 4.4 Magnets, alignment and new installations
   - 4.5 Radiation Protection
   - 4.6 Status of the 2 MeV Electron Cooler for COSY/HESR
5. Preparations for FAIR
   - 5.1 Barrier-bucket operation at COSY for HESR

5.2 Redesign of the HESR RF-system
5.3 Recent developments of the HESR stochastic cooling system
5.4 An efficient threshold and noise extraction algorithm suitable for FPGAs
5.5 Characterization of a silicon pixel readout chip for the PANDA Micro Vertex Detector
5.6 Progress in the dE/dx particle identification method with the PANDA-type straw tube tracker
5.7 Measurements at COSY with the Bonn beam telescope
5.8 Antiproton-proton elastic scattering as a day-one experiment at HESR

6. Technical Developments

6.1 Electronics laboratory
6.2 How to solder temperature diodes

Study of the $pn \to \{pp\}_s\pi^-$ reaction near the threshold at ANKE

With the advent of chiral perturbation theory (χPT), the low-energy effective field theory of QCD, accurate calculations have become possible for hadronic reactions. The extension of the approach to pion production in nucleon-nucleon collisions requires new high precision experimental information in the near-threshold region.

Of especial interest are the processes $pp \to \{pp\}_s\pi^0$ and $pn \to \{pp\}_s\pi^-$, with the formation of a $^1S_0$ proton pair (diproton) in the final state. The measurements of $d\sigma/d\Omega$, A_y and the spin-correlation coefficients $A_{x,x}$ and $A_{x,z}$ will permit an amplitude analysis that should provide a non-trivial test of the χPT predictions. A combined study of these processes will lead to the isolation of the Low Energy Constant (LEC) d of the $4N\pi$ contact operator in χPT.

The ANKE spectrometer is particularly well suited for the study of reactions with a final diproton. The excellent resolution in the excitation energy of the proton pair, $\sigma_{E_{pp}} < 0.5$ MeV, allows one to select the range of low $E_{pp} < 3$ MeV. This ensures the dominance of the $^1S_0$ state of the final proton pair. Single and double polarisation experiments can be conducted through the use of the polarised COSY beams and the ANKE polarised internal target.

As a first step in the proton–neutron programme, measurements with a polarised proton beam incident on an unpolarised deuterium cluster target were performed at ANKE in 2009 at a beam energy of $T_p = 353$ MeV.

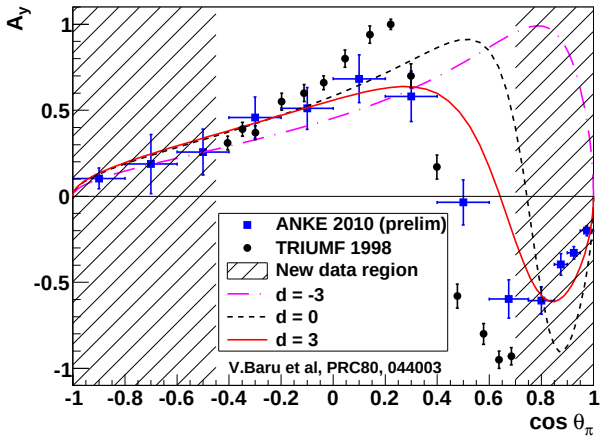

Fig. 1: A_y in the $\vec{p}n \to \{pp\}_s\pi^-$ reaction at T_n=353 MeV (blue squares). Also shown are the results of χPT calculation for $d = 3$ (red solid line), $d = 0$ (black dashed line), and $d = -3$ (magenta dot-dashed line). The data from TRIUMF are shown as black circles.

The results for the $\vec{p}n \to \{pp\}_s\pi^-$ reaction are presented in Figs. 1 and 2. The ANKE data are shown together with the results from TRIUMF [H. Hahn *et al.*, Phys. Rev. Lett. **82** (1999) 2258] and compared to the prediction of the IKP theory group [V. Baru *et al.*, Phys. Rev. C **80** (2009) 044003].

The value of LEC $d = 3$ is favoured, though it must be stressed that the pion d–waves have not yet been included in the calculations.

The results were obtained with a 40 MeV wide range of effective beam energy in the free pn-scattering, *i.e.*, $T_{\rm free} = 353 \pm 20$ MeV. The $E_{pp} < 3$ MeV cut was imposed on the data but, to facilitate the comparison with previous results, the cross section has been recalculated for the $E_{pp} < 1.5$ MeV cut used at TRIUMF. This was done using the Migdal-Watson approximation for the final state interaction in the $^1S_0$ proton pair. The main advantage of the ANKE measurement is the extended angular range compared to the pre–existing data.

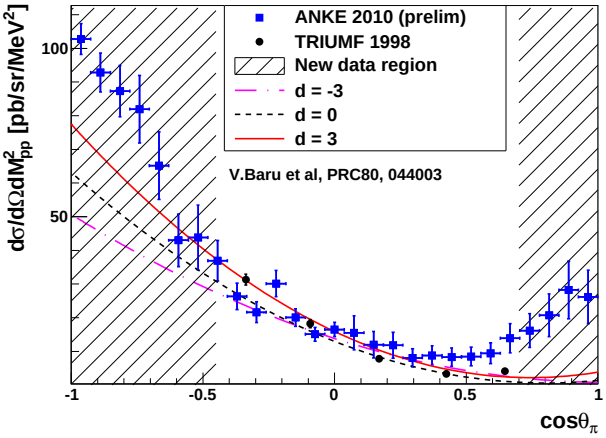

Fig. 2: ANKE Preliminary results for the cross section of the $\vec{p}n \to \{pp\}_s\pi^-$ reaction at T_n=353 MeV in the $E_{pp} < 1.5$ MeV range. The conventions are the same as those used in the caption to Fig. 1.

The transitions involving the $4N\pi$ contact interaction correspond to the p-wave pion production in the $np \to \{pp\}_s\pi^-$ reaction. The magnitude of one of the p-wave amplitudes is fixed completely by the measurement of $(1 - A_{x,x})d\sigma/d\Omega$ for $np \to \{pp\}_s\pi^-$. The double polarisation experiment for the measurement of $A_{x,x}$ and $A_{y,y}$, scheduled for 2011, will greatly improve our knowledge of the LEC d.

This experiment will provide the most systematics-free way to fix the value of d. At the same time, the magnitude of the other p-wave amplitude and its relative phase will be deduced from a combined analysis of these results with our cross section and analysing power data for $pp \to \{pp\}_s\pi^0$ and $np \to \{pp\}_s\pi^-$, which have already been taken. Two determinations of the LEC d will therefore be possible.

Analyzing power of $\vec{p}d \to {}^3\mathrm{H}\pi^+$ and $\vec{p}d \to {}^3\mathrm{He}\pi^0$ at $T_p = 353$ MeV measured at ANKE-COSY*

V. Shmakova[1,2], S. Dymov[2,3] for the ANKE collaboration

The study of coherent pion production on very light nuclei $p + A \to (A+1)\pi$ in the Δ-resonance region is important for the understanding of the structure of the nuclei and the properties of the πN and ΔN interactions. The good results obtained with microscopic models with explicit Δ-excitation in the two-nucleon sector calls for tests of the models to be made in the three-nucleon case, where production of the Δ may involve 3N forces. The phenomenological approach using impulse approximation with $pp \to d\pi^+$ amplitudes as input was successful near the reaction threshold but only partial progress has been achieved at higher energies [1]. The new high quality ANKE results, which supplement data available from other laboratories, will present further challenges for theory.

The proton analyzing power (A_y) has been extracted for the $\vec{p}d \to {}^3\mathrm{H}\pi^+$ and $\vec{p}d \to {}^3\mathrm{He}\pi^0$ reactions as byproducts of the April 2009 study of $pn \to \{pp\}_s\pi^-$ process. A polarized proton beam with kinetic energy 353 MeV was incident onto the cluster deuterium target.

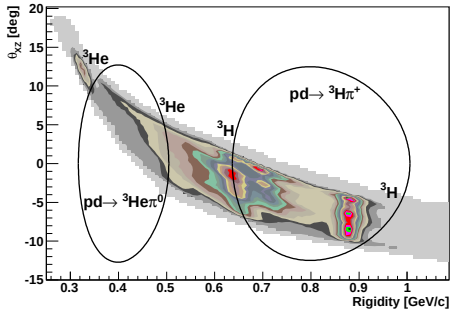

Fig. 1: Acceptance of the ANKE forward detector. Kinematical loci for the processes under study are shown.

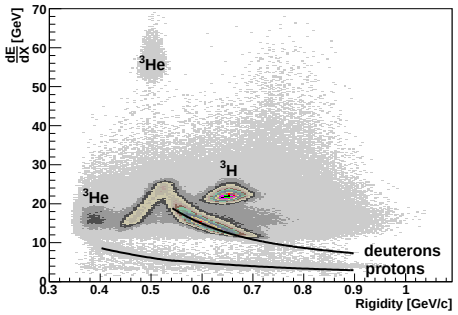

Fig. 2: Distribution of the energy losses in the first layer of the hodoscope versus particle rigidity, as obtained with the high dE/dx trigger.

The final ^{3}He and ^{3}H were detected in the ANKE Forward Detector (FD). As shown in Fig. 1, the FD acceptance covered the forward and backward c.m. angles of the ejected nuclei to give the four kinematical branches of the reactions studied. The criterium for particle identification (see Fig. 2) was based on the energy loss information from the FD hodoscope. A dedicated trigger selecting events with high energy losses in the first layer of the hodoscope was used for the detection of three of the four branches.

The asymmetry measured is $\xi = (N\uparrow\eta - N\downarrow)/(N\uparrow\eta + N\downarrow)$, where $N\uparrow$ and $N\downarrow$ are the numbers of events with proton spin oriented up and down, respectively, and η is the ratio of the luminosities collected for the two beam spin states. This ratio was obtained by comparing the rates of ejectiles emitted at $\theta = 0^\circ$ or $\phi = \pm 90^\circ$, which do not depend on the beam polarisation. The vector analyzing power A_y is related to the experimental asymmetry ξ as $A_y = \xi/P\cos\phi$, where the value of polarization $P = 0.65$ was obtained from the analysis of $\vec{p}n \to d\pi^0$ reaction.

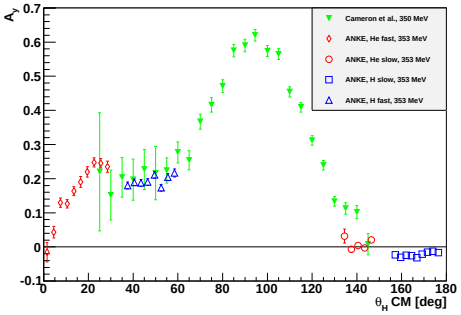

Fig. 3: Analyzing power of $\vec{p}d \to {}^3\mathrm{He}\pi^0$ at 350 MeV.

Isospin conservation ensures that the A_y for the ${}^3\mathrm{H}\pi^+$ and ${}^3\mathrm{He}\pi^0$ final states should be equal. The ANKE results for $\vec{p}d \to {}^3\mathrm{H}\pi^+$ and $\vec{p}d \to {}^3\mathrm{He}\pi^0$ are shown in Fig. 3 together with the TRIUMF data [2] for the π^0 case at 350 MeV. The results cover the previously unexplored angular ranges and improve on the precision of the TRIUMF data in the overlapping regions. Differential cross sections are currently being analyzed.

References:

[1] W.R. Falk, Physical Review C 50 (1994) 1574.
[2] J.M. Cameron *et al.*, Nucl. Phys. A 472 (1987) 718.

[1] IKP, Forschungzentrum Jülich, 52425 Jülich, Germany
[2] LNP, JINR, 141980 Dubna, Russia
[3] Phys. Inst. II, Universität Erlangen-Nürnberg, 91058 Erlangen, Germany

* Supported by the COSY-FFE programme.

Double pi0 production in pp collisions at Tp = 1.4 GeV

T. Tolba and J. Ritman for the WASA at COSY collaboration

Double pion production in proton-proton collisions is of special interest for the study of the mutual excitation of two baryons into their excited states and the subsequent decay. Here, the simplest case (i.e. the excitation of the two nucleons into their first excited state, the Δ(1232)) is considered.
The theoretical models [1, 2] describing the $NN \rightarrow NN\pi\pi$ reaction predict that near threshold the ππ production is dominated by the excitation of the Roper resonance $N^*(1440)P_{11}$ in one of the nucleons, followed by its s-wave decay $N^* \rightarrow N(\pi\pi)_{I=0}$ (where I indicates the isospin of the ππ system). As the beam energy increases, the double p-wave decay $N^* \rightarrow \Delta(1232)\pi \rightarrow N(\pi\pi)_{I=0}$ gives an increasing contribution to the cross section. At higher energies (T_p>1.3 GeV) the double Δ(1232) excitation is expected to be the dominant reaction mechanism for ππ production.
Recently, this reaction has been studied exclusively with high-statistics from threshold (T_p=650 MeV) up to T_p=1.3 GeV [3, 4, 5, 6]. The results and the theoretical expectations are in good agreement at low and intermediate energies. At T_p=1.36 GeV [6] and T_p=1.48 GeV [8], only the total cross section values are available, while the differential cross section values are absent in both measurements.
The reaction $pp \rightarrow pp\pi^0\pi^0$ has been investigated using the WASA at COSY facility [9] at T_p=1.4 GeV. The beam energy chosen corresponds to a total center-of-mass energy of $\sqrt{s}$=2.48 GeV, i.e. twice the Δ mass - an optimal condition for the exciting the ΔΔ system.
The event sample selection demands at least one of the two produced protons to be detected in the forward detector, while the other proton can be scattered outside the geometrical boundaries of the forward detector. The two pions are reconstructed in the central detector by reconstructing two γ-pairs each with $m_{\gamma\gamma}=m_{\pi^0}$. With these selection criteria, the geometrical acceptance found to be ∼45%. Furthermore, a kinematic fit with six constraints (four for total energy-momentum conservation and two for the masses of both π^0 meson) is applied in order to suppress the contribution from possible background channels, to recover the information of the unmeasured proton (scattered outside the geometrical boundaries of the forward detector) and to improve the reconstruction resolution. The data are corrected for the detector acceptance generated by a Monte Carlo Toy model (tuned in order to match the data) [10].
The preliminary total cross section is found to be $(324 \pm 21_{systematic} \pm 58_{normalization})$ μb, the statistical error found to be negligible in this work (∼10^{-3}). This result is shown in Fig. 1 and verifies the rising trend of the cross section value starting at ∼1170 MeV, where the ΔΔ excitation is expected to start to dominate the production process. The result, also, fits well to the CELSIUS data at lower energies [4, 5] as well as to the previous low-statistics bubble-chamber results at low and high energies [3, 8]. In order to study the $2\pi^0$ production mechanism, differential cross section distributions have been evaluated. Fig. 2 shows differential cross section distribution of the $p\pi^0$ invariant mass pairs normalized to equally populated phase space. Here, a significant enhancement at the mass of the Δ(1232) resonance is observed. The results of the total and differential cross sections are compared to the theoretical expectations. Clear evidence for the ΔΔ excitation

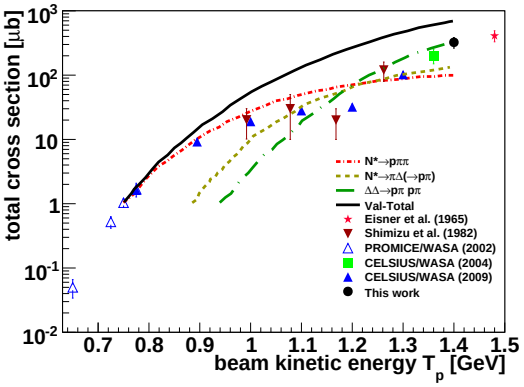

Fig. 1: Excitation function of the total cross section for $pp \rightarrow pp\pi^0\pi^0$. The preliminary result from this work is located at T_p = 1400 *MeV*.

is observed, without a significant signature for a contribution of the Roper N*(1440).

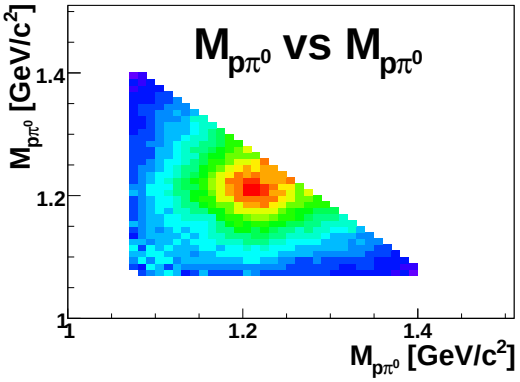

Fig. 2: $p\pi^0$ invariant mass differential cross section.

The investigation of the production of charged pions ($\pi^+\pi^-$) is the next step in the study of the double pion production in *NN* collisions. This final state is of special interest in order to study the contribution from the vector meson $\rho^0(770)$ which is expected to play an important role at this beam energy. Moreover, the extension to higher proton energies will shed a light on the role which higher resonances contribute to this channel.

References:

[1] L. Alvarez-Ruso et al. Nucl. Phys. A 633 (1998) 519.
[2] X. Cao, et al., Phys. Rev. C 81 (2010) 065201.
[3] F. Shimizu et al., Nucl. Phys. A 386 (1982) 571.
[4] T. Skorodko, et al., Physics Letters B 679 (2009) 30.
[5] J. Johanson, et al., Nucl. Phys. A 712 (2002) 75.
[6] T. Skorodko, et al., Physics Letters B 695 (2011) 115.
[7] I. Koch, PhD Thesis, Uppsala University (2004).
[8] A. M. Eisner, et al., Phys. Rev. 138 (1965) B670.
[9] H. H. Adam, et al., arXiv:nucl-ex/0411038 (2004).
[10] T. Tolba, PhD Thesis, Ruhr-Universitaet Bochum (2010).

Coherent production of pion pairs in the reaction $pd \to pd\pi\pi$

T. Azaryan[1], S. Dymov[1,2], V. Komarov[1], A. Kulikov[1], G. Macharashvili[1,3], H.Ströher[2] for the ANKE collaboration

The reaction $pd \to pd\pi\pi$ was studied at ANKE for beam energies 0.8, 1.1, 1.4 and 2.0 GeV. The proton-deuteron pairs, emerging with high momenta P_p =0.5 - 1.6 GeV/c, P_d =0.6 - 1.8 GeV/c were detected at small angles with respect to the proton beam and the reaction kinematics was reconstructed event-by-event. First results of the data analysis were presented last year [1]. The missing mass spectra of the reaction reveal a prominent peak in the region of low-mass pion pairs. For beam energies of 1.1 and 1.4 GeV the invariant mass of the deuteron-pion pair system exhibits a resonance-like distribution. For the lower and higher energy, the acceptance of the setup does not allow to observe the whole peaks at other energies and only low- and high-mass parts of them could be obtained (Fig.1 left). At the same time the invariant mass of the proton-pion pair system $M_{p\pi\pi}$ exhibits quite a different behavior: the events are concentrated at high masses near the relevant kinematic boundary and do not seem to show any structure there (Fig.1 right).

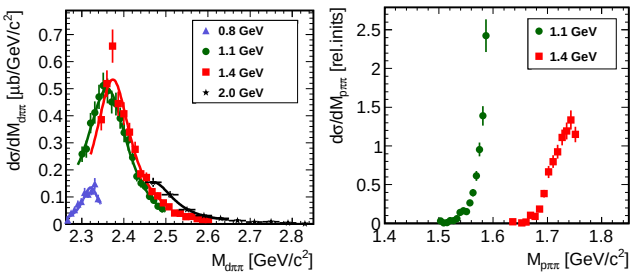

Fig. 1: $d\pi\pi$ and $p\pi\pi$ system invariant mass.

Such features can be understood by interpreting the reaction as a process of meson exchange between the projectile proton and the deuteron in which a significant momentum and energy is coherently transferred to the deuteron. The produced excited two-baryon system decays then to the pion pair and deuteron (Fig.2a). Such an excitation may include the following two main mechanisms shown in Fig.2: excitation of the Roper resonance or of two $\Delta(1232)$ resonances.

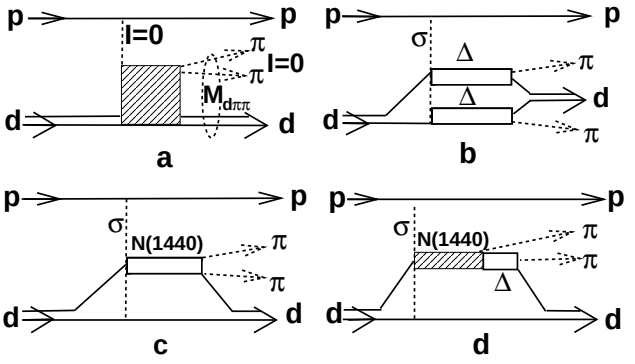

Fig. 2: Schematic presentation of the reaction mechanisms.

Each of these channels separatly should produce a peak, at 2.31 GeV/c^2 for the first and 2.46 GeV/c^2 for the second process, respectively. They overlapp due to the rather large inherent widths. The $M_{\pi\pi}$ distribution in separate intervals of $M_{d\pi\pi}$ reveals a hump at 320±10 MeV/c^2 with an intrinsic width of about 50 MeV/c^2 FWHM (Fig.3). A low-mass hump was obtained in the calculations of Ref. [2] as a manifestation of the Roper mechanism with the $N(1440) \to \Delta\pi \to N\pi\pi$ mode of decay. This ABC type enhancement, as an indication of the Roper mechanism contribution, dominates in our data at the lower part of the $M_{d\pi\pi}$ peak and disappears with $M_{d\pi\pi}$ growth. The relatively low width of the $M_{d\pi\pi}$ peak follows from the interference of amplitudes of the two mechanism channels due to their strong coupling. The coupling may be caused by the transitions $N(1440) + N \to \Delta + \pi + N \to \Delta + \Delta \to N + \pi + \Delta \to N + N(1440)$ in the intermediate state of the reaction. Confirmation of such an explanation requires comprehensive theoretical consideration.

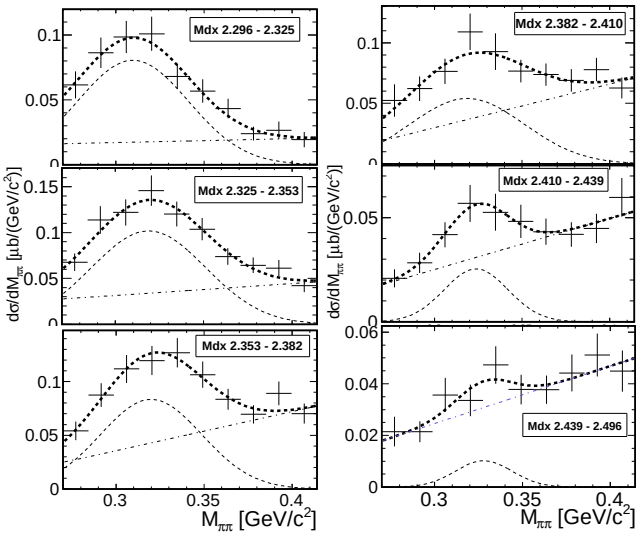

Fig. 3: $M_{\pi\pi}$ distributions at 1.1 GeV

References:

[1] V. Komarov et al., IKP Ann.Rep.2009.
[2] L.Alvarez Russo,Phys. Lett. B **452**, 207 (1999).

[1] LNP JINR, 141980 Dubna, Russia
[2] IKP FZJ, 52425 Jülich, Germany
[3] HEPI TSU, 0186 Tbilisi, Georgia

The η meson mass determination with ANKE at COSY*

P. Goslawski[1], I. Burmeister[1], M. Mielke[1], M. Papenbrock[1], D. Schröer[1], A. Täschner[1] and A. Khoukaz[1]
and the ANKE-Collaboration

Recent measurements on the η-meson mass performed at different experimental facilities (i.e. CERN-NA48, COSY-GEM, CESR-CLEO, DAΦNE-KLOE, MAMI-Crystall Ball) resulted in very precise data but differ by up to more than eight standard deviations, i.e. $0,5\,\mathrm{MeV/c^2}$ [1]. In order to clarify this situation a high precision measurement using the ANKE spectrometer at the COoler SYnchrotron has been realized.
Using the two-body reaction $\mathrm{d\,p} \rightarrow {}^3\mathrm{He}\,\eta$ at low excess energies the η-mass can be determined only from pure kinematics by the determination of the production threshold. Therefore, fifteen data points at fixed excess energies in the range of $Q = 1 - 15\,\mathrm{MeV}$ were investigated. The final momentum p_f of the ^{3}He-particles

$$p_f\,(s) = \frac{\sqrt{\left[s - (m_{^3\mathrm{He}} + m_\eta)^2\right] \cdot \left[s - (m_{^3\mathrm{He}} - m_\eta)^2\right]}}{2 \cdot \sqrt{s}}\,,$$

measured with the ANKE spectrometer, is very sensitive on the η-mass and the total energy $\sqrt{s}$, where the latter one is completely defined by the masses of the initial particles and the momentum of the deuteron beam. For a precise determination of the production threshold both the final momenta of the ^{3}He-particles and the corresponding beam momenta have to be measured with high accuracy.
First, the beam momenta for fifteen fixed energies were determined using an artificial spin resonance. This spin resonance was induced by a horizontal rf-magnetic field of a solenoid to depolarize a vector polarized accelerator beam [2]. The depolarizing resonance frequency f_r depends on the kinematical γ-factor (i.e. the beam momentum $p = m\sqrt{\gamma^2 - 1}$) and the beam revolution frequency f_0 via the resonance condition:

$$f_r = (k + \gamma G)\, f_0\,,$$

where k is an integer and G the gyromagnetic anomaly of the beam particle. By measuring this two frequencies the beam momenta in the threshold range of 3.1 - 3.2 GeV/c were determined with an accuracy of $\Delta p/p < 8 \cdot 10^{-5}$, i.e. with less than 250 keV/c [3].
Second, the momenta of the ^{3}He-nuclei of the reaction $\mathrm{d\,p} \rightarrow {}^3\mathrm{He}\,\eta$ have to be determined for every energy. The reaction can be identified by an energy loss cut on the ^{3}He band and a time of flight cut. Using these two cuts the background, consisting mainly of protons and deuterons of the dp elastic scattering and the deuteron break-up, can be suppressed. The final state momentum of the $^3\mathrm{He}\,\eta$ channel can be visualized by plotting the transversal versus the longitudinal reconstructed momentum in the CM system, as shown in in figure 1. For a two body final state reaction, one expects a centered momentum locus with a fixed radius p_f given by the equation above. By studying carefully the momentum dependence on cos(θ) and ϕ the detector calibration can be checked and improved, which is currently in progress. The final state momentum of the $^3\mathrm{He}\,\eta$ channel

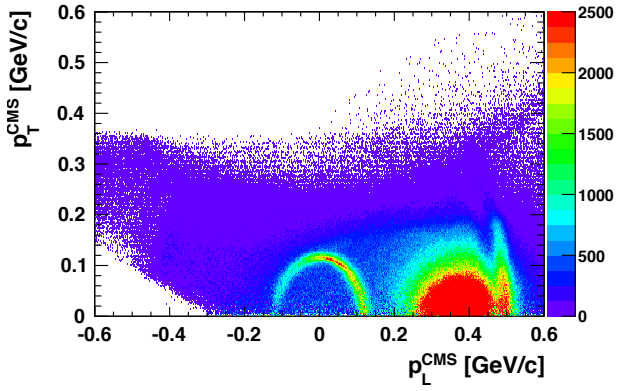

Fig. 1: Momentum plot to identify the $^3\mathrm{He}\,\eta$ reaction.

can be extracted as shown in figure 2. The background, originating mainly from the multi pion production and the deuteron break-up, can be described very well by sub-threshold data ($Q \approx -5\,\mathrm{MeV}$). Although currently

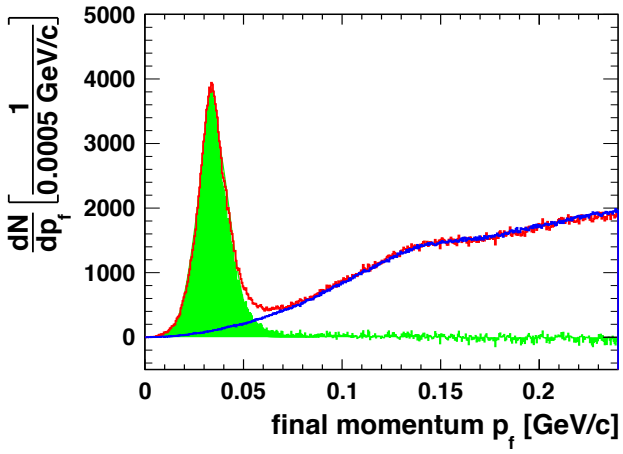

Fig. 2: Momentum p_f (red) at an excess energy of $Q \approx 0.6\,\mathrm{MeV}$, the background description (blue) and the extracted $^3\mathrm{He}\,\eta$ signal (green).

detailed investigation are performed on the fine calibration of the forward detector system, already now it is obvious that the accuracies of the beam momenta and the $^3\mathrm{He}\,\eta$ final state momenta allow for an η mass determination with the desired resolution of better than 100 keV.

References:

[1] C. Amsler et al., Phys. Lett. B **667**, 1 (2008).
[2] Ya. S. Derbenev et al., Part. Accel. 10, 177 (1980).
[3] P. Goslawski, Diploma thesis, Westfälische-Wilhelms Universität Münster (2008); P. Goslawski et al., Phys. Rev. ST Accel. Beams 13 (2010) 022803.

[1]Institut für Kernphysik, Westfälische-Wilhelms Universität Münster, 48149 Münster, Germany
*Supported by FZ Jülich FFE

The $pp \to pp\eta$ reaction dynamics studies at $3.35\mathrm{GeV/c}$ beam momentum

B.R. Jany[a,b,*]

The $pp \to pp\eta$ reaction at an incident proton momentum $3.35\mathrm{GeV/c}$ ($T = 2.54\mathrm{GeV}$) was measured with the WASA-at-COSY detector setup [1] via η meson decay into three neutral pions. All final state particles were measured, the two protons were detected in the Forward Detector of the WASA, while the three pions were reconstructed from the decay into six photons in the Electromagnetic Calorimeter.
The reaction was measured for the momentum of the η meson in the CM system in the rage of $q_\eta^{CM} = 0.45 - 0.7\mathrm{GeV/c}$ and for the cosine of the scattering angle of the η meson in the CM frame in range of $\cos(\theta_\eta^{CM}) = -1.0 - 0.0$. The detail investigations of the reaction dynamics were performed to understand the production process.

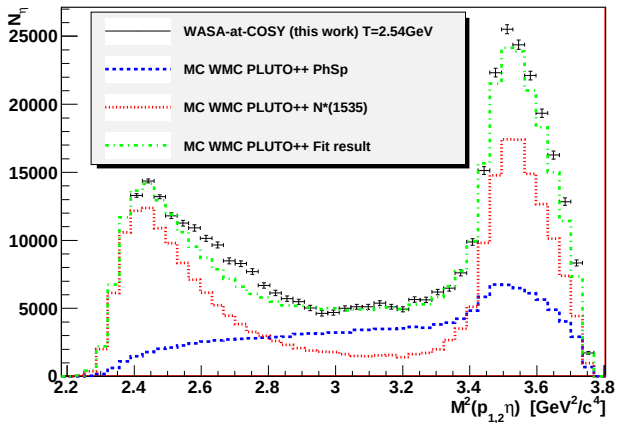

Fig. 1: Invariant mass squared of the proton-η system, the lines correspond to the Monte-Carlo simulation assuming different production mechanism. The experimental data are described by the 43% contribution of the $N^*(1535)$ and 57% contribution of the homogeneous and isotropic phase space. The spectra is not corrected for acceptance or efficiency.

The invariant mass squared of the proton-η system was studied (Fig. 1) and compared with the Monte-Carlo predictions assuming production mechanism via excitation of the $N^*(1535)$ and the production via homogeneously and isotropically populated phase space. Assuming that only these two processes contribute to the production of the η meson, the relative contribution of this processes were fitted to the experimental data, fitted curve see Fig. 1. The fit results in a 43% contribution of the $N^*(1535)$ and 57% of phase space in the production mechanism.
Also the angular distribution of the η meson was investigated by studying the cosine of the scattering angle of the η meson in the CM frame $\cos(\theta_\eta^{CM})$ for different momenta of the η meson in the CM system q_η^{CM} (Fig. 2). It is seen that when the momentum q_η^{CM} increases the angular distribution of $\cos(\theta_\eta^{CM})$ changes from almost flat one to highly anisotropic. This effect have never been measured before. The experimental data were also compared withe the existing Monte-Carlo model [3], based on the experimental measurements [2]. It is seen that the Monte-Carlo model follows only

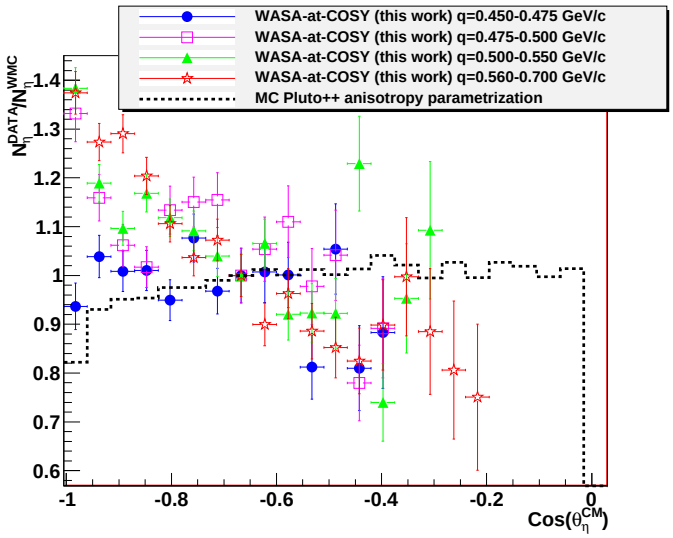

Fig. 2: The angular distribution of the η meson in the CM system for the different η meson momentum in the CM frame, the line corresponds to the Monte-Carlo model [3] based on experimental measurements [2]. The angular distribution changes while the η momentum increases.

the angular distribution for the lowest measured momentum range $q_\eta^{CM} = 0.450 - 0.475\mathrm{GeV/c}$. The angular distribution for the higher momentum range is not described by the model since it does not include the changes of the distribution as a function of the momentum.
The production dynamics of the η meson was studied in details. It is shown that the production mechanism proceeds via excitation of the $N^*(1535)$ baryon resonance in 43%. For the first time the momentum dependence of the angular distribution of the η meson was measured.

References:

[1] H. H. Adam, et al. (2004), `nucl-ex/0411038`.
[2] F. Balestra, et al. *Phys. Rev. C*, 69(6):064003, Jun 2004.
[3] I. Frohlich, et al. *PoS*, ACAT2007:076, 2007, `nucl-ex/07082382`.

[a] Institut für Kernphysik and Jülich Center for Hadron Physics, D-52425 Jülich, Germany

[b] Institute of Physics, Jagiellonian University, PL-30059 Cracow, Poland

* Supported by COSY-FFE

Study of the eta meson production with the polarised proton beam

M. Hodana[a,b], P. Moskal[a,b], I. Ozerianska[a] for the WASA-at-COSY collaboration

One of the interesting unsolved problem as regards the $\vec{p}p \to pp\eta$ reaction is the difficulty in reproducing the pp invariant mass distributions [1, 2, 3, 4]. Calculations which include NN FSI and $N\eta$ FSI do not match existing data [2]. To explain the unexpected shape of the distribution, possibility of higher partial-waves is considered. Taking into account a P-wave contribution one could reproduce the pp invariant mass distribution but not the close to threshold cross section dependencies [5]. To solve this discrepancy, a D_{13} resonance has been included [6] in the calculations. However, the data collected so far are insufficient for the unambiguous extraction of the S-wave or P-wave contributions.

Polarisation observables can probe interference terms between various partial amplitudes even if they are negligible for the spin averaged distributions. Therefore, for better understanding of the η meson production process, relative magnitudes from the partial waves contributions must be well established.

Up to now there are only three measurements of the analysing power for the $\vec{p}p \to pp\eta$ reaction which have been performed with low statistics and the determined value of analysing power is essentially consistent with zero [7, 8, 9] within large error bars of about ± 0.15.

Therefore in November 2010, the azimuthally symmetric WASA detector and the polarised proton beam of COSY, have been used [12] to collect a high statistics sample of $\vec{p}p \to pp\eta$ reactions in order to determine the analysing power as a function of the invariant mass spectra of the two particle subsystems and subsequently to perform the partial wave decomposition with an accuracy by far better than resulting from measurements of the distributions of the spin averaged cross sections.

For the determination of the analysing power of the η meson at a given value of the polar and azimuthal angle, it is required to measure left-right asymmetry of yields of the η meson, in the frame turned by the ϕ angle with respect to the laboratory coordinate system.

The large acceptance of the WASA detector allows to determine asymmetry of the η meson production as a function of the polar and azimuthal angle. The whole angular range is covered even at excess energies far from the threshold.

The measurement of the $\vec{p}p \to pp\eta$ reaction was carried out for two beam momenta of 2.026 GeV/c and 2.188 GeV/c, corresponding to excess energies of 15 MeV and 72 MeV. 118 hours of effective data taking included 74 hours with polarisation of 70% for the lower beam momentum and 44 hours with polarisation of 60% for the higher beam momentum. Vertically polarised proton beam, was stored and accelerated in the COSY ring. Direction of the polarisation was flipped from cycle to cycle. Protons from the $p\vec{p} \to pp\eta$ reaction, were registered in the Forward Detector and photons coming from the η decay channels were detected in the electromagnetic calorimeter. Both, the invariant mass of the decay products and the missing mass of two outgoing protons, are used for the identification of the η meson.

Determination of the beam polarisation and control of the systematics is achieved by measuring asymmetries for elastically scattered protons. Angular range of elastic scattered protons amounts to $60^\circ - 85^\circ$. In this range, analysing power for Q = 15 MeV and Q = 72 MeV is within 0.27 - 0.36 [10].

Average luminosity was estimated using trigger which requires at least one hit in the Central Plastic Barrel together with at least one hit in the Forward Plastic Barrel. For this trigger, prescaling factor was set to 600. With an assumption that 350 kHz [11] corresponds to the luminosity of $10^{31} cm^{-2} s^{-1}$, the achieved averaged luminosity amounts to $1.7 \cdot 10^{30} cm^{-2} s^{-1}$ and $2.3 \cdot 10^{30} cm^{-2} s^{-1}$ for the beam momentum of 2.026 GeV/c and 2.188 GeV/c, respectively. The main trigger used in the experiment required at least one matching track in Forward Trigger Hodoscope, Forward Window Counter and Forward Range Hodoscope in coincidence with at least two neutral groups in calorimeter. Cross sections for the $pp \to pp\eta$ reaction amounts to about $1 \cdot 10^3$nb for Q = 15 MeV and $5 \cdot 10^3$ nb for Q = 72 MeV, respectively [2]. Geometrical acceptance (Acc) together with expected number of $\eta \to \gamma\gamma$ and $\eta \to 3\pi^0$ events are given in Table 1.

Q $[Mev/c]$	P [MeV/c]	σ_{tot} [mb]	Acc	$N_{\eta\to\gamma\gamma}$	$N_{\eta\to}3\pi^0$
15	2026	10^3	0.55	99708	81661
72	2188	5*10^3	0.63	447789	375558

Table 1: Estimation of the number of produced eta mesons corrected for the geometrical acceptance of the detector system

The expected result should shed a light on the still not explained origin of structures in the invariant mass distributions observed independently by the TOF [1], COSY-11 [2, 4], and CELSIUS/WASA [3] collaborations.

We acknowledge support by the FFE grants from the Research Center Jülich.

References:

[1] M. Abdel-Bary et al., Eur. Phys. J. **A16** (2003) 127.
[2] P. Moskal et al., Phys. Rev. **C 69** (2004) 025203.
[3] H.Petrn et al., Phys. Rev. C 82 (2010) 055206
[4] P. Moskal et al., Eur. Phys. J. **A43** (2010) 131.
[5] K. Nakayama et al., Phys. Rev. C **68** (2003) 045201.
[6] K. Nakayama, SLAC eConf C070910
[7] R. Czyżykiewicz et al., Phys.Rev.Lett. **98** (2007) 122003.
[8] P. Winter et al., Eur. Phys. J. **A18** (2003) 355.
[9] F. Balestra et al. Phys. Rev. **C69** (2004) 064003.
[10] W. Scobel, *Nucl.Phys.News 11N4:21-26* (2001).
[11] H. Calén, priv. com. (2010).
[12] P. Moskal, M. Hodana, e-Print: arXiv:1101.5486

[a] M. Smoluchowski Institute of Physics, Jagiellonian University, 30-059 Cracow, Poland
[b] IKP, Forschungszentrum Jülich, D-52425 Jülich, Germany

Investigation of the ^{3}Heη-final state in dp-collisions*

I. Burmeister[1], P. Goslawski[1], M. Mielke[1], M. Papenbrock[1], D. Schröer[1], A. Täschner[1] and A. Khoukaz[1]
for the ANKE-Collaboration

Previous investigations on the reaction dp$\rightarrow$ η^3He at low excess energies have shown unexpected results in the total and differential cross section as seen by measurements accomplished at ANKE [1]. The total cross section shows a steep rise at threshold followed by a plateau for a wide energy range. The differential cross sections show a strongly increasing asymmetry with rising excess energies.

For the interpretation of these results the possibility of an η^3He quasi-bound state was discussed [2]. As a theoretical approach for the interpretation of the data a final state interaction model is used. In detail a description with two poles in the production amplitude f is chosen [1]. One of the poles is determined near the reaction threshold which is a necessary prerequisite for a bound or quasi-bound state.

Another criterion for a quasi-bound state is a fast change of the magnitude and the phase of the s-wave. This value is attainable by the interference of the s- and p-wave contribution to the scattering process. This interference changes the angular distribution and can be obtained by the asymmetry factor α defined as the slope of the angular distribution at $\cos\theta = 0$ [2]:

$$\alpha = \frac{\mathrm{d}}{\mathrm{d}(\cos\theta)} \ln\left(\frac{\mathrm{d}\sigma}{\mathrm{d}\Omega}\right)_{\cos\theta=0} \qquad (1)$$

The results presented in [1] were achieved using a continuous linear ramp in beam momentum provided by the COSY accelerator. This allows a precise determination of the total cross section in small steps which in turn limits the angular resolution for statistical reasons.

New data were taken in a beam time for the determination of the η mass at ANKE which are also used to determine total and differential cross sections of the reaction dp$\rightarrow$ η^3He. For this measurement COSY was operated at fixed beam momenta which were dermined with highest precision by spin resonance measurements [3]. Thereby the excess energy for the 15 different settings above threshold is known with high accuracy (i.e. 0.05 MeV). Due to the large statistics collected in this experiment, angular distributions of high quality will be accessible. The reaction itself is identified by using the missing mass technique. The background can be described by using data taken below the reaction threshold. This is demonstrated exemplarily for one angular bin at $Q = 8.1$ MeV excess energy in Fig. 1.

Using this background correction and counting the missing mass peak content for all angular bins allows to determine angular distributions. Very preliminary examples are shown in Fig 2. Although detector effficiency corrections are not yet included the relevance of higher partial waves already at excess energies above 4 MeV ist clearly visible. In the final analysis the angular distributions will allow for the precise determination of the asymmetry factor α. This provides the possibility to investigate the η^3He final state and might provide further important hints for a quasi-bound state.

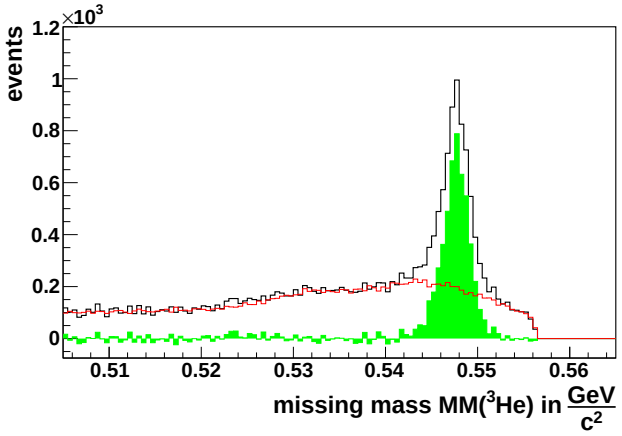

Fig. 1: ^{3}He missing mass distribution (black) at an excess energy of $Q = 8.1$ MeV and $\cos\theta_{^3\mathrm{He}} = [-0.6, -0.5]$. The background can be well discribed by subthreshold data (red) to extract the η^3He signal (green).

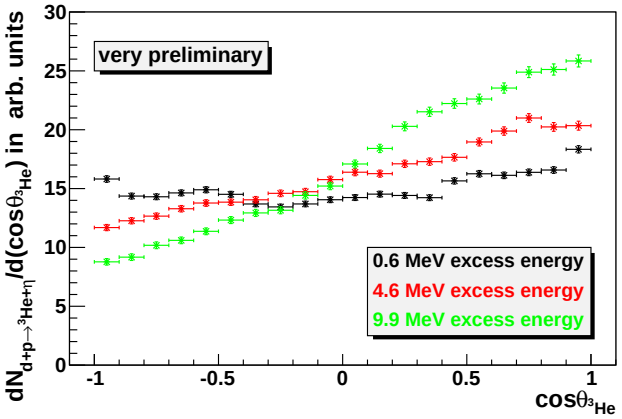

Fig. 2: Preliminary angular distributions of emitted ^{3}He-nuclei for three different excess energies.

The preliminary results demonstrate that the data set allows for the determination of total and differential cross sections with high statistics and unattained angular resolution. Although still preliminary the presented results indicate that new high quality data will be available in future.

References:

[1] T. Mersmann et al., Phys. Rev. Lett. **98**, 242301 (2007).
[2] C. Wilkin et al., Phys. Lett. B 654 (2007) 9296.
[3] P. Goslawski, Diploma thesis, Westfälische Wilhelms Universität Münster (2008); P. Goslawski et al., Phys. Rev. ST Accel. Beams 13 (2010) 022803.

[1]Institut für Kernphysik, Westfälische-Wilhelms Universität Münster, 48149 Münster, Germany
*Supported by FZ Jülich FFE

Status of the search for $(^4\text{He-}\eta)_{bs}$ by means of the WASA-at-COSY facility

M. Skurzok[a], P. Moskal[a,b] for the WASA collaboration

Measurement of the ^{4}He-η bound states is performed with unique precision with the WASA detector installed at the Cooler Synchrotron COSY. Signals of the η-mesic nuclei are searched for via studying the excitation function of specific decay channels of the ^{4}He-η system, formed in deuteron-deuteron collision [1]. The measurement is performed for beam momenta varying continously around the threshold. The beam ramping technique allows to reduce the systematic uncertainities. The existence of the bound system should manifest itself as a resonance-like structure in the excitation curve of eg. $dd \rightarrow (^4\text{He-}\eta)_{bs} \rightarrow {}^3\text{He}p\pi^-$ reaction below the $dd \rightarrow {}^4$He-η reaction threshold. This reaction is schematically presented in Fig. 1.

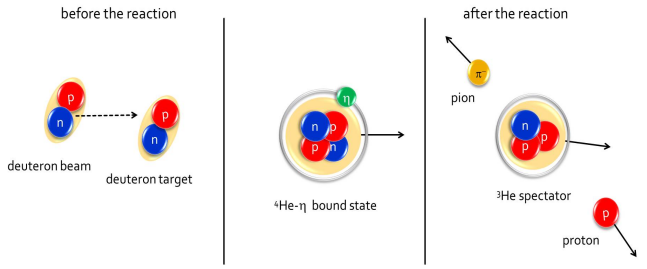

Fig. 1: Schematic picture of the $dd \rightarrow (^4\text{He-}\eta)_{bs} \rightarrow {}^3\text{He}p\pi^-$ reaction. Red and blue circles represent protons and neutrons respectively, further more π^- meson is depicted as yellow circle. The beam momentum is indicated by the dashed arrow [2].

During the experiment, in November 2010, two channels of the eta-mesic helium decay were measured: $dd \rightarrow (^4\text{He-}\eta)_{bs} \rightarrow {}^3\text{He}p\pi^-$ and $dd \rightarrow (^4\text{He-}\eta)_{bs} \rightarrow {}^3\text{He}n\pi^0 \rightarrow {}^3\text{He}n\gamma\gamma$. The measurement was performed with the beam momentum ramping from 2.127GeV/c to 2.422GeV/c, corresponding to the range of excess energy Q$\in$(-70,30)MeV.

For both of reactions the geometrical acceptance of the detector as a function of the excess energy Q near the kinematical threshold for η meson production was determined in simulations [2]. It is presented in Fig. 2 for different bound state widths and AV18 model describing nucleon momentum distribution inside the ^4He nuclei. The detailed description of the simulations is presented in Ref. [2]. The acceptance is almost a constant function of the excess energy and its average value is about 53% and 50% for $dd \rightarrow (^4\text{He-}\eta)_{bs} \rightarrow {}^3\text{He}p\pi^-$ and $dd \rightarrow (^4\text{He-}\eta)_{bs} \rightarrow {}^3\text{He}n\pi^0 \rightarrow {}^3\text{He}n\gamma\gamma$, respectively. The high acceptance values allow high statistics measurements of these final states.

During the experiment, data were effectively taken for about 167 hours. However, because the cooling system of Superconducting Solenoid failed, the measurement with magnetic field was carried out for only 41 hours. The total integrated luminosity was estimated based on the trigger used for the elastic proton-proton scattering (trigger No. 17 assuming that 220kHz corresponds to L=$4{\cdot}10^{30} cm^{-2}s^{-1}$) and is equaled to about L=$8.5{\cdot}10^{30} cm^{-2}s^{-1}$. Taking into account the fact that there were two reactions measured, in total more than 40 times higher statistics were collected than in 2008. At present the data analysis is in progress. In optimistic case the statistics could be sufficient to observe a signal from the η-mesic helium and in the pesimistic scenario we will decrease the upper limit of the cross section for the ^{4}He-η bound state production by a factor of about six.

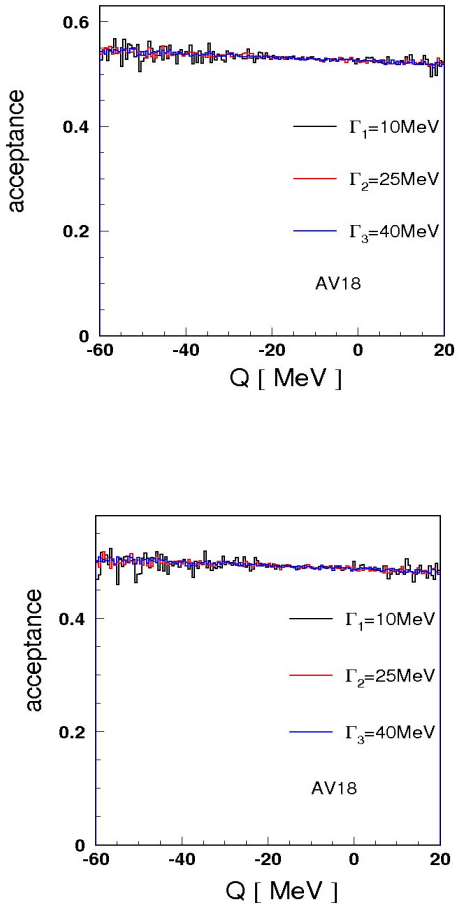

Fig. 2: Geometrical acceptances of the WASA-at-COSY detector for the $dd \rightarrow (^4\text{He-}\eta)_{bs} \rightarrow {}^3\text{He}p\pi^-$ (top) and $dd \rightarrow (^4\text{He-}\eta)_{bs} \rightarrow {}^3\text{He}n\pi^0 \rightarrow {}^3\text{He}n\gamma\gamma$ reaction (down). Acceptance is calculated for three different bound state width values and AV18 potencial model describing the momentum distribution of the nucleons inside ^{4}He.

We acknowledge support by the Foundation for Polish Science - MPD program, co-financed by the European Union within the European Regional Development Fund and by the FFE grants of the Research Center Juelich.

References:

[1] P. Moskal, *arXiv:0909.3979* (2009).
[2] M. Skurzok, *Diploma Thesis, Jagiellonian University of Cracow* (2010), Berichte des FZ-Jülich, Jül-4332 (2010), *arXiv:1009.5503* (2010).

[a] M. Smoluchowski Institute of Physics, Jagiellonian University, 30-059 Cracow, Poland
[b] IKP, Forschungszentrum Jülich, D-52425 Jülich, Germany

Measurement of Angular Distribution for pd $\rightarrow {}^3$He ($\eta \rightarrow \gamma\gamma$) reaction at Q=61 MeV with WASA-at-COSY

Anna Jany[a,*] for the WASA-at-COSY Collaboration

We report on the studies of angular distribution for pd $\rightarrow {}^3$He ($\eta \rightarrow \gamma\gamma$) reaction investigated with the WASA-at-COSY. An experimental data set was taken in October/November 2008, at 1.7 GeV/c beam momentum corresponding to Q=61 MeV. The two photon decay of the η meson was registered in coincidence with the ^{3}He. The two photons were detected in the central part of the WASA-at-COSY apparatus, whereas the ^{3}He was observed in its forward part [1]. The η meson has been identified via missing mass and invariant mass techniques, as shown in Fig. 1. As can be seen, the signal-

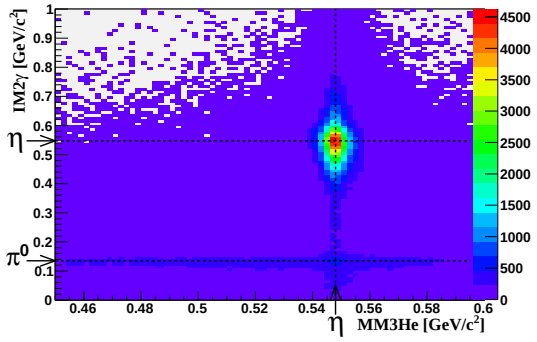

Fig. 1: Invariant mass IM2γ versus missing mass MM3He.

to-background ratio is big enough for easy selection of the η meson by putting the gate on the invariant mass of the two photons (IM2γ). The selected events have been used to construct the angular distribution of the η meson in the CM of the ^{3}He-η system. For each individual bin of the $\cos(\theta)\eta_{CM}$ of 0.03 length, the still existing background in missing mass of ^{3}He (MM3He) has been approximated by a second order polynomial. The preliminary data, corrected for the total efficiency and normalized to the total cross section taken from [2], have been compared with ANKE data [2] taken at the same Q, as presented in Fig. 2. Taking into account, that

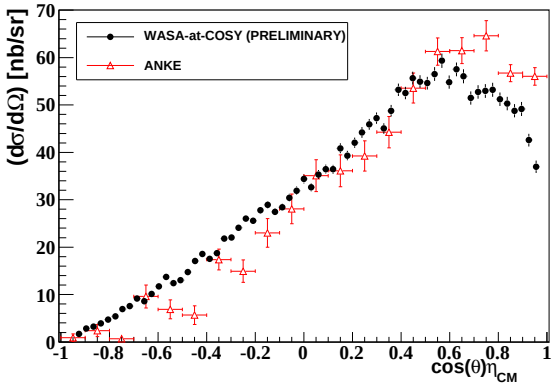

Fig. 2: The present result (full circles) compared to the ANKE data [2] measured at Q=60MeV (triangles).

the completely different experimental methods were used in both measurements, the agreement between the two results is quite good. It should be pointed out, that our data were obtained with significantly higher statistics than those from the ANKE experiment. This allowed to obtain smaller statistical errors even using the smaller $\cos(\theta)\eta_{CM}$ bins.
Using the present, preliminary data, the partial wave analysis has been made. Since the considered reaction is induced by unpolarized proton beam impinging onto unpolarized deuteron target and polarization of outgoing ^{3}He is not measured, the angular distribution can be decomposed into series of Legendre polynomials, as follows:

$$\frac{d\sigma}{d\Omega}(\theta) = \frac{1}{4k^2} \cdot |\sum_{l=0}^{l_{max}} (2l+1) S_l P_l(\theta)|^2 \qquad (1)$$

where k is the CM p+d wave number and the dynamics of the process is determined by complex S-matrix elements S_l for this reaction. The formula (1) was fitted to the experimental angular distribution treating the S_l elements as free parameters. The fit was performed independently for different l_{max} values, from 1 to 4. The result is presented in Fig. 3.

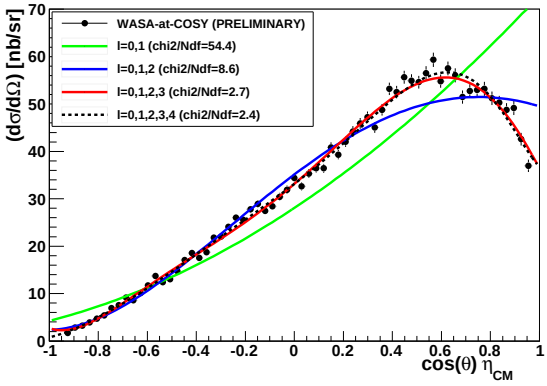

Fig. 3: Experimental angular distribution and results of the partial wave fits.

The best fit was obtained for $l_{max} = 4$, what is in agreement with conclusions of [2]. The corresponding probabilities $|S_l|^2$ of the reaction for given l - orbital momentum, as well as relative probabilities $|S_l|^2/|S_0|^2$ are listed in Table 1.

l	$\lvert S_l\rvert^2$ [10^{-5}]	$\lvert S_l\rvert^2/\lvert S_0\rvert^2$
0	8.57(98)	1
1	3.86(53)	0.45(1)
2	1.18(40)	0.14(3)
3	0.27(6)	0.031(3)
4	0.016(7)	0.0019(6)

Table 1: The probabilities $|S_l|^2$ of the reaction for given l and the relative to $l = 0$ probabilities $|S_l|^2/|S_0|^2$.

As can be seen in Fig. 3 and in Table 1, the contribution of g - wave ($l = 4$) is almost negligible, however all smaller l - values are significant and decrease monotonically with l.

References:

[1] H.H.Adam et al., arXiv:nucl-ex/0411038 (2004).
[2] T.Rausmann et al., Phys. Rev. C **80**, 017001 (2009).

[a] Institute of Physics, Jagiellonian University, PL-30059 Cracow, Poland

* Supported by COSY-FFE

Preliminary analysis of the $\eta \to \pi^+\pi^-\pi^0$ decay

Patrik Adlarson*

The $\eta \to \pi^+\pi^-\pi^0$ is an important decay since its largest contribution comes from the strong isospin violation part which in turn makes it possible to set important constraints on quark mass ratios m_s/m_d and m_u/m_d. This requires that experimental results and theoretical calculations are well understood. On the experimental side there have been many measurements studying $\eta \to 3\pi^0$ (see e.g. [1]-[5]), but only one recent measurement with large statistics for the charged decay $\eta \to \pi^+\pi^-\pi^0$ done by KLOE ([6]). Their experimental result shows a deviation in comparison to Chiral Perturbation Theory calculation, therefore making it important to perform an independent measurement.

In 2008 and 2009 WASA-at-COSY measured $pd \to {}^3\mathrm{He}X$ at 1 GeV, with the intent of detecting η decays. Approximately $3 \cdot 10^7$ η were collected during that time. In the beam time in 2008, 11.8 million $pd \to {}^3\mathrm{He}\eta$ events were saved on disk. This contribution shows preliminary results of the $\eta \to \pi^+\pi^-\pi^0$ experimental data obtained with the WASA-at-COSY for the 2008 beam time. η is identified by selection of the peak in the M_x distribution as shown in figure 1.

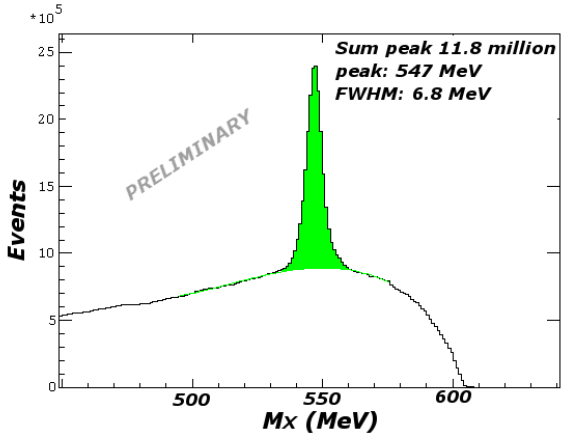

Fig. 1: Results from 2008 data. Missing Mass calculated for the identified ^{3}He shows a distinct peak corresponding to η.

To separate $\eta \to \pi^+\pi^-\pi^0$ from other background channels one requires a ^{3}He detected in FD, at least two tracks of opposite polarity reconstructed in the MDC, and a photon pair with the invariant mass close to π^0. In addition, several cuts are imposed on the data to further reduce contributions from chance coincidental events and background channels. The three main cuts are conditions on $\mathrm{MM}^2({}^3\mathrm{He}\pi^+\pi^-)$, $\mathrm{MM}^2({}^3\mathrm{He}\pi^0)$ and $\mathrm{MM}(\pi^+\pi^-)$. After implementation of the cuts the preliminary analysis gives approximately 254 000 $\eta \to \pi^+\pi^-\pi^0$ candidates from the 2008 data. Basic distributions obtained for this event sample are shown in figure 2.
The final goal of the analysis is to obtain a Dalitz Plot with the axes defined as

$$X = \sqrt{3}\frac{(T_+ - T_-)}{Q_\eta},\ Y = \frac{3T_0}{Q_\eta} - 1 \qquad (1)$$

where T_+, T_- and T_0 represent the kinetic energies of π^+, π^- and π^0 in the rest frame of η, and

$$Q_\eta = T_+ + T_- + T_0. \qquad (2)$$

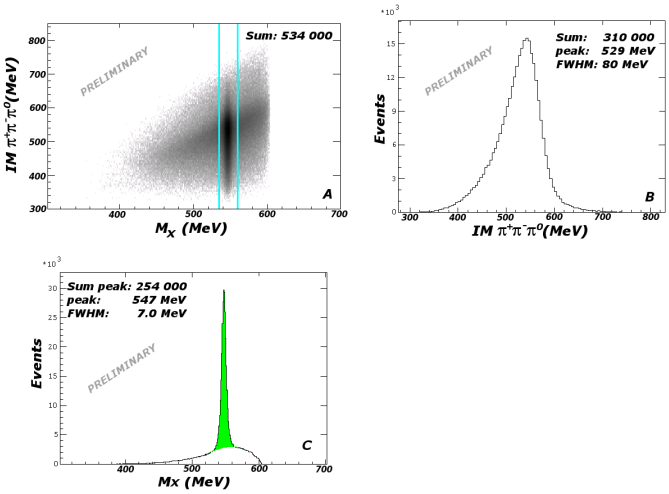

Fig. 2: Scatterplot of $MM(^3\mathrm{He})$ vs $IM(\pi^+\pi^-\pi^0)$ after a crude selection criterion (A). The blue lines mark the interval which is projected onto the IM-axis (B). The projection of the scatterplot onto MM_x with η candidates is marked in green (C).

As may be seen from figure 2, the resolution of the Forward Detector is better than the resolution in the invariant mass of the decay products measured in the Central Detector. The four-momentum resolution for the individual decay products may be improved by using the kinematical fit procedure. This requires a good understanding of the detector performance which is achieved by Monte Carlo simulation using the GEANT package [3].
Reasonable agreement between experimental data and simulation has been obtained as seen by comparing distributions of ΔX and ΔY distributions of simulated data and experimental data in figure 3. The ΔX and ΔY are defined as:

$$\Delta X = X_{kfit} - X_{rec},\ \Delta Y = Y_{kfit} - Y_{rec}. \qquad (3)$$

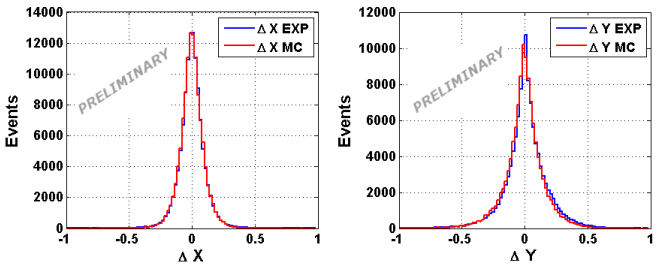

Fig. 3: *(left:) Experimentally obtained ΔX (blue) compared to ΔX obtained in MC simulation (red). (right:) Experimentally obtained ΔY (blue) compared to ΔY obtained in MC simulation (red).*

Here $X_{kfit}(Y_{kfit})$ is the X(Y)-value obtained after kinematical fit and $X_{rec}(Y_{rec})$ is the reconstructed X(Y)-value before kinematical fit. If the simulated data agrees well with the experimental data, the bin width of the Dalitz plot may be from the width of ΔX_{tr} and ΔY_{tr} distributions:

$$\Delta X_{tr} = X_{kinfit} - X_{true},\ \Delta Y_{tr} = Y_{kinfit} - Y_{true}, \qquad (4)$$

where $X_{true}(Y_{true})$ is the actual $X(Y)$-value used in the simulation. The distributions are shown in figure 4 and give a full width at the half of the maximum of 0.15.

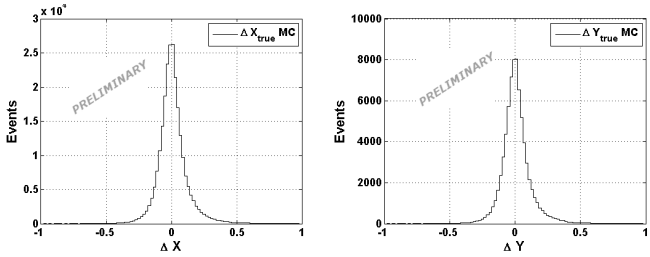

Fig. 4: *(left:) ΔX_{tr} for MC . (right:) ΔY_{tr} for MC.*

The bin width is therefore preliminarly chosen as 0.2. For each bin in the Dalitz Plot the number of $\eta \to \pi^+\pi^-\pi^0$ decays will be found as the peak in the MM(^{3}He) using different peak estimation methods, as illustrated in figure 5.

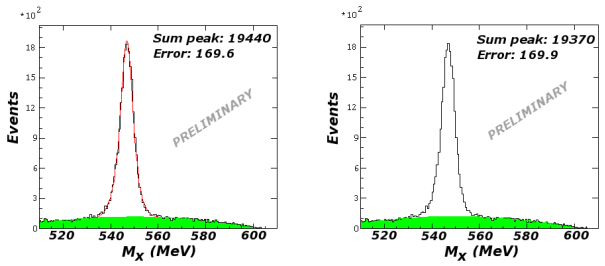

Fig. 5: The MM(^{3}He) content for the bin region $-0.3 < X < -0.1$ and the total projection on the Y-axis using two different peak estimation methods- fitting a polynomial over the background region and two gaussians on the peak (left), and by subtracting the background by a fitting a polynomial and summing the counts in the peak region (right).

The projections of the Dalitz plot on the X- and Y-axis, not corrected for acceptance, are shown in figure 6 which compares the experimental result (black point with statistical error bars) with Monte Carlo weighted with the leading order result of Chiral Perturbation Theory (blue solid line), the NLO result (green solid line), the NNLO result (red solid line), as well as weighting the simulation with the result found by KLOE (black solid line).

References:

[1] Crystal Ball Collaboration, W. Tippen *et al*, Phys. Rev. Lett. **87**, 192001 (2001).

[2] CELSIUS/WASA Collaboration, M. Bashkanov *et al*, Phys. Rev. C. **76**, 048201 (2007), arXiv:0708.2014 [nucl-ex].

[3] CERN, GEANT - Detector Description and Simulation Tool, CERN Program Library Long Writeup W5013

[4] KLOE Collaboration, F.Ambrosino *et al* in *Proceedings of LP07 conference*, pp. S8-356, Kyungpook National University Press, 2007, arXiv:0707.4137 [hep-ex].

[5] WASA-at-COSY Collaboration, P. Vlasov *et al*, Phys. Lett. B **677**, 24 (2009), arXiv:0811.2763 [nucl-ex].

[6] KLOE Collaboration, F.Ambrosino *et al*, JHEP 05 **006** (2008), arXiv:0801.2642 [hep-ex].

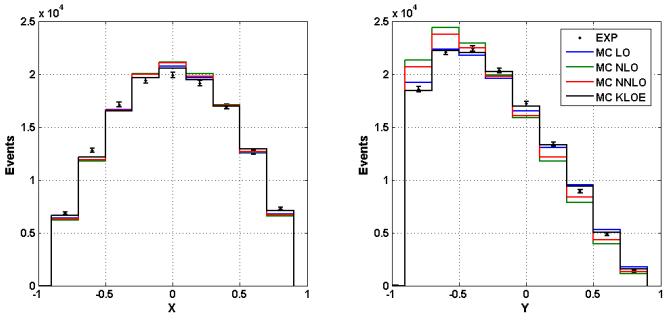

Fig. 6: *Dalitz Plot projections on the X-axis (left) and on the Y-axis (right) for the average experimental values (black points) with their statistical errors, compared to the LO result (blue line), NLO result (green line), NNLO result (red line) of Chiral Perturbation Theory and the KLOE result (black solid line). The simulation is normalized to the sum of the experimental points. The distributions are not acceptance corrected.*

* Department of Physics and Astronomy University of Uppsala, patrik.adlarson@fysast.uu.se

Feasibility of the $\pi^0 \to e^+e^-$ measurement in the $pp \to pp\pi^0$ reaction at T_{beam} =550 MeV

C.-O. Gullström*

A test run of π^0 production in proton proton collisions was performed in spring 2010. The goal of the run was the feasibility of measuring $\pi^0 \to e^+e^-$ decay with WASA-at-COSY. The decay have an extremely low branching ratio of $(7.44 \pm 0.29) \times 10^{-8}$ (when correcting for final state radiation). This result is based on 795 events from the KTeV Collaboration [1]. It is three standard deviations larger then the Standard Model prediction of $(6.23 \pm 0.09) \times 10^{-8}$ [2], which has lead to speculations about new physics. One explanation is the existence of a new vector boson U with a mass of $m_U \sim 10 - 100$ MeV. The new boson would be responsible for annihilation of a neutral scalar particle χ with a mass of $m_\chi \sim 1 - 10$ MeV [3]. The annihilation $\chi\chi \to U \to e^+e^-$ could account for the observed 511 keV line from the galactic center.

The WASA-at-COSY test run was performed at a beam energy of 550 MeV to achieve the largest π^0 production cross-section while staying below threshold for the two pion production. The π^0 meson production corresponds to 4% of the total pp cross section at this energy. The π^0 events are tagged by the missing mass of the two outgoing protons. The two protons are emitted at scattering angles, θ, up to 45°. Therefore the protons are measured in the Forward Detector (FD), with the angular coverage $3° < \theta < 18°$ and the forward part of the Central Detector (CD), with the angular coverage $20° < \theta < 45°$. The best signal to background ratio is found for the case of two FD proton tracks followed by FD–CD combination. The case with two CD proton tracks were found to have too high background level. Figure 1 shows the missing mass squared of the two outgoing protons showing a signature of the $pp \to pp\pi^0$ reaction.

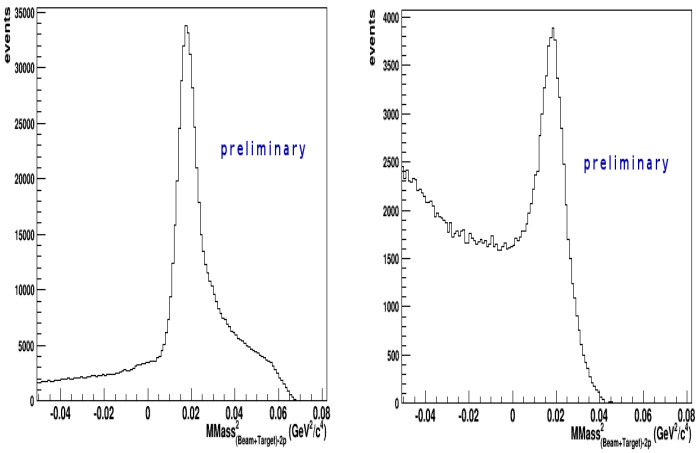

Fig. 1: Left: Missing mass squared of two protons from the test run. Right: two proton tracks in the FD, Left: FD–CD proton tracks combination.

The most common decay, $\pi^0 \to \gamma\gamma$, has a branching ratio (BR) of 98.8%. The most common π^0 decay with charged particles is the Dalitz (conversion) decay $\pi^0 \to e^+e^-\gamma$ with BR of 1.13%. Since the decay contains a lepton pair it is more appropriate for $\pi^0 \to e^+e^-$ normalization and monitoring due to similarities in the reconstruction procedures.

The distribution of the lepton pair invariant mass, q, in the $\pi^0 \to e^+e^-\gamma$ decay is related to the internal structure of the π^0 via a transition form factor. This decay could also be used to search for the light dark matter candidates. If the mass of the hypothetical particle is below the π^0 mass a peak would appear in the q distribution. Figure 2 shows the invariant mass of γe^+e^- from spring 2010 data and figure 3 shows the q distribution. The result is compared to the simulations of $\pi^0 \to e^+e^-\gamma$ and $\pi^0 \to \gamma\gamma$ (with photon conversion in the detector material) decays. The $\pi^0 \to e^+e^-$ events are supposed to be located at the high end of the distribution. In order to see the peak one would need to improve resolution by means of fine tuning the detector calibration and the reconstruction algorithm.

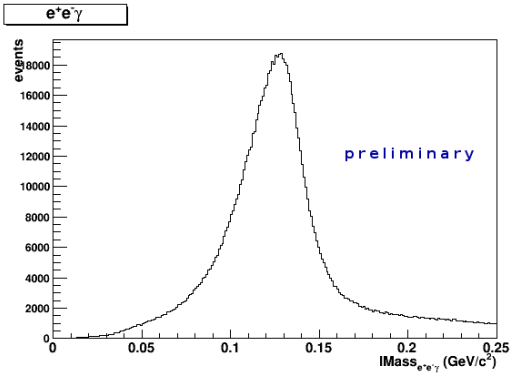

Fig. 2: Invariant mass of $e^+e^-\gamma$ from the test run.

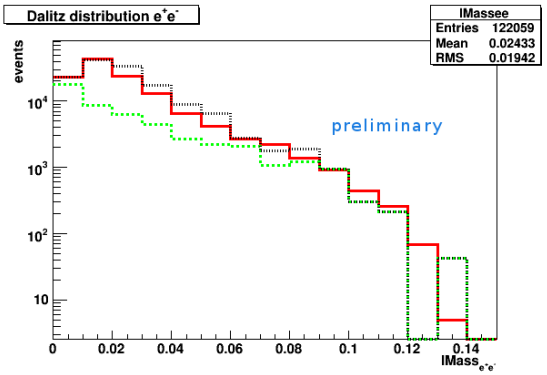

Fig. 3: Invariant mass of the e^+e^- pair. Red line: data, green line: simulation of $\pi^0 \to e^+e^-\gamma$, black line: simulation of $\pi^0 \to e^+e^-\gamma$ and $\pi^0 \to \gamma\gamma$.

References:

[1] E. Abouzaid *et. al,* Phys. Rev. D **75** (2007)
[2] A.E. Dorokhov arXiv:0805.0994v1 [hep-ph]
[3] C. Boehm and P.Fayet, Nucl. Phys. B **683** (2004)

*Department of Physics and Astronomy, Uppsala University, Sweden

Measurement of $\eta \to \pi^+\pi^- e^+ e^-$ with WASA at COSY

D. Coderre* and J. Ritman* for the WASA-at-COSY Collaboration

The large number of η-mesons collected at the WASA facility at COSY has made possible the study of rare decay modes of the η. The branching ratio of the channel $\eta \to \pi^+\pi^- e^+ e^-$ has recently been determined to be $2.68 \pm .11\text{x}10^{-4}$ [1]. Predictions from modern theories are at least two standard deviations away from the measured value. WASA-at-COSY will make use of data collected in both the $pd \to {}^3He\eta$ and $pp \to pp\eta$ production reactions to make a new measurement of the absolute branching ratio of $\eta \to \pi^+\pi^- e^+ e^-$ as well as the branching ratio relative to $\eta \to \pi^+\pi^-\gamma$.

It has also been suggested that this reaction could provide an observable for a type of flavor-conserving CP-violation not explained by the CKM mechanism in the standard model [2][3]. Contributions of the CP-violating electric transition could be observed by detecting an asymmetry in the angle between the decay planes of the pions and electrons, which can be measured by the WASA drift chamber. This asymmetry arises due to mixed electric and magnetic transition terms in the decay amplitude. Using the non-conventional operator suggested in [2], there are virtually no experimental restrictions on the magnitude of this asymmetry and it could have a value of up to 1% [3]. The current experimental upper limit is on the order of a few percent [1].

WASA currently has a total of 12 weeks of data from proton-deuteron reactions taken in 2008 and 2009 yielding over 30 million η-mesons. The unique signature of the ^{3}He ion in the WASA forward detector allows data-taking to proceed with no bias on the decay of the η. The ability to cleanly trigger on the ^{3}He also keeps the background suppressed, with the cross-section of multipion production on the same order of magnitude as η production. In 2010, WASA collected 8 weeks of data from proton-proton reactions with the goal of accumulating high statistics of η mesons to measure rare decays. The cross-section for η production is a factor of 10 higher than in pd, resulting in a sample of 10^8 η mesons. Due to a large background from multi π production, the main experiment trigger was biased towards charged decays of the η.

For analysis of the signal channel, the forward-scattered hadron(s) must be reconstructed in the WASA forward detector and the η decay products must be reconstructed in the central detector. Based on Monte Carlo studies, the combined geometrical acceptance and reconstruction efficiency for p-d and p-p at this stage is 23% and 10%, respectively. The lower acceptance in the p-p reactions is a result of the increased Lorentz boost of the produced η-mesons.

The identification of pions and electrons is important for proper mass assignments and for the decay plane measurement. First, E/dE plots are made using various sub-detector combinations in the WASA central detector. These bands are trained into neural networks which can be queried for single-track probabilities at run time. Additionally, because the dilepton pair in this decay originates from a virtual photon, the opening angle between the electron and positron is usually smaller than the angle between the two pions or a mismatched pair and this information can also be used. According to simulations, the pions and electrons are correctly identified in over 90% of events.

After particle identification, the decay of interest makes up

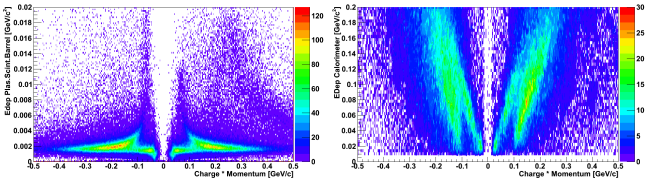

(a) q*Mom. vs. dE/dx Plas. Barrel (b) q*Mom. vs. Edep Calorimeter

Fig. 1: Particle identifcation plots showing clear signals from both electrons and pions. (Fall 2009 data)

just 15% of the remaining η signal. Two separate steps are taken to further suppress background. In the first step, a kinematic fit is performed with constraints on energy and momentum conservation. A cut on the probability suppresses events coming from other reactions. After this, the most significant background remaining comes from the conversion of real photons in the beam pipe. These channels are sensitive to a selection on the primary vertex. For this, the electron and positron helices are traced toward the origin and the point of closest approach is calculated. This value is correlated with the invariant mass of the dilepton pair calculated at the beam pipe. In the resulting distribution, electron/positron pairs coming from the beam pipe are easily separated from those coming from the origin. After this background suppression, the signal content of the remaining event sample is about 80%.

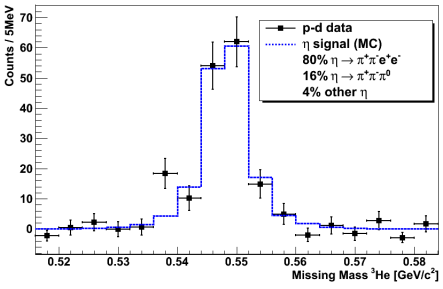

Fig. 2: Events from pd data remaining after all cuts and subtraction of continuum multi-π background. Total signal content about 130 events.

A clean sample of signal events has been identified in pd reactions. Work is ongoing to determine the absolute and relative branching ratios of the signal channel. The decay has also been observed in proton-proton data, but that analysis is still in its early stages.

References:

[1] The KLOE Collaboration, Phys. Lett. B675 (2009) 283-288.

[2] C.Q. Geng,J.N. Ng, and T.H. Wu, Mod. Phy. Lett. A 17 (2002) 1489.

[3] D.N. Gao, Mod. Phys. Lett. A 17 (2002) 1583.

* Institut für Kernphysik, Forschungszentrum Jülich and Institut für Experimentalphysik I Ruhr Universität Bochum

The $\eta \to \gamma\, e^+e^-$ Decay from pd Reactions with WASA-at-COSY

M.Hodana[a,b] and P.Moskal[a,b]

We report on the analysis of the pd $\to$ ^{3}Heη $\to$ ^{3}Heγe^-e^+reaction, measured with the WASA-at-COSY detector at proton beam momentum of 1.69 GeV/c. Experiment was performed in November 2008. Data collected during 4 weeks, yields approximately 10 million of η mesons tagged by the ^{3}He ions measured in the Forward Detector.

The aim of the conducted analysis is the investigation of the electromagnetic structure of the η meson by determining the transition form factor. The probability of creation of a dielectron pair in considered decay is proportional to the probability of emission of a virtual photon with a time-like four-momentum. The square of this four-momentum vector is equal to the square of the mass of created dielectron pair. By studying the probability of given decay as a function of the dielectron pair mass, one obtains information about the hadron-photon transition and hence about the electromagnetic structure of decaying neutral meson [1].

In order to obtain a clean data sample consisting of η events, selection of ^{3}He in Forward Detector (FD) is applied as shown in Fig.1:left. After selection of ^{3}He ions a sample of over 4×10^6 events corresponding to the η meson production is clearly seen over the continuous background of the multi-meson production (Fig.1:right,blue curve).

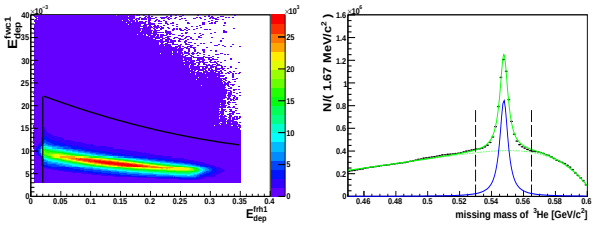

Fig. 1: Left: Energy loss in the first layer of the thin forward detector array (FWC) versus energy loss in the first layer of the forward range hodoscopes (FRH) - the band of ^{3}He particles is visible. Right: Missing mass of ^{3}He after ^{3}He selection. Both spectra contain around 40% of η produced in 2008 run. We see in the signal region of the missing mass spectrum (broken lines) around 4.35×10^6 η s.

Selection in Central Detector (CD) aims at choosing decay channel of interest. We demand (i) that two tracks corresponding to the oppsitely charged particles are reconstructed and, (ii) that at least one neutral particle was registered and, (iii) that the signals are correlated in time with signals observed in Forward Detector within 12 ns and 31 ns window for charged and neutral tracks, respectively. Energy deposited by neutral particle has to be higher than 100MeV. Additionaly, for a given event, in the η center of mass system, there has to be only one such neutral candidate, forming with a lepton pair $\Delta\phi$ angle in a range from 60° to 300° (see Fig.2).

In order to supress background from $\eta \to \gamma\gamma$ decay, where one of photons undergoes conversion into

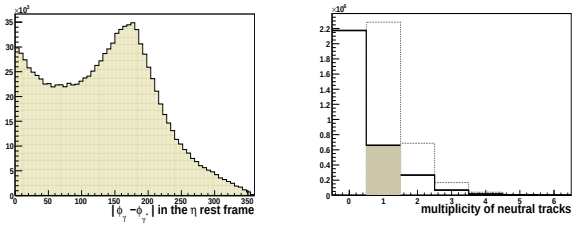

Fig. 2: Left: Difference in azimuthal angle between virtual and real photon in the η center of mass frame ($\Delta\phi$). Right: Multiplicity of neutral tracks before cut on $\Delta\phi$ (broken line) and after (solid line). Events with exactly one neutral tracks inside $\Delta\phi$ cut (shadowed region) are accepted.

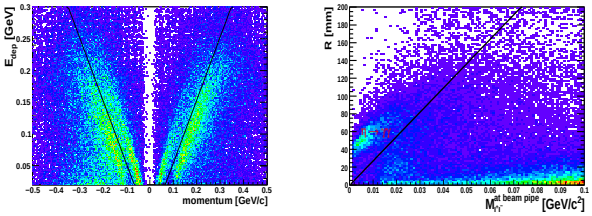

Fig. 3: Left: Selection of e^+e^- particles in Central Detector. Bands of e^+ and e^- particles are visible above solid lines. Picture was obtained with restriction that the opening angle of e^+e^- particles is less than 10°. Right: Radius of point of closest approach as a function of invariant mass of a lepton pair. Events coming from $\eta \to \gamma\gamma$ decay, in which real photon converts into lepton pair are clearly visible.

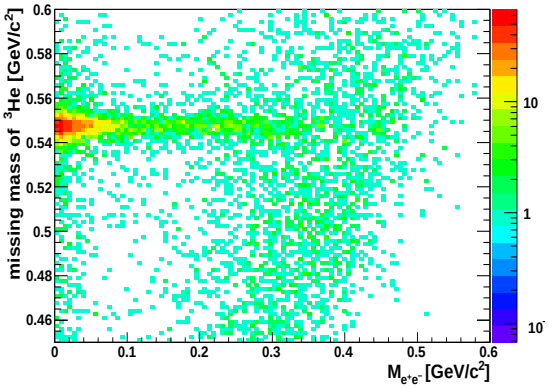

Fig. 4: Missing mass of ^{3}He as a function of invariant mass of lepton pair after cuts described in the text. Plot contains 30% of avaiable data.

e^+e^- pair in the beam pipe, the radius of point of closest approach (R) is used as presented in Fig.3:left. Identification of electrons is done using E/dE plot as shown in Fig.3:right. Additional restriction is placed on the missing mass of $e^+e^-\gamma$ and $\Delta\phi$ angle between virtual and real photon. That reduces futher, background coming

from η decay channels with pions.
Spectrum of missing mass of ^{3}He as a function of invariant mass of lepton pair after applying cuts described above is shown in Fig.4. Plot was made using data sample showed in Fig.1:right.

References:

[1] L. G. Landsberg, Physics Reports, **128** (6), p.301-376, Nov 1985.

[a] Institute of Physics, Jagiellonian University, PL-30059 Cracow, Poland

[b] Institut für Kernphysik and Jülich Center for Hadron Physics, D-52425 Jülich, Germany

* Supported by COSY-FFE

Measurement of the $\eta \to e^+e^-e^+e^-$ double Dalitz decay

P. Wurm and M. Büscher
for the WASA-at-COSY Collaboration

The Wide Angle Shower Apparatus (WASA) is a large-acceptance detector to study the decay channels of light mesons [1]. A huge number of η mesons is being produced in proton-deuteron and proton-proton collisions. The data permit the study of very rare η-decay channels, like the double Dalitz decay, where the η meson decays via two virtual photons into two electron-positron pairs. The current upper limit for the branching ratio amounts to 6.9×10^{-5} with a 90% confidence level [2]. One objective of the WASA-at-COSY experiment is to determine and establish a finite value of this branching ratio. A first analysis is based on a $p\,d \to {}^3\mathrm{He}\,\eta$ beam time in 2008, which comprises approximately 10^7 η mesons [3]. From these data 30 ± 10 double Dalitz decay event candidates have been extracted.

The analysis presented here is based on a total amount of 3×10^7 η mesons, which have been produced in $p\,d \to {}^3\mathrm{He}\,\eta$ reactions during two beam times in 2008 and 2009. Figure 1 shows the ^{3}He-missing mass spectrum from the 2009 data set.

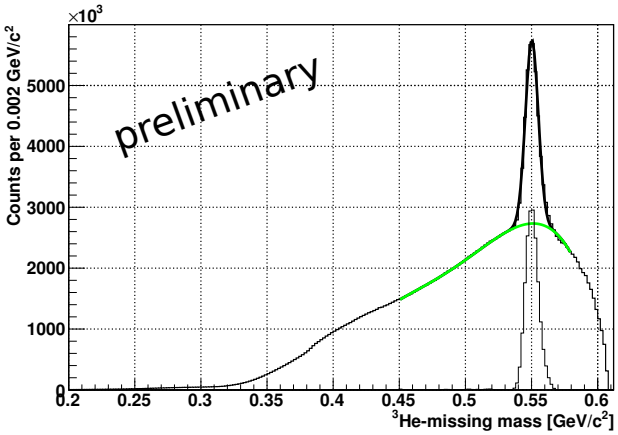

Fig. 1: ^{3}He-missing mass distribution from the 2009 data set.

The η signal is extracted by fitting the spectrum with a Gaussian function for the signal plus a polynomial, for the background coming from direct pion production. The signal is peaked around a mass of $547.9\,\mathrm{MeV/c^2}$ and contains approximately 1.9×10^7 η mesons. After each cut the ^{3}He-missing mass spectrum serves as the reference spectrum for the total number of η events.

A set of cuts has been developed, which suppresses the background channels as strongly as possible while leaving the number of $\eta \to e^+e^-e^+e^-$ events as high as possible. The considered background channels are listed in Table 1.

Due to the large amount of pions from the strong η decays, an effective method to distinguish between electrons (positrons) and pions must be found. The WASA detector provides particle identification via the momentum information, which is measured by the Mini Drift Chamber (MDC) as well as the energy deposit in the Plastic Scintillator Barrel (PSB) and in the Scintillator Electromagnetic Calorimeter (SEC). Figure 2 shows the simulated electron (positron) and pion bands.

Table 1: η-decay channels for background studies and their branching ratios (from Ref. [4])

decay product	branching ratio
$\gamma\gamma$	0.3931 ± 0.002
$\pi^0\pi^0\pi^0$	0.3257 ± 0.0023
$\pi^+\pi^-\pi^0$	0.2274 ± 0.0028
$\pi^+\pi^-\gamma$	0.0460 ± 0.0016
$e^+e^-\gamma$	0.007 ± 0.0007
$\pi^+\pi^-e^+e^-$	0.000268 ± 0.000011

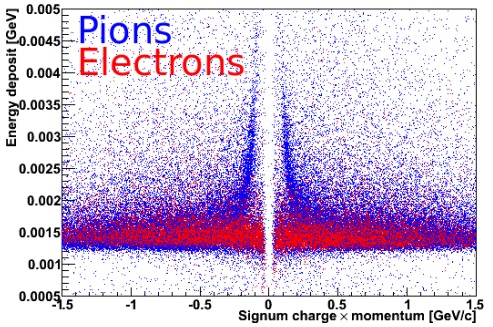

(a) Energy deposit in PSB as a function of the momentum times the particles charge.

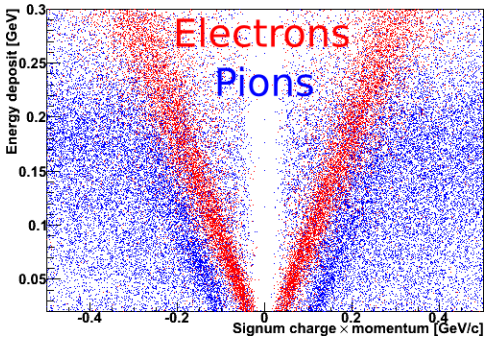

(b) Energy deposit in SEC as a function of the momentum times the particles charge.

Fig. 2: Particle identification plots.

The decision, whether the particle is an electron (positron) or a pion, is based on artificial neural networks (ANN) implemented in ROOT [5]. After the particle identification, an event-candidate must have at least two electrons and two positrons. Out of these tracks all possible pair-combinations are build, which can be the decay product of one of the two virtual photons. In the following, each combination is evaluated to be an double Dalitz decay event.
Another source of background are events, where a photon converts into an electron-positron pair. In case of the single Dalitz decay $\eta \to e^+e^-\gamma$, there is the same

number of electrons and positrons in the final state as in case of the double Dalitz decay. To suppress such events, the invariant mass of each lepton-pair is calculated from the four-vectors at the beam pipe. For conversion events, the invariant mass is zero, since the lepton-pair comes from a real photon.
The next cuts make use of the decay-specific kinematics of the double Dalitz decay. The opening angle α between the electron and the positron from the same virtual photon peaks at small values. Due to the two body decay $\eta \rightarrow \gamma^*\gamma^*$, the two virtual photons must be emitted back-to-back in the CM system. In the laboratory system, the opening angle β between the virtual photons is mainly populated in the range of large values.

Figure 3 shows the development of the ^{3}He-missing mass spectrum after the described cuts.

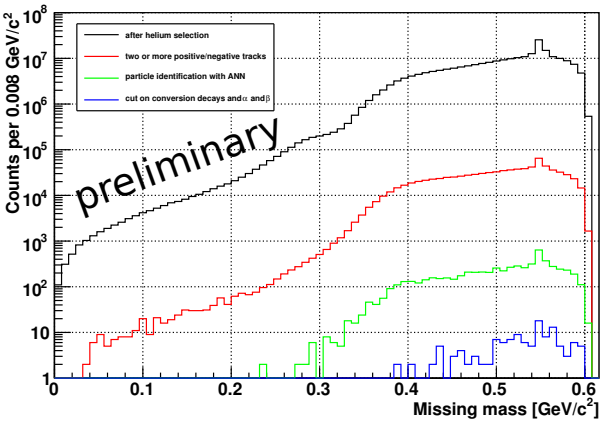

Fig. 3: Development of the ^{3}He-missing mass spectrum after different cuts.

After all these cuts and after the direct pion background subtraction, around 20 double Dalitz decay event candidates remain in the signal region around the η peak.

References:

[1] H. H. Adam et al. (WASA-at-COSY Collaboration), arXiv:nuclex/0411038 (2004)
[2] R. R. Akhmetshin et al. (CMD-2), Phys. Lett. B501 191-199 (2001), Preprint hep-ex/0012039
[3] L. Yurev (WASA-at-COSY Collaboration), Study of the decay $\eta \rightarrow e^+e^-e^+e^-$ with WASA-at-COSY, PhD thesis (2011)
[4] K. Nakamura et al. (Particle Data Group), J. Phys. G 37, 075021 (2010)
[5] R. Brun et al., ROOT - An Object Oriented Data Analysis Framework, Proceedings AIHENP'96 Workshop, Lausanne, Sep. 1996, Nucl. Inst. and Meth. in Phys. Res. A 389 81-86 (1997)

Identification of the $pn \to d\omega$ reaction at ANKE

S. Barsov[1], R. Schleichert[2], D. Chiladze[3], S. Dymov[3], A. Dzyuba[1], D. Oellers[2], S. Merzlyakov[2], S. Mikirtychyants[1,2], S. Trusov[2], C. Weidemann[2] for the ANKE collaboration.

As it was reported in [1], the experiment aimed at the determination of total and differential cross sections of the $pn \to d\omega$ reaction in the excess energy range $Q < 100$ MeV has been carried out at ANKE. The pn initial state was defined event-by-event due to the detection of a "spectator" proton (p_{sp}) emitted from the windowless deuterium cluster target. Two Silicon Tracking Telescopes (STT) were installed close to the deuterium jet to provide the momentum reconstruction for protons with kinetic energy from 2.7 MeV to 30 MeV. Since the ANKE acceptance for ω-decay products is very small, the reaction under investigation has to be identified among other $pd \to p_{sp}dX$ reactions.

Deuterons arisen from the $pn \to d\omega$ reaction within the (1.2 - 2.7) GeV/c momentum range, as well as other fast charged particles, were detected in the Forward detector consisted of 3 multiwire chambers, 17 scintillator detectors arranged in 2 layers and one layer of 16 Cherenkov counters. Having determined momenta of particles, one can separate fast deuterons from a large proton background by means energy losses in scintillators in combination with Cherenkov counter responses as presented in Fig. 1.

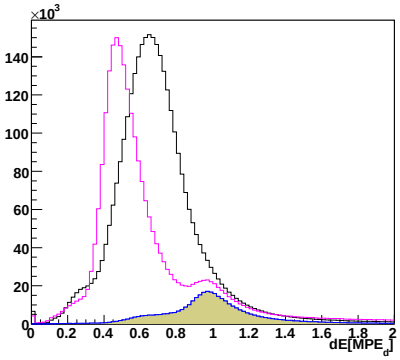

Fig. 1: Energy loss distributions of particles detected in one layer of 9 Fd scintillator detectors. The energy is presented in units of the most probable deuteron energy loss (MPE_d) which is momentum dependent. Shown in black is the initial distribution divided by the factor 5. It is dominated of the proton component. A cut on Cherenkov signal amplitudes effectively suppresses a high-momentum proton contribution and produces the distribution shown in magenta. The shadowed distribution is obtained for particles those energy losses in another scintillator layer are, in addition, restricted to the (0.8 - 1.5) MPE_d range.

Finally, particles populating the shadowed histogram in Fig. 1 within the (0.8 - 1.5) MPE_d range were accepted as deuterons. Using the method described in [2], the efficiency of deuteron separation was determined to be about 85%.

The histogram in Fig. 2 represents general features of a missing mass distribution from the $pd \to p_{sp}dX$ reaction. The large physical background from a multi-particle production is strongly peaked near the kinematical limit due to a specifics of the Fd acceptance. A clear evidence for the ω-peak can be still achieved at $Q > 60$MeV. However, at lower Q values the maximum of background continuum is shifted towards the ω mass. To determine the background shape under the ω-peak in a model-independent way, measurements were done at two proton beam energies.

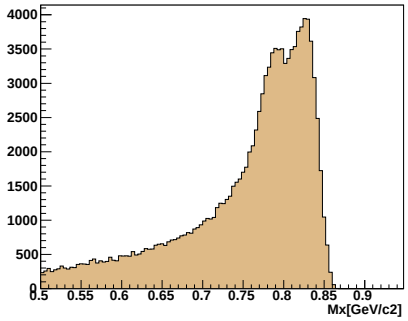

Fig. 2: The missing mass distribution of $pd \to p_{sp}dX$ reaction within the 60-80 MeV Q-range. The ω-meson is visible as the peak in vicinity of 0.783 GeV/c^2

Then, a kinematical transformation of the experimental missing mass distribution from one beam momentum to the other [3, 4] can be used as shown in Fig. 3. The same procedure was tested to be applicable for any selected Q-range. However, the extraction of ω-events was found to be affected by an overlap of the resulting peaks. A further analysis is in progress to take this into account.

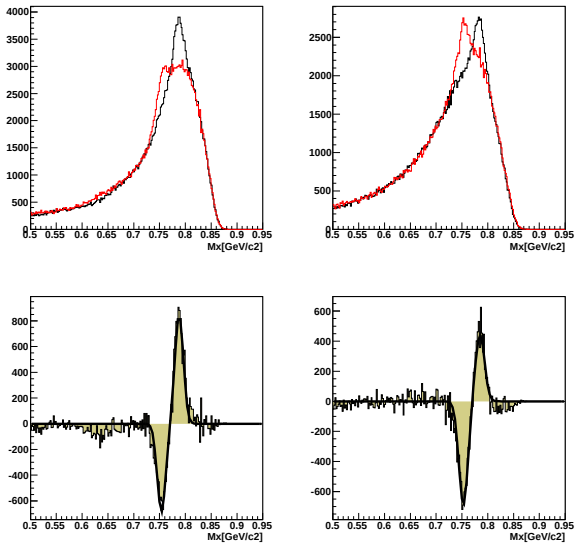

Fig. 3: Upper panels represent overall missing mass plots of the $pd \to p_{sp}dX$ reaction with p_{sp} detected either in the STT1(left side) or in the STT2(right side). Black histograms are obtained at the 2.124 GeV beam energy. The red ones are actually measured at the other beam energy of 2.219 GeV but kinematically transformed to the 2.124 GeV. The lower frames present the corresponding bin-by-bin differences of these two sets of distributions.

References:

[1] IKP Annual Report 2008, p.19
[2] I.Lehmann et al., NIM A 530, 275 (2004)
[3] F.Hibou et al., PRL 83, 492 (1999)
[4] S.Barsov et al., EPJ A 21, 521 (2004)

1 PNPI, 188350 Gatchina, Russia
2 IKP, FZ Jülich, 52425 Jülich, Germany
3 JINR, 141980 Dubna, Russia

Recent results from the charge-exchange breakup reaction $dp \to \{pp\}_s n$ study at ANKE*

D. Chiladze[1,2], D. Mchedlishvili[1,2], A. Kacharava, N. Lomidze[2], G. Macharashvili[2,3], M. Nioradze[2], H. Ströher, M. Tabidze[2], and C. Wilkin[4] for the ANKE collaboration

A good understanding of the Nucleon–Nucleon interaction still remains one of the most important goals of nuclear and hadronic physics. Apart from their intrinsic importance for the study of nuclear forces, *NN* data are necessary ingredients in the modelling of meson production and other nuclear reactions at intermediate energies. It goes without saying therefore that any facility that could make significant contributions to this important database should do so.

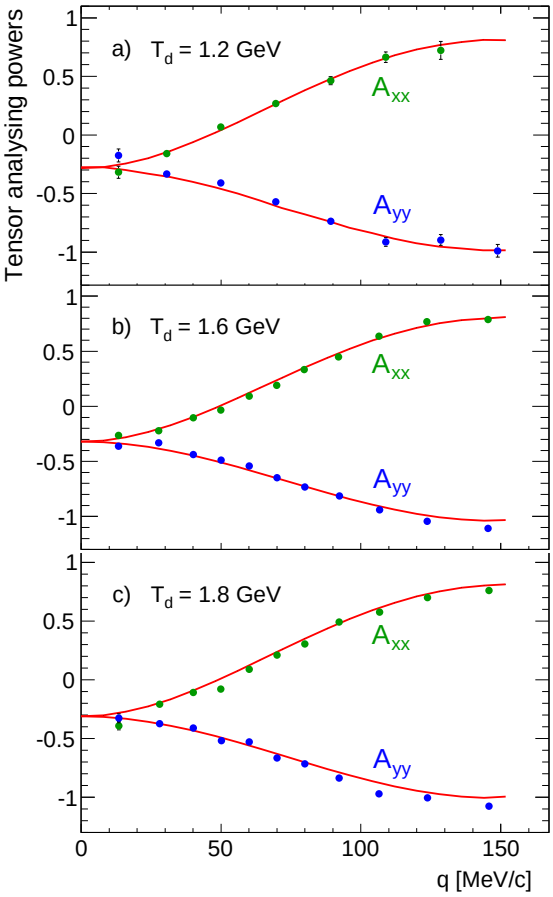

Fig. 1: Cartesian tensor analysing powers A_{xx} (green dots) and A_{yy} (blue dots) of the $dp \to \{pp\}_s n$ reaction at beam energies of $T_d = 1.2, 1.6$, and 1.8 GeV for low diproton excitation energy, $E_{pp} < 3$ MeV. The solid red curves are results of an impulse approximation calculation, where the input np amplitudes were taken from the SAID program at the appropriate energies.

The ANKE collaboration has embarked on a systematic programme to measure the differential cross section, analysing powers, and spin correlation coefficients of the $\vec{d}\vec{p} \to \{pp\}_s n$ deuteron charge–exchange breakup reaction. The aim is to deduce the energy dependence of the spin–dependent np elastic amplitudes. By selecting the two final protons with low excitation energy, typically $E_{pp} < 3$ MeV, the emerging diproton is dominantly in the $^1S_0$ state.

In impulse approximation the deuteron charge-exchange reaction can be considered as an $np \to pn$ scattering with a spectator proton. The spin dependence of the np charge-

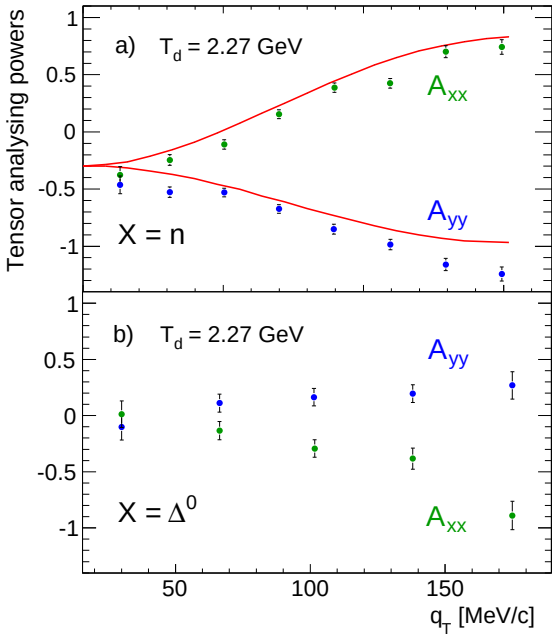

Fig. 2: Cartesian tensor analysing powers for the $dp \to \{pp\}_s X$ reaction at $T_d = 2.27$ GeV: with a neutron (a) or Δ^0 isobar (b) in the final state. In the Δ case the variable used is the transverse momentum transfer q_T. The red solid lines for the neutron are the results of an impulse approximation calculation.

exchange amplitude in the cm system can be displayed in terms of five scalar amplitudes as:

$$\begin{aligned} f_{np} &= \alpha(q) + i\gamma(q)(\vec{\sigma}_1 + \vec{\sigma}_2)\cdot\vec{n} + \beta(q)(\vec{\sigma}_1\cdot\vec{n})(\vec{\sigma}_2\cdot\vec{n}) \\ &\quad + \delta(q)(\vec{\sigma}_1\cdot\vec{m})(\vec{\sigma}_2\cdot\vec{m}) + \varepsilon(q)(\vec{\sigma}_1\cdot\vec{l})(\vec{\sigma}_2\cdot\vec{l}), \end{aligned}$$

where α is the spin–independent amplitude between the initial neutron and final proton, γ is a spin–orbit contribution, and β, δ, and ε are spin–spin terms. In the $^1S_0$ limit of the impulse approximation, the $\vec{d}\vec{p} \to \{pp\}_s n$ observables are directly related to the np spin–dependent amplitudes through:

$$\begin{aligned} \frac{d^4\sigma}{dt\,d^3k} &= \tfrac{1}{3} I \left\{ S^-(k, \tfrac{1}{2}q) \right\}^2, \\ I &= |\beta|^2 + |\gamma|^2 + |\varepsilon|^2 + |\delta|^2 R^2, \\ I A_y^d &= 0, \; I A_y^p = -2\mathrm{Im}(\beta^*\gamma), \\ I A_{xx} &= |\beta|^2 + |\gamma|^2 + |\varepsilon|^2 - 2|\delta|^2 R^2, \\ I A_{yy} &= |\delta|^2 R^2 + |\varepsilon|^2 - 2|\beta|^2 - 2|\gamma|^2, \\ I C_{y,y} &= -2\mathrm{Re}(\varepsilon^*\delta) R, \; I C_{x,x} = -2\mathrm{Re}(\varepsilon^*\beta), \end{aligned}$$

where $R = \left\{ S^+(k, \frac{1}{2}q) / S^-(k, \frac{1}{2}q) \right\}^2$ and $S^\pm$ are form factors that can be evaluated using low energy *NN* information. Here $\vec{k}$ is the pp relative momentum in the diproton and $\vec{q}$ the momentum transfer between the deuteron and diproton.

Although corrections due to final *P*- and higher pp waves have to be taken into account in the detailed analysis, it is clear that in the low E_{pp} limit a measurement of the differential cross section, A_{xx}, and A_{yy} would allow the extraction of $|\beta(q)|^2 + |\gamma(q)|^2$, $|\delta(q)|^2$, and $|\varepsilon(q)|^2$ over a range of values of q.

For the above to be the realistic objectives, the methodology has to be checked in energy regions where the np amplitudes are reasonably well known. An extended paper (*D. Chiladze et al., Eur. Phys. J. A 40 (2009) 23*) has recently been published with this in mind. The new ANKE results for the deuteron Cartesian tensor analysing powers A_{xx} and A_{yy} at three beam energies are shown in Fig. 1 as functions of the momentum transfer. The agreement between the experimental data and the impulse approximation predictions obtained using the reliable SAID np amplitudes as input at T_n = 600, 800, and 900 MeV, is very encouraging. This success provides a motivation for repeating these measurements at higher energies where the np input is far less certain.

The maximum deuteron energy available at COSY is $T_d \approx$ 2.3 GeV (1.15 GeV per nucleon) and the ANKE results for A_{xx} and A_{yy} near this energy are shown in Fig. 2a. The neutron–proton amplitudes are here not as well known and the deviations of the data from the predicted curves strongly suggest that there are deficiencies in the SAID values of the np amplitudes in this region.

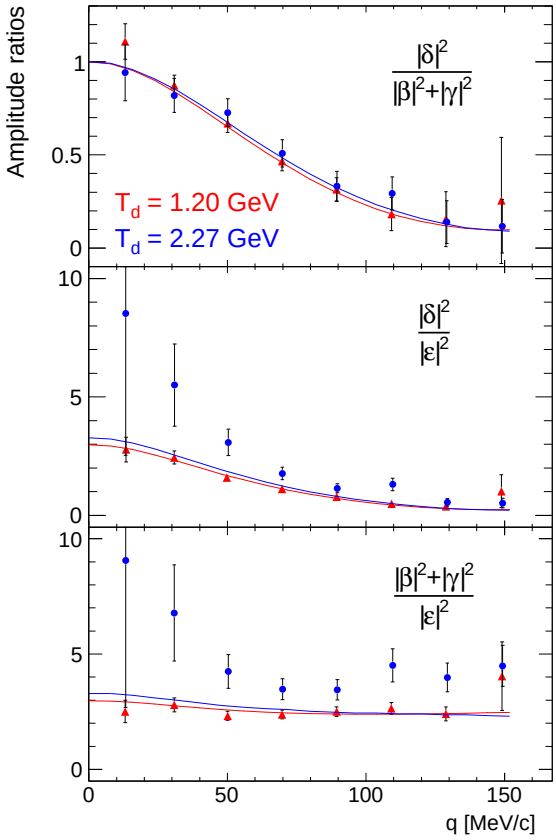

Fig. 3: Measured observable ratios as functions of q for two different beam energies. Solid lines are impulse approximation predictions.

The deficiencies of the SAID input np amplitudes at 1.135 GeV can be shown more explicitly by forming the following combinations of the observables:

$$\begin{aligned}(1-A_{yy})/(1+A_{xx}+A_{yy}) &\approx (|\beta|^2+|\gamma|^2)/|\varepsilon|^2\,,\\ (1-A_{xx})/(1+A_{xx}+A_{yy}) &\approx |\delta|^2/|\varepsilon|^2\,,\\ (1-A_{xx})/(1-A_{yy}) &\approx |\delta|^2/(|\beta|^2+|\gamma|^2)\,.\end{aligned}$$

The variation of these quantities with q are presented in Fig. 3 for the 1.2 and 2.27 GeV data. Whereas at the lower energy all the ratios are well described by the model, at the higher it is seen that it is only $|\delta|^2/(|\beta|^2+|\gamma|^2$ which is well understood. It seems that the SAID program currently overestimates the values of $|\varepsilon|$ at small q. This will become clearer when absolute values of the cross sections are extracted at 2.27 GeV.

The final goal is to go to even higher energies by using a proton beam (available up to 3 GeV at COSY) incident on a polarised deuterium target, $pd \to \{pp\}_s n$. This could be very fruitful because so little is known about the spin dependence of the np charge exchange reaction much above 1 GeV.

In order to determine the relative phases of the spin-spin amplitudes $(\beta, \delta, \varepsilon)$ it is necessary to determine the spin correlation parameters $C_{x,x}$ and $C_{y,y}$. A large amount of data was successfully obtained from the first double–polarised neutron–proton scattering experiment at ANKE (*cf.* Annual Report 2009). The *preliminary* results for the vector-vector spin correlation coefficients in the $\vec{d}\vec{p} \to \{pp\}_s n$ reaction at T_d = 1.2 GeV are shown in Fig 4, where they are seen to be in satisfactory agreement with impulse approximation predictions. The analysis of the higher energy data is in progress.

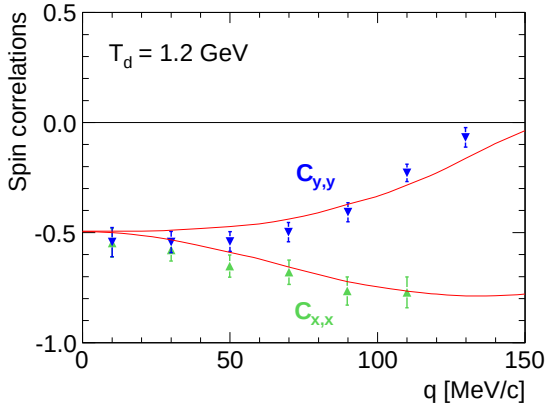

Fig. 4: Vector spin–correlation coefficients in $\vec{d}\vec{p} \to \{pp\}_s n$ reaction at $T_d = 1.2$ GeV. The red curves are the predictions of the impulse approximation calculation.

It was shown at Saclay that at $T_d = 2$ GeV the $\Delta(1232)$ isobar can be excited in the $\vec{d}p \to \{pp\}_s \Delta^0$ reaction and substantial tensor analysing powers were measured. In impulse approximation, these are also sensitive to a spin–transfer from the neutron to the proton in $np \to p\Delta^0$. The Δ^0 is seen clearly also in the ANKE charge-exchange breakup data at 1.6, 1.8, and 2.27 GeV. The values of A_{xx} and A_{yy} deduced at 2.27 GeV and shown in Fig. 2b are very different to those measured for the 'normal' neutron breakup with even changes of the signs. ANKE will therefore also provide useful information on the spin structure of Δ excitation in neutron–proton collisions.

[1] IKP FZJ, 52425 Jülich, Germany
[2] HEPI, TSU, 0186 Tbilisi, Georgia
[3] LNP, JINR, 141980 Dubna, Russia
[4] Phys. and Astronomy Dep., UCL, London, WC1E 6BT, UK

* Supported by COSY FFE program and GNSF grant No. ST09-1024-4-200.

Vector analyzing power of the $\vec{p}p \to \{pp\}_s\pi^0$ reaction at intermediate energies at ANKE/COSY*

D. Tsirkov[1,2], S. Dymov[1,3], V. Komarov[1], A. Kulikov[1], G. Macharashvili[1,4] for the ANKE collaboration

A successful ChPT analysis of the $NN \to NN\pi$ processes involving relatively high momentum transfers has only been developed in recent years [1]. The theory involves a contribution in the effective chiral Lagrangian from a so–called $(\bar{N}N)^2\pi$ contact operator, the strength of which is denoted by a low energy contact parameter d, which must be determined from experimental data. A ChPT analysis is currently focused on a set of experimental data for $pn \to \{pp\}_s\pi^-$ reaction at 353 MeV, however, the contaminations in these processes from pion d–waves are not yet included [1]. Though $(\bar{N}N)^2\pi$ does not contribute to the $pp \to \{pp\}_s\pi^0$ amplitude, the π^0 production data will provide information on the pion d–waves. It was one of the main aims for the present A_y measurement at 353 MeV.

At higher energies, in the $\Delta(1232)$ resonance region, the reaction $pp \to \{pp\}_s\pi^0$ was studied for the first time at ANKE [2]. The experiment revealed a wide peak in the energy dependence of the cross section at small angles. A consistent picture of the process is still lacking, so we have performed measurements of the cross section and A_y in the energy region 500–700 MeV where the forward cross section is maximal.

Measurements were performed in April 2009 with the ANKE spectrometer [3] at COSY-Jülich. The transversely polarized proton beam, with energies $T_p = 353$, 500, 550 and 700 MeV, interacted with the hydrogen cluster-jet target. The setup and procedure for data handling are described in detail in [2].

To start to identify the $pp \to \{pp\}_s\pi^0$ reaction, proton pairs were selected from all the registered two–track events, using the measured momenta of the both particles and their time-of-flight difference [4]. Then we applied the cut $E_{pp} < 3$ MeV to identify pairs where the $^1S_0$ state dominates.

We can reconstruct the kinematics of the $pp \to \{pp\}_sX$ process event–by–event and obtain a missing–mass spectrum. The main sources of the background are random coincidences and a signal from the $pp \to \{pp\}_s\gamma$ channel. To find the numbers of $\{pp\}_s\pi^0$ events, we fitted the M_X^2 distributions by the sum of a linear accidental background and simulated peak shapes for γ and π^0 [4]. The polarization asymmetry is given by

$$\varepsilon = \frac{N_\uparrow/L_\uparrow - N_\downarrow/L_\downarrow}{N_\uparrow/L_\uparrow + N_\downarrow/L_\downarrow}\,.$$

The analyzing power A_y is connected to it through:

$$A_y = \frac{\varepsilon}{P\,\langle\cos\phi_{pp}^{\rm cm}\rangle}\,.$$

Since the $\cos\phi_{pp}^{\rm cm}$ acceptance is concentrated near 1, essentially all the statistics collected effectively contribute to A_y.

The polarization P of the beam was evaluated using the $pp \to pp$ and $pp \to d\pi^+$ reactions detected in parallel. The two methods agreed within measurement errors and resulted in an average $P = 0.67 \pm 0.01$.

In 353 MeV case, if only waves up to $\ell = 2$ are retained, A_y must originate from a Ss:Sd interference. The cross section can be described with $a + b\cos^2\theta_{pp}^{\rm cm}$ [8]. Interpolating the CELSIUS data [5] gives the values of $a = 204\pm10$ nb/sr and $b = -112\pm23$ nb/sr. Then fitting the A_y distribution with

$$A_y = \frac{c\sin 2\theta_{pp}^{\rm cm}}{a + b\cos^2\theta_{pp}^{\rm cm}}\ [8]$$

leads to $c = 48\pm4$ nb/sr. When the results of the full model [1] are available, the current data will provide a valuable test of the theoretical approach.

In the $\Delta(1232)$ region, the small angle predictions of the Niskanen model [7] approach the data at 500 MeV but are in full disagreement at 700 MeV. The reason for the disagreement in respect of both the cross section [2, 6] and analyzing power is unclear.

In order to improve the results, the setup geometry will be defined more precisely, reducing the angular uncertainty at 353 MeV from 5° to ≈ 2°. The systematic uncertainties will also be reduced by applying more precise dead-time and luminosity corrections.

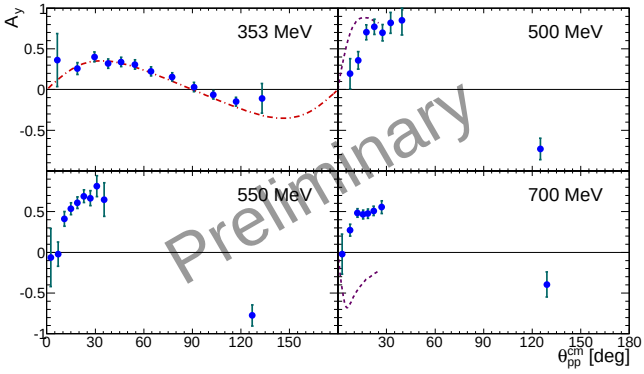

Fig. 1: Preliminary values of A_y for the $\vec{p}p \to \{pp\}_s\pi^0$ reaction at all the measured energies. The errors shown are purely statistical; the overall systematic uncertainty from the beam polarization and luminosity is about 3%. The angular uncertainty is about 5° near 90° at 353 MeV and less than 1.5° at other energies. The dash-dotted line represents the fit using CELSIUS data for the cross section [5]. The dashed line corresponds to the predictions by Niskanen [6, 7].

References:

[1] V. Baru *et al.*, Phys. Rev. C **80** 044003 (2009).
[2] V. Kurbatov *et al.*, Phys. Lett. B **661** 22 (2008).
[3] S. Barsov *et al.*, Nucl. Instrum. Methods Phys. Res. A **462** 354 (2001).
[4] D. Tsirkov *et al.*, J. Phys. G **37** 105005 (2010).
[5] R. Bilger *et al.*, Nucl. Phys. A **693** 633 (2001).
[6] J. A. Niskanen, Phys. Lett. B **642** 34 (2006).
[7] J. A. Niskanen, private communication (2008).
[8] C. Hanhart, Phys. Rep. **397** 155 (2004).

[1] LNP JINR, RU-141980 Dubna, Russia
[2] IKP FZJ, D-52425 Jülich, Germany
[3] Phys. Inst. II, UEN, D-91058 Erlangen, Germany
[4] HEPI TSU, GE-0186 Tbilisi, Georgia
* supported by COSY-FFE

Analysis of the $pd \to pp_{(STT)} + X$ reaction at 353 MeV using ANKE STT's*

N. Lomidze[1], G. Macharashvili[1,2], and M. Tabidze[1] for the ANKE/PAX collaboration

In this note preliminary results of the analysis of experimental data of the April 2009 beamtime are presented. In the experiment 2 STT's (left and right) have been used with layer thicknesses of: 70 μm (I) and 300μm (II).

For the analysis the root files containing a list of 2-dimensional hits in layers were chosen. The tracks were reconstructed using the hit list and the following information about each track was reorded: the energy deposit in the first and second layer, the polar(θ) and azimuthal(ϕ) angles, Y and Z coordinates at $X = 0$. The data for 11 runs (from 17434 to 17445) was analysed. The total number of the events was equal to 9 908 692. Among them the number of one-track events was 9 529 546 (96.2 %), of two-track event - 358 258 (3.6%)and more then two - 20 888 (0.2 %) (Fig. 1).

For the selection of the deuteron breakup reaction $pd \to ppn$, the particle identification parameter ($pid = (dE_1 + dE_2)^{1.62} - dE_2^{1.62}$) was used and the distance between two straight line in space, which was calculated by the formula:

$$distance = \frac{|det|}{\sqrt{(det_1^2 + det_2^2 + det_3^2)}} \qquad (1)$$

where:

$$det = \begin{vmatrix} X_2 - X_1 & Y_2 - Y_1 & Z_2 - Z_1 \\ \sin(\theta_1)cos(\phi_1) & \sin(\theta_1)sin(\phi_1) & \cos(\theta_1) \\ \sin(\theta_2)cos(\phi_2) & \sin(\theta_2)sin(\phi_2) & \cos(\theta_1) \end{vmatrix} \qquad (2)$$

$$det_1 = \begin{vmatrix} \sin(\theta_1)sin(\phi_1) & \cos(\theta_1) \\ \sin(\theta_2)sin(\phi_2) & \cos(\theta_2) \end{vmatrix} \qquad (3)$$

$$det_2 = \begin{vmatrix} \cos(\theta_1) & \sin(\theta_1)cos(\phi_1) \\ \cos(\theta_2) & \sin(\theta_2)cos(\phi_2) \end{vmatrix} \qquad (4)$$

$$det_3 = \begin{vmatrix} \sin(\theta_1)cos(\phi_1) & \sin(\theta_1)sin(\phi_1) \\ \sin(\theta_2)cos(\phi_2) & \sin(\theta_2)sin(\phi_2) \end{vmatrix} \qquad (5)$$

In Fig. 2 the distribution of the pid parameter for events in which 2 tracks were detected in the STT-s are presented (upper left panel). For the further analysis we chose the tracks which had $4.0 < pid < 5.5$. The distribution of the missing mass for such events is presented in Fig. 2 (upper right panel). In the area of the mass of the neutron is a concentration of events. This suggests that we can see breakup reactions.

The distribution of the distance between the two tracks in space is presented in Fig. 2 (lower left panel). For the further analysis we chose the tracks which had $distance < 5\ mm$. The distribution of the missing mass for remainig events is presented in Fig.2 (lower right panel). In Fig. 3 (upper panel) the distribution of the missing mass for the events in which both tracks were detected in same STT (blue histogram) and for events in which both tracks were detected in different STT (red histogram), are presented. They differ greatly from each other. The reason for this difference is not clear and requires further study.

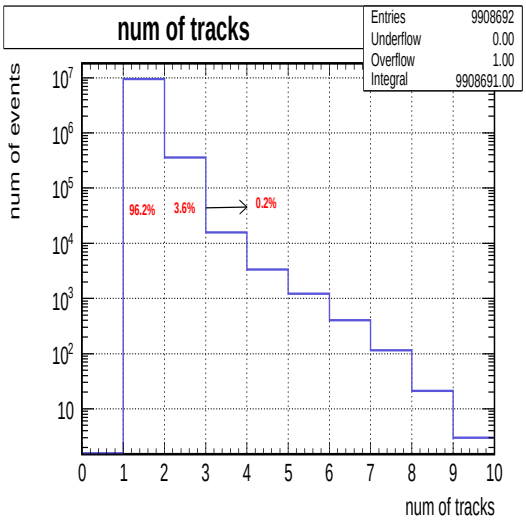

Fig. 1: The distribution of number of tracks in event

To isolate the $pd \to pd$ elastic scattering reaction, events with one track were chosen. This track was detected in one of the STT's. For this track $pid > 6.0$ (deuteron) was used. The distribution of the missing mass for such events is presented in Fig. 3 (lower panel). In the area of the mass of the proton is a concentration of events. This suggests that we can see the elastic scattering reaction.

Next step is: to prepare analysis code using the Neural Network (NN) method, developed by G. Macharashvili.

[1] HEPI, TSU, 0186 Tbilisi, Georgia
[2] LNP, JINR, 141980 Dubna, Russia

* Supported by DFG grants (436 RUS 113/964/0-1, 436 RUS 113/965/0-1) and GNSF grant (No. ST09-1024-4-200).

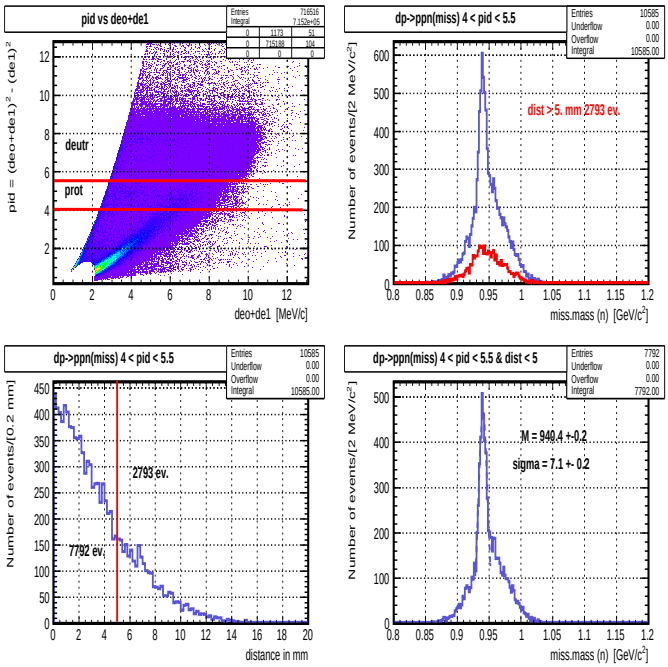

Fig. 2: Upper left panel: the two dimensional distribution *pid* vs $dE_1 + dE_2$, upper right panel: the distribution by the missing mass for events with $4.0 < pid < 5.5$ (blue) and for the events with the additional cut - $distance > 5.0$ mm, lower left panel: the distribution of the distance, lower right panel: the distribution of the missing mass after $4.0 < pid < 5.5$ and $distance < 5.0$ mm cuts

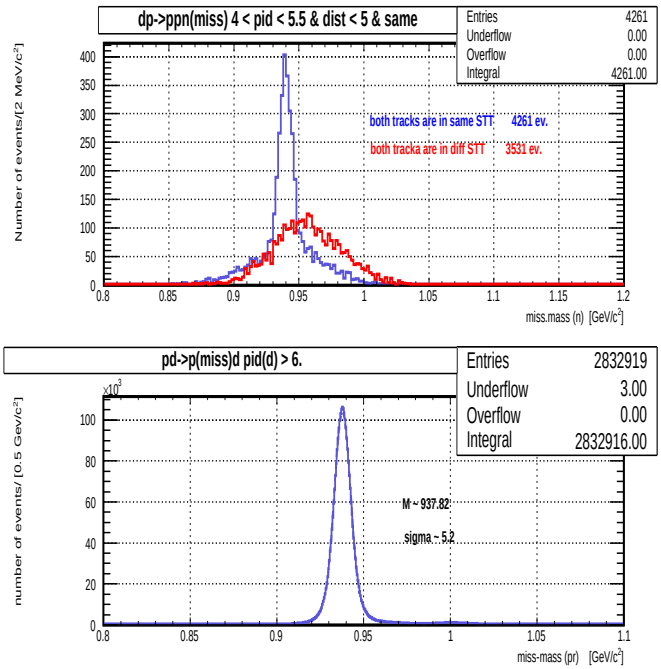

Fig. 3: Upper panel: the two-track events distribution of the missing mass in case when both track are in the same STT (blue) and in case when they are in the different STT (red), lower panel: the one-track events distribution of the missing (proton) mass in case when $pid > 6.0$ (deuterons stopped)

Neural Network Application for Proton Kinetic Energy Reconstruction in ANKE STT*

N. Lomidze[a], G. Macharashvili[a,b] and M. Tabidze[a]
for the ANKE/PAX Collaboration

In this note the procedure of proton/deuteron separation and proton kinetic energy reconstruction in the ANKE silicon detectors using the Neural Network (NN) method, as well as the preliminary results are presented. For this aim we have used the simulated proton tracks (100000) from the pd-elastic and deuteron breakup process at $T_p = 49.3$ MeV, detected in the first (I) and second (II) silicon layers with thickness of 300 μm (ANKE type STT). The process was simulated using the GENBOD event generator and the GEANT3 framework (MC) for the ANKE Feb'08 setup. During the simulation, all GEANT flags for the secondary interaction was set to 0 (switched OFF).

As an input variables for the NN method we have chosen the energy deposit in each silicon layer (smeared by Gaussian with $\sigma = 100$ KeV as an intrinsic resolution) and the track path length, wich was estimated using layer thickness and track polar (θ) and azimuthal (ϕ) angles. In our opinion superior of choosing the path length is, since the energy deposit in the layers directly depends on this variable. On the other hand, in case of different layer (I and II) thicknesses, track angles θ and ϕ are the same while the estimated path lengths are different and it is extra information for NN input.

In case proton/deuteron separation the output variable for the NN was *Particle type*, which is equal to 1 for deuterons, and to 0 for protons. The results from the NN procedure (the back-propagation learning method with $E_{poch} = 500$ and *hyperbolic tangent* function has been used) are presented on Fig. 1. Half of the whole statistics was used for the training (learning) procedure and half - for the testing procedure. From the lower panel distributions it is clear, that using the NN method we can separate with high (99%) accuracy deuterons and protons.

In case of proton kinetic energy reconstruction the task has been performed in two steps. At first, we have determined over them if the protons was stopped in second (II) layer or not. As an input for the NN method, we have chosen the same variables as was described above. The output variable for NN method was the *status* of protons, which is equal to 0 for stopped protons, and to 1 for passed ones. The results from the NN procedure with $E_{poch} = 500$ are presented on Fig. 2. From the lower panel distributions we see, that using the NN method we can distinguish with high accuracy whether, a proton was stopped ($NNstatus < 0.3$) or passed ($NNstatus > 0.6$) the second layer. Efficiency (contamination) of each cut is 95.6% (3.4%) and 98.0% (0.6%) respectively. The same procedure, but using a *sigmoid* instead of the *hyperbolic tangent* function also was tested, but no significant improvement has observed.

For stopped protons the kinetic energy equals the sum of energy deposits in I and II layer. For passed protons the kinetic energy reconstruction is necessary. For this task special simulations were performed: single proton tracks were simulated with uniformly θ and ϕ inside I and II layer acceptance and uniform momentum in the range of 20-240 MeV/c. For track transporting GEANT4 framework was used.

For NN input the same variables as described above where used, while as output variable the proton kinetic energy has been taken. The results from NN procedure with $E_{poch} = 500$ are presented in Fig. 3. From lower left panel we see, that using this method we can reconstruct the proton kinetic energy in a wide energy range with less than 5% accuracy. For $T_p = 40$ MeV NN results are practically the same.

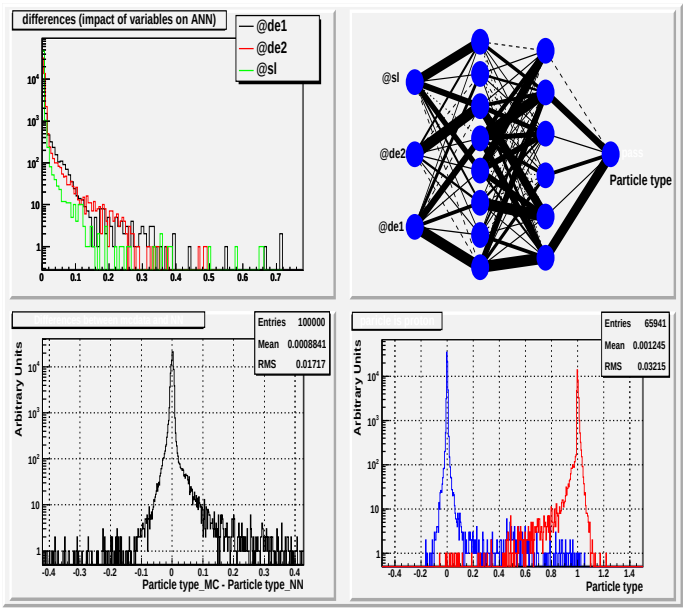

Fig. 1: Neural Network method application for the particle type determination: *upper left panel:* Impact of the input variables on NN method; *upper right panel:* NN structure; *lower left panel:* The differences in 'Particle type' variable between input (MC data) and output (NN data); *lower right panel:* Particle type NN output, blue line corresponds to protons, red line - deuterons.

[a] HEPI, TSU, 0186 Tbilisi, Georgia.
[b] LNP, JINR, 141980 Dubna, Russia.

* Supported by DFG (436 RUS 113/964/0-1; 436 RUS 113/965/0-1) and GNSF (ST09-1024-4-200) grants.

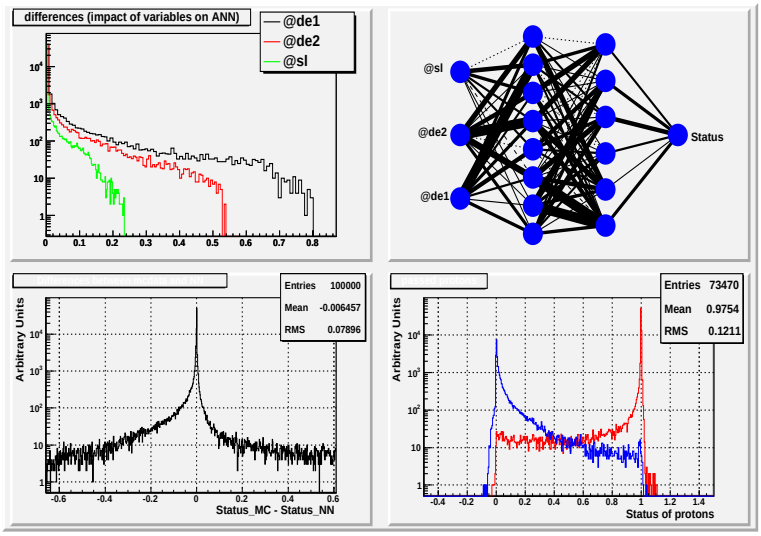

Fig. 2: Neural Network method application for the proton status determination: *upper left panel:* Impact of the input variables on NN method; *upper right panel:* NN structure; *lower left panel:* The differences in 'Status' variable between input (MC data) and output (NN data); *lower right panel:* Status of NN output, blue line corresponds to stopped protons, red line - passed ones.

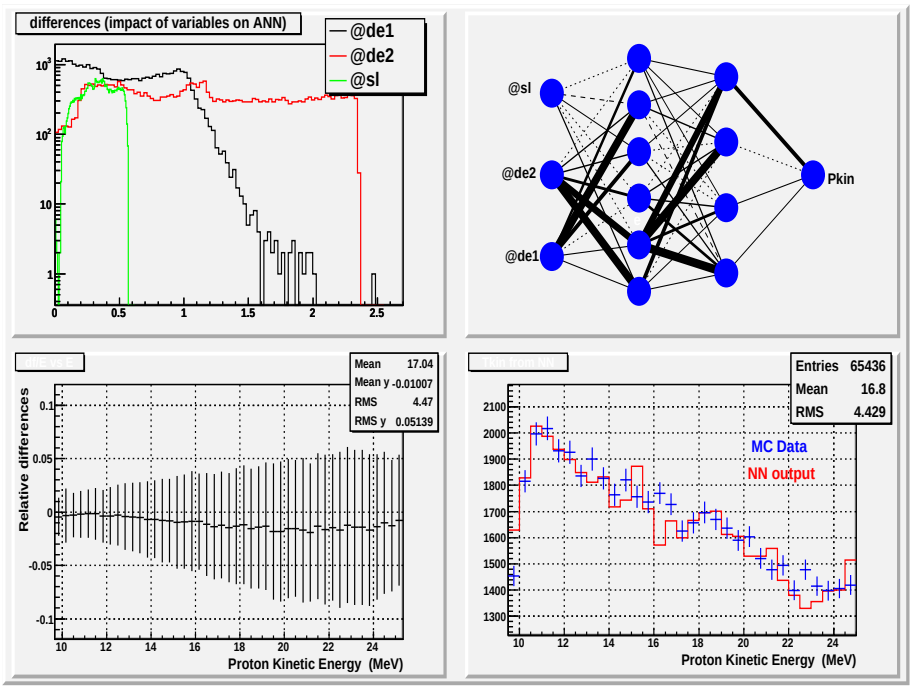

Fig. 3: Neural Network method application for proton kinetic energy determination: *upper left panel:* Impact of the input variables on NN method; *upper right panel:* NN structure; *lower left panel:* The profile histogram for relative differences between proton kinetic energy and reconstructed one; *lower right panel:* The proton kinetic energy, blue line corresponds for MC input, red line - NN output.

Formation of the $^1S_0$ diproton in the reaction $pp \to \{pp\}_s\pi^0$ in the Δ isobar region

O.Imambekov and Yu. Uzikov

The reactions with the diproton $pp(^1S_0)$ in the final or initial state can give more insight onto the short-range dynamics of the reaction and the nucleon-nucleon interaction in addition to the corresponding reactions with the deuteron. Indeed, the contribution of non-short range mechanisms related to excitation of the Δ-isobars in intermediate states of the considered reactions is expected to be considerably suppressed for the case of the diproton (or the spin-singlet deuteron), as compared to the deuteron case due to isospin symmetry and conservation of angular momentum and parity [1, 2].

According to ANKE-COSY measurements [3], the cross section of the reaction $pp \to \{pp\}_s\pi^0$, where $\{pp\}_s$ is the proton pair in the $^1S_0$ state at small excitation energy $E_{pp} < 3$ MeV, demonstrates a clear bump at beam energy $\sim 0.6-0.7$ GeV for the cms diproton scattering angle $\theta_{cm} = 0^\circ$. The microscopical model [4], which includes $\Delta(1232)$-isobar excitation via coupled channel and the s-wave πN-rescattering and successfully applied to the $pp \to d\pi^+$ reaction, fails to describe the data [3]. In view of this failure, a more simpler approach that is the one pion exchange model (OPE) which includes the on-mass-shell subprocesses $\pi^0 p \to \pi^0 p$ and accounts for the final state pp-interaction, was used in theoretical analysis of this reaction [5]. It was found that the OPE model fairly well explains the shape of the observed bump and suggests that it is related the $\Delta(1232)$ isobar excitation [5].

Here we present results of calculations [6] performed using the box diagram (Fig. 1) with explicite consideration of the Δ-isobar. The direct term (Fig. 1a) can be written as

$$A^{dir}_{\sigma_1\sigma_2} = -8m_p^2 m_\Delta \left(\frac{f_{\pi NN}}{m_\pi}\right)\left(\frac{f_{\pi N\Delta}}{m_\pi}\right)^2 \int \frac{d^3q}{(2\pi)^3} \frac{4\pi f(q,k_{pp};E_{pp})}{k_{pp}^2 - \mathbf{q}^2 + i\varepsilon} \frac{F_{\pi NN}(t)}{m_\pi^2 - t - i\varepsilon} \frac{F_{\pi N\Delta}(t)}{m_\Delta^2 - P_\Delta^2 - i m_\Delta \Gamma} \Re_{\sigma_1\sigma_2}(\mathbf{k},\mathbf{k}',\mathbf{Q}), \quad (1)$$

where $f(q,k_{pp};E_{pp})$ is the half-off-shell amplitude of the pp-scattering in the $^1S_0$ state at on-shell momentum $k_{pp} = \sqrt{E_{pp}m_p}$, $t = k_\pi^2$ is the squared 4-momentum of the intermediate pion, P_Δ, m_Δ and Γ_Δ are the 4-momentum, mass and the full energy-dependent width of the Δ-isobar, respectively; $f_{\pi NN}$ and $F_{\pi NN}$ are the πNN coupling constant and the πNN form factor, respectively; ${f^2}_{\pi NN}/4\pi = 0.0796$, $F_{\pi NN}(k^2{}_\pi) = \frac{\Lambda^2 - m^2{}_\pi}{\Lambda^2 - k^2{}_\pi}$; $f_{\pi N\Delta} = 2.15$ is the $\pi N\Delta$ coupling constant; the 3-momentum $\mathbf{Q}$ is determined by the πNN vertex, the spin-tensor $\Re_{\sigma_1\sigma_2}$ is related to the amplitude of the subprocess $\pi^0 p \to \Delta \to \pi^0 p$ and depends on the spin-projections of the intial protons σ_i and 3-momenta of the intermediate ($\mathbf{k}$) and final ($\mathbf{k}'$) π-mesons.

One can see from Fig. 2 that an explicite consideration of the Δ-isobar contribution within the box-diagram model is less succesfull in explanation of the data [3] than the OPE model [5, 6]. We found that neither energy and angular dependencies of the cross section are reproduced. However, for energy dependence the agreement becomes better if the Δ-propagator is taken off the loop integral. In this approximation the box-diagram is close to the OPE model and provides a similar agreement with the data.

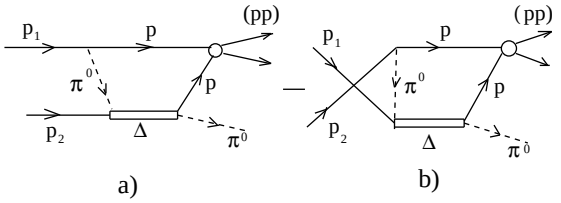

Fig. 1: The box-diagrams of the Δ mechanism: direct (a) and exchange (b) terms.

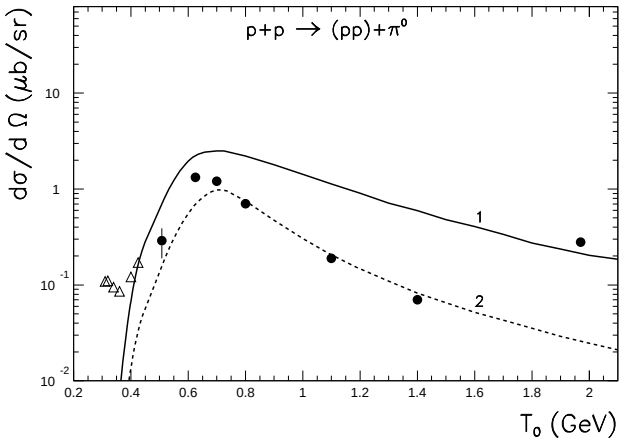

Fig. 2: The forward differential cross section of the reaction $pp \to \{pp\}_s\pi^0$ versus the beam energy. The curves show the box-diagram calculations with the Δ-propagator being under the loop integral (1) and outside the integral (2). The curve 2 is multiplied by the factor 0.2. Data (•) are taken from Ref. [3].

Very similar result we have got when applying the box diagram to the $pp \to d\pi^+$ reaction at beam energies 0.5-1.5 GeV.

References:

[1] O. Imambekov, Yu.N. Uzikov, Yad. Fiz. 52 (1990) 1361

[2] Yu.N. Uzikov, Pis'ma v ZHETF, **75** (2002) 7.

[3] V. Kurbatov et al., Phys. Lett. **B 661**, (2008) 22.

[4] J.A. Niskanen, Phys. Lett. **B 642**, (2006) 34.

[5] Yu.N. Uzikov, in Proc: 19th International Baldin Seminar on High Energy Physics Problem, (September, 2008, Dubna), Eds. A.N. Sissakian et al. (JINR, Dubna, Russia, 2008), v. 2 p. 307; arXiv:0803.2342 [nucl-th]

[6] O.Imambekov, Yu.N. Uzikov: In proc. of XX Int. Baldin Seminar on High Energy Physics Problem (September, 2010, Dubna) (in press).

* Joint Institute for Nuclear Researches, Moscow reg., Dubna, Russian Federation

Acceptance studies for the $pp \rightarrow nK^+\Sigma^+$ reaction at COSY-TOF

Paweł Klaja[a] for the COSY-TOF collaboration

The COSY-TOF detector setup was recently upgraded with a new tracking system [1]. A high statistics measurement with this setup in August 2010 was dedicated to hyperon production with a polarized proton beam of 2.95 GeV/c momentum. The main goal of this experiment was to measure the spin triplet component of the $p\Lambda$ scattering length, the spin transfer coefficient of the $pp \rightarrow pK^+\Lambda$ reaction and the investigation of N^* resonances.
In addition the $pp \rightarrow nK^+\Sigma^+$ reaction can be studied at an excess energy of Q = 128.7 MeV. Beside the straw tube tracker (STT), the silicon quirl telescope (SQT) [2] and the calorimeter are essential for the measurement of the $pp \rightarrow nK^+\Sigma^+$ reaction being performed. The schematic drawing of two plane quirl-like SQT with example of two hit event is presented in the left panel of Figure 1. The scheme of 84 block calorimeter detector is shown in the right panel of this figure.

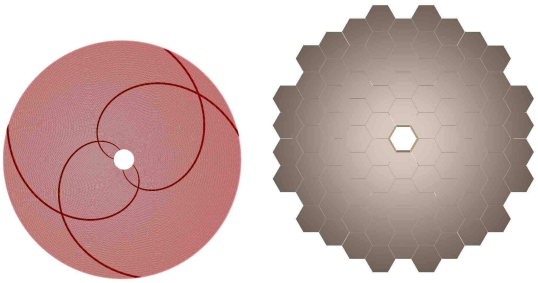

Fig. 1: Detector front views. **(left)** Silicon quirl telescope (SQT). **(right)** Calorimeter. Note different dimensions of both detectors, diameters of 7.0 cm for SQT and 142.1 cm for the calorimeter, respectively.

All particles in exit channel can be measured. The kaon track can be reconstructed using the straw detector and the neutron track can be fitted as a line from the target to the calorimeter block. For the Σ^+ hyperons one can use the SQT detector. Since the distance between target and SQT is 2.57 cm one can divide the data into two parts according to the range of the Σ^+. First, when the Σ^+ is registered in the SQT, the neutron hits calorimeter and the K^+ meson track is reconstructed with the straw tube tracker. The second scenario differs by the Σ^+ decaying before the SQT and thus the hyperon is no longer registered in the detectors. In this case, one can look for an additional charged track in the STT which does not point to the target. This could be a π^+ meson originating from the decay $\Sigma^+ \rightarrow n\pi^+$.
Monte Carlo simulations of the $pp \rightarrow nK^+\Sigma^+$ reaction were performed in order to check the acceptance of the detector setup. As it was mentioned earlier not all hyperons reach the SQT detector. In order to check the fraction of simulated particles which could be measured, the laboratory range the Σ^+ was determined. The Σ^+ range distribution is presented in the left panel of Figure 2. The dashed line corresponds to the SQT position at 2.57 cm from the target.
Hit coordinates in the silicon quirl telescope were calculated for those Σ^+ hyperons which reached the SQT. The resulting Σ^+ hit distribution is shown in the right panel of Figure 2.

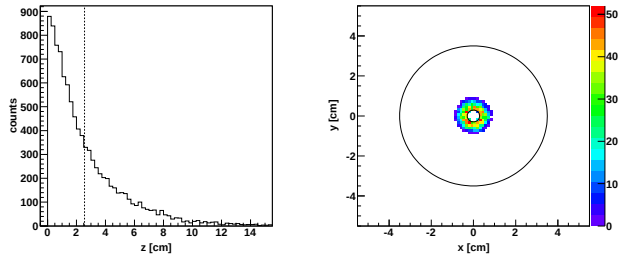

Fig. 2: **(left)** Σ^+ range in the laboratory. The vertical dashed line corresponds to the z-position of the silicon quirl telescope. **(right)** x-y hit position distribution in the silicon quirl telescope. Circles visualize the dimensions of the SQT, the inner and outer radii are equal to 0.3 cm and 3.5 cm, respectively.

Around 30% is lost due to the hole in the center of the detector.
The angular acceptance of the calorimeter for neutrons was studied since the detection of neutrons is crucial for the identification of the $pp \rightarrow nK^+\Sigma^+$ reaction. The left panel of Figure 3 shows the simulated primary neutron polar angle distribution. As it can be noticed only 30% of the neurons can be measured due to the 10° polar angle coverage of the calorimeter.

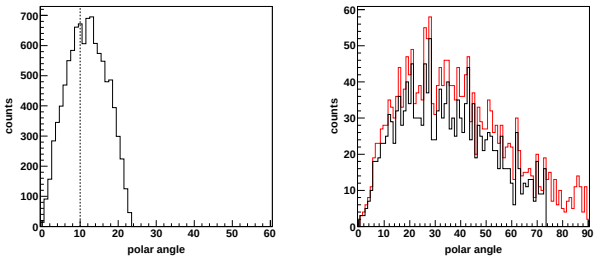

Fig. 3: **(left)** Primary neutron polar angle distribution. Vertical dashed line shows maximal polar angle coverage of calorimeter. **(right)** Decay charged pion ($\Sigma^+ \rightarrow n\pi^+$) polar angle distribution. Red histogram depicts all generated pions, black one shows only those which reach stop detectors.

Also, the posibility to measure the π^+ mesons produced in the Σ^+ decay to n and π^+ was determined. The charged pion ($\Sigma^+ \rightarrow n\pi^+$) polar angle distribution is presented in the right panel of Figure 3. The black histogram represents pions which reached the stop detectors[1] and the red histogram shows a total amount of generated pions.
Further acceptance studies using experimental data are needed for selection of $pp \rightarrow nK^+\Sigma^+$ reaction events.

References:

[1] Stop detectors = quirl, ring and barrel detector in the COSY-TOF detector system.

[1] Commissioning of the COSY-TOF Straw Tracker, IKP Annual report highlights 2008.
[2] W. Gast, IKP Annual report 2009.

[a] Physikalisches Institut, Friedrich-Alexander-Universität Erlangen-Nürnberg, 91058 Erlangen, Germany

Multifragmentation of Aluminium Nuclei by GeV Protons

M. Fidelus for the PISA collaboration

Double differential cross sections $\frac{d\sigma}{d\Omega dE}$ of proton induced reactions on ^{27}Al have been measured for three proton beam energies: 1.2, 1.9, and 2.5 GeV. Isotopically identified hydrogen, helium, lithium, beryllium and boron ejectiles have been detected at seven scattering angles: 15.6° , 20° , 35° , 50° , 65° , 80° , and 100° . The present results agree well with the scarce data from literature measured at similar proton beam energies and extend considerably the existing data bank on ejectile species and double-differential-cross section spectra towards the high energy regime.

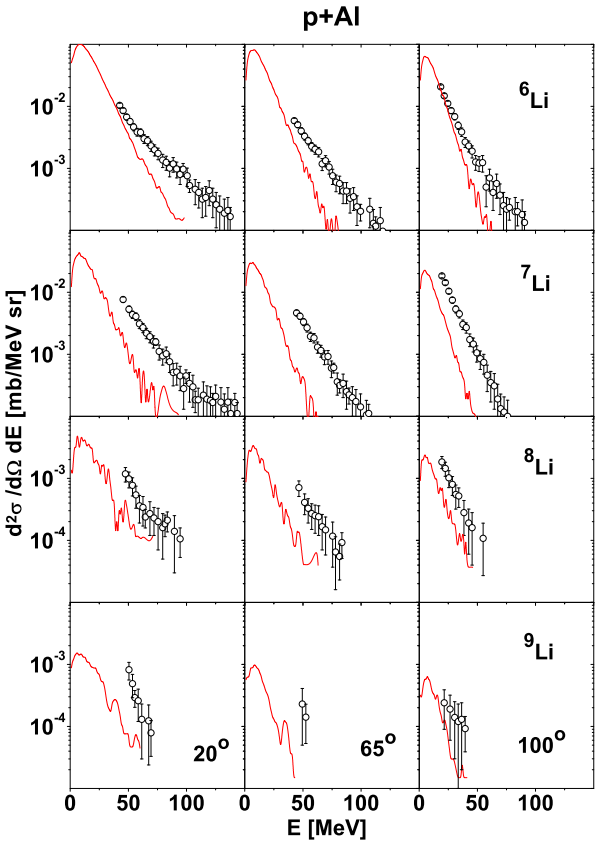

Fig. 1: The experimental spectra (dots) and calculated spectra by INCL4.3+GEM2 evaporation (lines) of ^{6}Li , ^{7}Li, ^{8}Li , and ^{9}Li for p+Al collisions at T_p= 1.2 GeV.

The analysis of intermediate mass fragment (IMF) data (Li, Be and B ejectiles) has been performed in the frame of a two-step model. In this model the first stage of the reaction is described by an intranuclear cascade of nucleon-nucleon and pion-nucleon collisions leading to the emission of nucleons and light charged particles (i.e. particles with Z $\leq$ 2) leaving the residual nuclei in excited states. The deexcitation of the residual nuclei proceeds in the second stage of the reaction and is usually treated as sequential evaporation of particles from the equilibrated nuclear system. In the present analysis the INCL4.3 computer program of Boudard and collaborators [1] has been applied for the evaluation of the intranuclear cascade stage of the reaction and the GEM2 program of Furihata [2] has been used for the evaporation of IMFs from excited remnants of the cascade. Results of the calculations are shown in Fig. 1 together with spectra of Li isotopes measured at a proton beam energy of 1.2 GeV. As can be seen, the

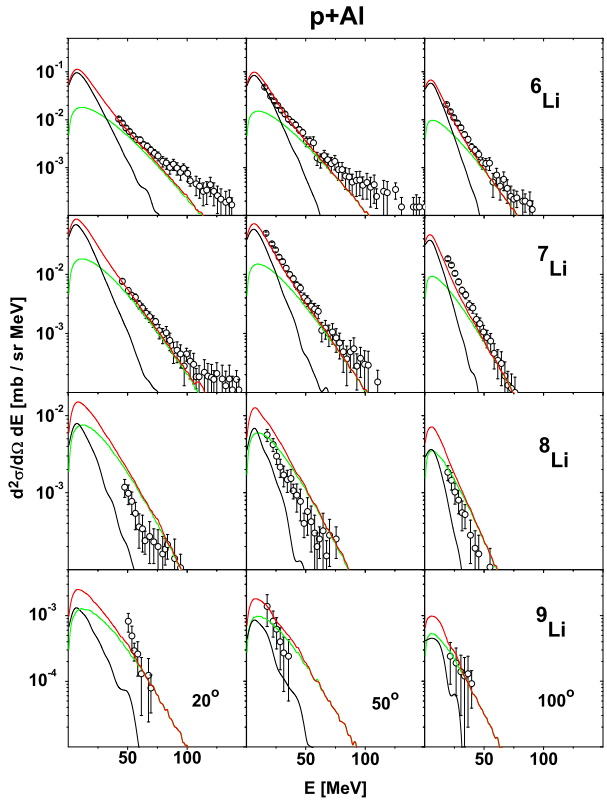

Fig. 2: Experimental spectra as in Fig. 1 but the lines (described in the text) represent evaporation and multifragmentation model calculations.

shape and magnitude of the spectra is not well reproduced by the model calculations.

Therefore the theoretical analysis has been performed assuming that in addition to the sequential evaporation of IMFs from excited nuclei, multifragmentation appears if the excitation energy per nucleon exceeds some critical value. This critical energy was treated as a free parameter. Results of this analysis are presented in Fig. 2, where the black lines show the contribution from sequential evaporation, the green lines depict the multifragmentation cross sections evaluated in the frame of the Fermi break up model by means of the ROZPAD computer program of Magiera [3]. The sum of both contributions is presented by the red lines.

A very good reproduction of all IMF spectra has been achieved with only one free parameter. The critical excitation energy is 7.7(8), 7.0(8), and 6.1(9) MeV/nucleon for proton beam energies of T_p=1.2, 1.9, and 2.5 GeV, respectively. This critical energy agrees well with the compilation of values obtained from caloric curve studies [4].

It is planned to apply the reaction models used in the present report to data obtained for other targets.

References:

[1] A. Boudard et al., Nucl. Phys. A **740**, 195 (2004)
[2] S. Furihata, Nucl. Instr. Methods in Phys. Res. B, **171**, 251 (2000)
[3] A. Magiera, unpublished
[4] J.B. Natowitz et al., Phys. Rev. C **65**, 034618 (2002)

Double-Polarized Fusion

R. Engels[a], N. Chernov[b], K. Grigoryev[a,b], S. Kiselev[c], L. Kotchenda[b], P. Kravtsov[b], L. Kröll[a], M. Marusina[c], M. Mikirtychyants[a,b], N. Nikolaev[a], F. Rathmann[a], H. Paetz gen. Schieck[d], H. Ströher[a], V. Trofimov[b], and A. Vasilyev[b]

In a collaboration between IKP, FZ Jülich, PNPI and ITMO, St. Petersburg, the influence of nuclear polarized projectiles on the differential and total cross section will be investigated for the *dd*-fusion reactions at low energies. For the $^3He(d,p)^4He$ and the $t(d,n)^4He$ reaction it was expected and has been shown, that aligned spins will increase the fusion rate by a factor up to 1.5 [1] because both reactions have a $J^\pi = 3/2^+$ resonance at energies below 100 keV. For the $d+d$ reactions no valid theoretical guidance exists [2]. The knowledge of the complete reaction matrix may allow to control the neutron rate in a fusion reactor and, therefore, to optimize the energy transport from the fusion plasma to the reactor walls. In addition, the lifetime of the reactor walls can be maximized, which will decrease the cost of investments for fusion energy.

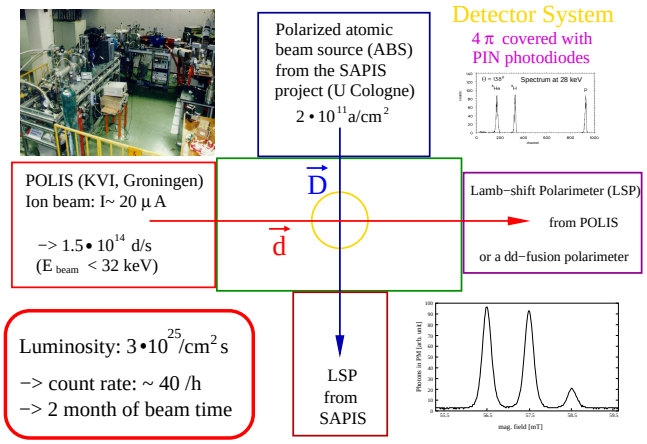

Fig. 1: Schematic setup of the experiment: The polarized deuteron beam will be produced by the POLIS source from KVI and the polarized deuterium jet target will be produced by the SAPIS ABS. The polarization of both, beam and target, will be measured with different Lamb-shift polarimeters. In addition, a nuclear-reaction polarimeter can be used for the ion beam.

In the framework of an ISTC (No. 3881) and a DFG project (EN 902/1-1) a double polarized experiment is in preparation at PNPI, St. Petersburg, to measure the spin-correlation coefficients $C_{z,z}$ and $C_{zz,zz}$ of the reactions $d(d,n)^3He$ and $d(d,p)t$ to determine the so-called 'quintet suppression factor' [2] for both reactions. To produce a polarized deuterium jet target the polarized atomic beam source (ABS) from the former SAPIS experiment [3] at the Institut für Kernphysik of the University of Cologne was dismounted and sent to Russia in 2009. In addition, the polarized ion source POLIS, which was in use at KVI, Groningen [4], was dismounted in spring and transported to Gatchina in summer of 2010. After some modification of the infrastructure at PNPI the ion source POLIS will be rebuilt in spring of 2011.

The polarization of both sources will be determined with a Lamb-shift polarimeter (LSP). In addition, a nuclear reaction polarimeter for the ion beam, based on the dd-reactions and the known analysing powers, was built and tested [5]. During this measurements it could be shown in Jülich, that photodiodes from Hamamatsu [6] are a cheap solution to detect the ejectiles (^{3}He, t and p) at energies between 0.8 and 3 MeV due to the large Q values of the reactions with a reasonable energy resolution. First tests with an α source showed an energy resolution of 28 keV. During the realistic tests with a deuteron beam on a CD_2 target an energy resolution of about 100 keV was reached due to the straggling in the thick target. Therefore, the necessary 4π detector around the interaction region of deuteron beam and target can be assembled from about 300 of these simple detectors.
The expected target density of $\sim 2 \times 10^{11}$ atoms/cm^2 and an ion beam of ~ 20 μA will provide a luminosity of 3×10^{25} cm^{-1}s^{-1}. Therefore, it will take about two months of beam time to measure the quintet suppression factor at 30 keV where a future fusion reactor will operate. With this setup additional spin-correlation coefficients can be measured at different energies to obtain futher information about the not well understood dd-fusion process.
On the other hand the astrophysical S-factor [7] can be investigated for different nucleus-electron spin-combinations. An ABS is able to produce a beam of deuteron atoms in different hyperfine states. Therefore, not only the nucleon spin can be changed but the electron spin, too. At energies below 10 keV the screening effect of the electron increases the total cross sections of the *dd* reactions due to the modified Coulomb barrier of the target atom. The influence of the electron spin in this case in completely unknown.

References:

[1] Ch. Leemann et al., Helv. Phys. Acta **44**, 141 (1971).
[2] H. Pätz gen. Schieck, EPJ A **44**, 321 (2010).
[3] R. Emmerich and H. Paetz gen. Schieck, NIM A**586**, 387 (2008).
[4] H.R. Kremers et al., NIM A **536**, 329 (2005).
[5] L. Kröll, *A dd nuclear reaction polarimeter for the polarized fusion project*, Diploma thesis, RWTH Aachen, 2010.
[6] Hamamatsu, PIN-Diode S3590-09.
[7] F. Raiola et al., Eur. Phys. J. **A 13**, 377 (2002).

[a] Institut für Kernphysik, Forschungszentrum Jülich, Germany
[b] St. Petersburg Nuclear Physics Iinstitute, Gatchina, Russia
[c] National Research University of Information Technology, Mechanics and Optics, ITMO, St. Peterburg, Russia
[d] Institut für Kernphysik, Universität zu Köln, Germany

Development of a Pellet Tracking System for PANDA and WASA

H. Calén, K. Fransson and M. Jacewicz
Uppsala University

This project aims at developing a system for optical tracking of pellets (PTR). It requires efficient detection and identification of individual pellets in a pellet stream of high intensity, typically 10k-20k pellets/second. The final goal is to be able to reconstruct the position (3d xyz) for pellets that are in the accelerator beam region at the time of a hadron reaction event with an accuracy of a few tenths of a millimeter.

During the last years the emphasis has been on development of a synchronized system of two cameras and on improving the efficiency of pellet detection [1]. Hydrogen pellets with $\phi \approx 25$ µm at the Uppsala pellet test station (UPTS) were used.

The most important measurements during 2010 concerned pellet signal time correlations and velocity estimates. For these studies the 2 cameras were placed at different vertical positions, one just below the vacuum injection capillary (VIC) and the second at the observation chamber 27 cm below (Fig.1). The large distance between the observation points, the velocity spread and the known inefficiencies were expected to make it difficult to observe a clear correlation. Never the less a correlation peak could be observed in the time difference distributions (Fig. 2) in agreement with simulation results. This peak corresponds to a pellet velocity of about 80 m/s and a velocity spread $\sigma_v/v \approx 1\%$. This velocity spread is small enough to allow for

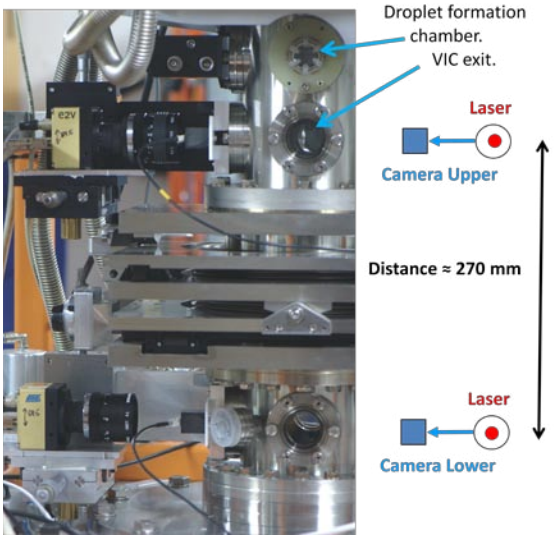

Figure 1. Two-camera setup at the UPTS.

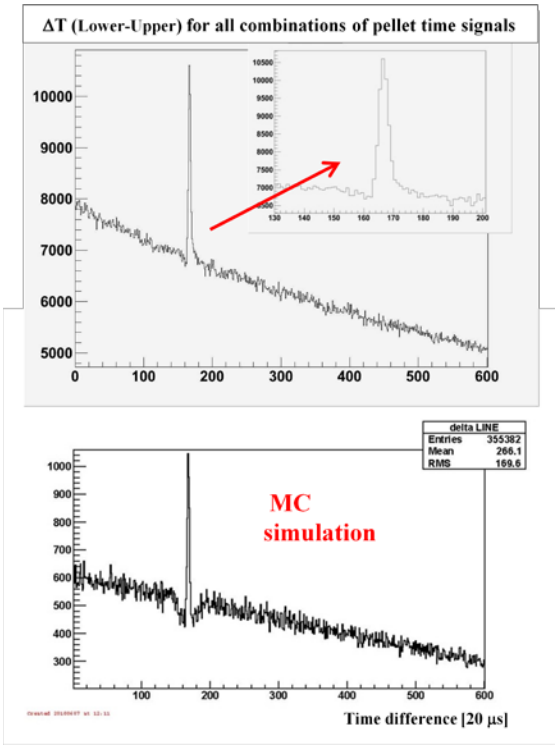

Figure 2. Time correlation measurement.

efficient pellet tracking in a future tracking system. Some similar measurements were also done with slightly varied conditions for the pellet generation. By changing the driving pressure, i.e. the pressure in/above

the liquid H_2 nozzle, and the nozzle vibration frequency the droplet size and velocity were varied. The droplet velocity was fairly independent of frequency and increased almost linearly with driving pressure (Fig.3 upper graph). Lower pressure or higher frequency was seen to result in smaller droplets as expected. Smaller droplets result in faster pellets (Fig.3 lower graph).

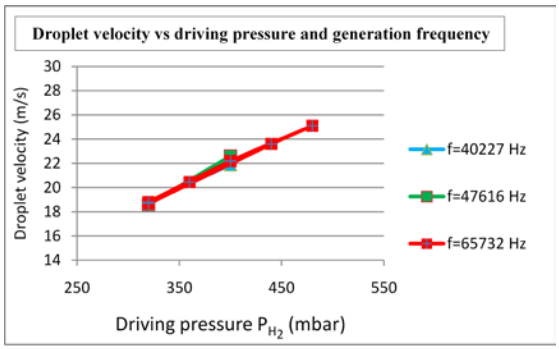

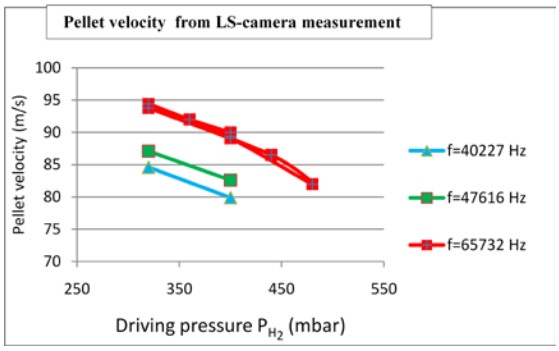

Figure 3. Droplet and pellet velocity

At these conditions (e.g. with estimated pellet sizes of 25-35 μm) a relative change in diameter, $\Delta\phi/\phi \approx 1\%$ gives a change in velocity of $\Delta v/v \approx 1.5\%$.

A minimal velocity spread is necessary for reaching an optimal pellet target performance. The presented measurement result gives important information on the uniformity required to reach this goal.

Continued development work including improvements in basic performance of the LS-camera system and pellet detection efficiency, the latter in particular if one wants to go to smaller pellets, are needed. To record and process the data from the LS-cameras a multi-camera read-out hardware with primary data selection by FPGAs and higher level processing will be developed.

In 2011 a prototype system that will allow tracking of individual pellets will be put in operation at UPTS (Fig. 4). In this system two pellet detection levels separated by 80 mm for 2-4 LS-cameras are placed after a collimator. Based on the experience from this system, the next step is to design a tracking system based on 6-8 LS-cameras for WASA.

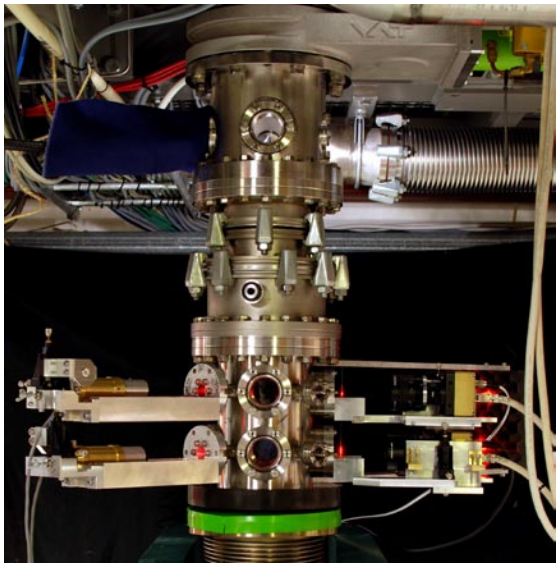

Figure 4. Prototype pellet tracking setup.

[1] K. Fransson and H. Calén, COSY/IKP Annual report, 2009.

The project is supported by COSY-FFE, EC FP7 and Swedish Research Council

Time calibration of the Forward Detectors for the usage of the Time-of-Flight method with WASA-at-COSY

M. Zieliński[a,b], and P. Moskal[a,b]

Investigatins of the η' meson decays produced in $pp \to ppX$ reaction using WASA-at-COSY apparatus [1] requires a high tagging efficiency by means of the missing mass technique. Therefore a high resolution of energy measurement for two outgoing protons is needed. To this end we developed energy reconstruction method based on a Time-of-Flight measurement using the scintillating layers of the WASA Forward Detector [2, 3]. Generaly all 14 layers (thin and thick) can be used for this pourpuse but for now we consider only 5 thin layers of FWC and FTH.

In order to use time information the time calibration of forward scintillating layers has to be done. For this pourpuse we analysed the experimental data from the reaction $pp \to ppX$ collected in 2008. As a first step a relative time offsets between each detection module of the FWC and FTH have to be established. The FWC detector is 48-fold segmented and is composed of two layers each with 24 elements made out of 3 mm plastic scintillator read out from one side by a photomultipler. The FTH consists of three scintillating layers composed of 96 individual modules read out by a photomiltiplier from one side. First layer is arranged with a cake-piece shaped modules and 2 others in a form of Archimedean spiral shape. The measured time information from the TDC unit for a single FWC and FTH element may be expressed as:

$$t^{FWC}_{TDC} = t^{FWC}_{real} + t^{FWC}_{offset} + t^{FWC}_{walk} + t^{FWC}_{light} - t_{trigger}, \qquad (1)$$

$$t^{FTH}_{TDC} = t^{FTH}_{real} + t^{FTH}_{offset} + t^{FTH}_{walk} + t^{FTH}_{light} - t_{trigger}, \qquad (2)$$

where t_{offset} denotes all the delays in the electronics and cables, t_{walk} is a effect related to the signal aplitude higth, t_{light} stands for the time of light propagation in scintillator and the $t_{trigger}$ denotes the time of the trigger signal. To calculate the Time-of-Flight TOF between FTH and FWC one can apply equations (1) and (2) as:

$$TOF = t^{FTH}_{TDC} - t^{FWC}_{TDC} + t^{FWC}_{offset} - t^{FTH}_{offset} + t^{FWC}_{walk} - t^{FTH}_{walk} + t^{FWC}_{light} - t^{FTH}_{light}. \qquad (3)$$

The unknown time offsets t_{offset} and effects of t_{walk} and t_{light} have to be established for each individual element in each scintillating layer.

In order to determine the offsets we have used events with proton track of energy greater then 100 MeV passing through FWC and FTH and assuming as a first approximation that the real time-of-flight between these layers is equal to 0. First by ploting the TOF as a function of element number in the FWC_1 and by correcting mean of the time distribution to asumed $TOF = 0$ (Fig. 1 left). Next assuming that the FWC offsets are correct, we have established with the same method offsets for each modul in the FTH_1 (Fig. 1 right).

Having the offsets established for each element the time walk effect t_{walk} may be calculated based on the signal amplitude information. This effect occures due to different signal hights of signals having the same rise time. To correct for this effect one can use a linear dependence between the time and the inverse of the square root of the charge [4]:

$$t = t' - \alpha - \beta \frac{1}{\sqrt{ADC}}, \qquad (4)$$

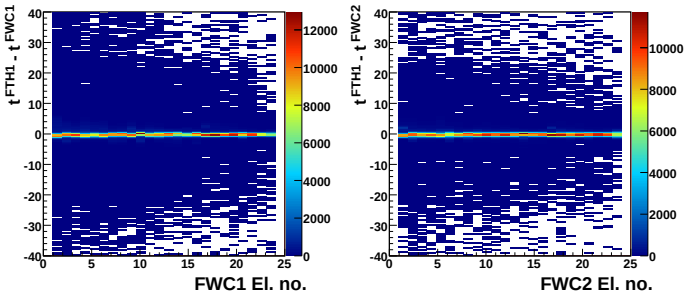

Fig. 1: Experimental data of time-of-flight as a function of element number (a) for FWC1 (b) FWC2.

where t stands for corrected time and t' for measured time. To determine the α and β coefficients we plotted the TOF for each individual module of scintillator as a function of square root of the ADC signal and fitted an linear function which is shown in Fig. 2 (left). Also the time of the light propagation

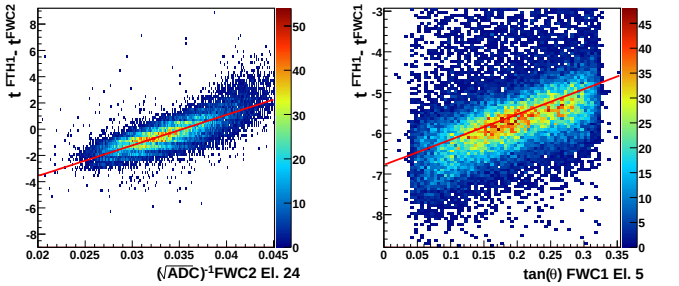

Fig. 2: (a) Experimental data of time-of-flight between FTH1 and FWC2 as a function of $\sqrt{ADC}^{-1}$ for element 24th of FWC2 with superimposed line $\Delta t = \alpha \cdot \frac{1}{\sqrt{ADC}} + \beta$ to establish a time "Walk effect". (b) Experimental data of time-of-flight between FTH1 and FWC1 as a function of $\tan\theta$ for element 4th of the FWC1 with superimposed line $\Delta t = \alpha \cdot \tan\theta + \beta$ to establish light propagation effects.

in the scintillator has to be taken in to account. To determine this effect based on the geomety of the FD we have found a time dependence on the theta angle as:

$$t = t' - \left(\frac{l_1}{v_1} - \frac{l_2}{v_2}\right) + \left(\frac{d_2}{v_2} - \frac{d_1}{v_1}\right) \cdot \tan\theta, \qquad (5)$$

where l_1, l_2 denotes the particle tracks lenght from the interaction point to the hit point in the detector, d_1, d_2 stands for the position of the FWC and FTH layers with respect to the assumed interaction point, v_1, v_2 are the vielocities of the light in the scintillator elements and θ is a angle of the particle track with respect to the beam direction. To correct for this effect we have plotted the TOF as a function of $\tan\theta$ which is shown in Fig 2 (right), and by fitting a linear function we have determined parameters $\alpha = \frac{d_2}{v_2} - \frac{d_1}{v_1}$ and $\beta = \frac{l_1}{v_1} - \frac{l_2}{v_2}$.

After correcting for the walk effect and taking into account the light propagation in scintillator we made another iteration

for the offset determination. Having these ralative offsets de-

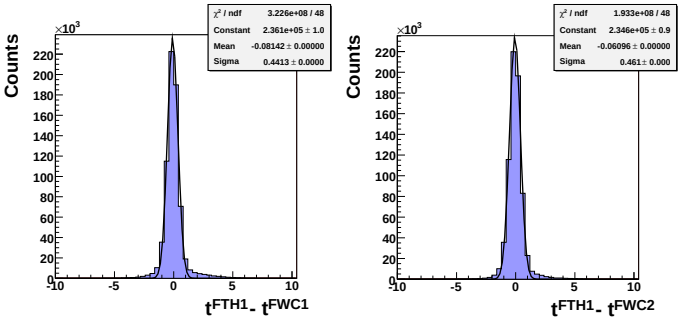

Fig. 3: Experimental data of time-of-flight between (a) FTH1 and FWC1, (b) FTH1 and FWC2 for all modules. The result of the fitted Gauss function is shown as a solid line. Fit parameter σ shows the time of flight resolution.

termined we ploted distributions of the time of flight between FTH_1-FWC_1 (Fig. 3 left) and FTH_1-FWC_2 (Fig. 3 right) and fitted the Gaussian function in range of the peak. The determined Time-of-Flight resolutions $\sigma(TOF_{FTH_1-FWC_1}) = 441ps$ and $\sigma(TOF_{FTH_1-FWC_2}) = 461ps$, which assuming the same resolution of the FWC and FTH gives σ of about 320 ps for individual layer (taking into account all detector modules).

References:

[1] H. H. Adam et al., `arXiv:nucl-ex/0411038` (2004)

[2] P. Moskal, A. Kupść, J. Złomańczuk, WASA-Note 061123PM (2006)

[3] M. J. Zieliński, Dip. Thesis, Jagiellonian University, JÜL-4277, `arXiv:0807.0576 [hep-ex]` (2008)

[4] P. Moskal, Dip. Thesis, Jagiellonian University, JÜL-2825 (1993)

[a] Institut für Kernphysik and Jülich Center for Hadron Physics, D-52425 Jülich, Germany

[b] Institute of Physics, Jagiellonian University, PL-30059 Cracow, Poland

Online control and data visualisation system for the COSY-TOF experiment

E. Borodina
for the COSY-TOF Collaboration

1.) Motivation

To improve the track reconstruction resolution and efficiency the Straw Tube Tracker (STT) detector has been recently installed at the COSY-TOF experiment. In order to get the track points near the primary vertex the Silicon Quirl Telescope (SQT) has been installed near the target. They improve both mass resolution and reconstruction efficiency significantly. These new detectors increase the number of channels of the COSY-TOF spectrometer by a factor of about 3. The increased complexity of the detector system required a new control and a 3D visualization software package. The development of this software and upgrades of the experiment visualization are described in the following.

2.) Description

The online control software consists of the conversion software, which transforms a binary data stream from the data acquisition system (DAQ) to a detector oriented event format, methods of Inter-Process Communications (IPC), the graphical user interface (GUI) and event display, based on 3D visualization of single selected events. To achieve data transfer through the network and real time data performance the IPC tools - sockets and shared memory - are used.The complete experiment geometry and single event displays are saved as a ROOT files.

Data processing at the COSY-TOF experiment starts with retrieving data from the DAQ, which provides data digitization, transport and management, first processing and storage. Parallel to the data storage the ”cluster2event” code recombines subevent data blocks from different electronic modules to full events. The converting code receives these event data from the DAQ socket, deciphers them from various hardware defined binary formats to the more user friendly TADE format (TDC-ADC-Detector-Element) based on physical data interpretation. The converting code is used for online data decoding and for offline analysis. In the latter case the data are stored on disk as ASCII files. Recently the converting algorithms ware optimized and the decoding speed was increased up to 1500 events/second.

Another part of the program package provides visualization of statistical experiment information and 3D visualization of single events (event display). The program creates in real time different types of spectra for all detectors and their elements and updates them continuously in the shared memory. Additional types of spectra are defined by the user in a special ASCII file. ”User friendly” data visualization is performed by a special GUI, ”TOF-ONLINE”, which is based on ROOT classes. It provides a convenient management of plots of data from selected detectors, real time visualization of various types of spectra, as well as additional services such as saving figures as vector graphic pictures, printing data, automatical spectra updating etc. (Fig. 1).

An additional program package was developed to calculate, plot and set new pedestal values automatically using current online data stream and to check the corresponding definition files.

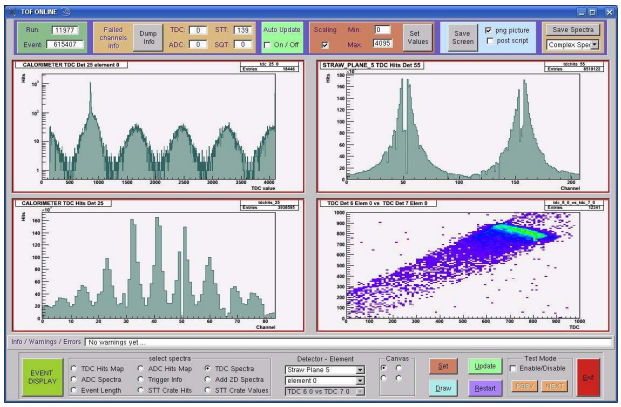

Fig. 1: Example of the GUI TOF-Online with examples of the default and user defined spectra.

3.) Event display

The event display, based on ROOT geometry classes, graphically shows detector components and events in different ways of visualization during online sessions. The whole TOF visualization is implemented as a set of sub-detectors as real 3D objects. The positions of the virtual detector elements can be adjusted for each experiment.
The navigation methods through detector elements to display single events were developed. By starting of the online control software the whole detector geometry will be loaded. Based on this, the geometry of single events will be created for selected cases (Fig. 2).

The event visualization has a number of options to change its settings. The user can switch on/off the detector parts to be visible. By the GUI the viewing angles, zoom factor and other parameters can be set. In addition an option to create 2D projections of events is provided. For optimal visualization of detector hits the transparent skeleton can be drawn. To adjust the new STT detector the additional GUI options to draw track points and reconstructed tracks, to select different planes and orientations etc. can be chosen.

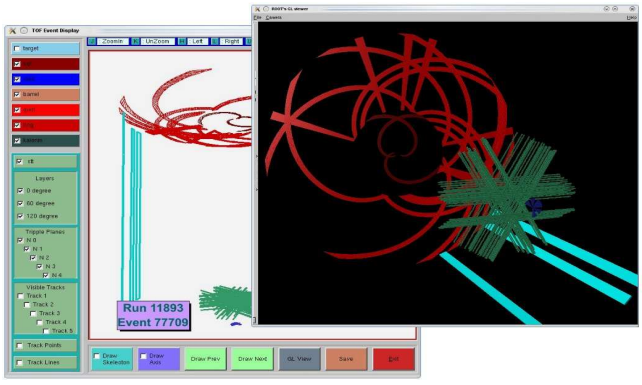

Fig. 2: Example of the GUI with the event display of a the PKL event candidate using 3D view (left) and OpenGL view(right).

4.) Online track reconstruction

The track reconstruction provides not only the best way of the events visualization and selection, but is also a useful feature to test the event display software routines. For example, in the case of the by error mixed tubes positioning it is not possible to reconstruct the track, since track trajectory, defined by several other hits, will lay outside of the wrong positioned STT tube.

There are two ways to reconstruct the tracks. The first is to reconstruct 2D track for each of the STT planes orientations. In this case we get 3 orientation instead of 6 due to combining together orientation with 180 degree angles difference. The second way is to calculate the track hits XY coordinates for each of the STT triple plane, and then combine them together to 3D track. For the online reconstruction the compromise between time and precision should be found, therefore the second way was chosen due to the very quick and simple calculation of the triple hits.

At the first step each hitted straw tube position is calculated in the triple plane (group of 3 neighboring planes, rotated by 60 degree) coordinates. Then the tubes of each of 3 planes and their sublayers (each plane has 2 sublayers), which could compose a hit, will be combined to triplets. For each triplet the track coordinates in this triple plane will be calculated. Then the track points are translated from the local STT planes coordinates in 3D global coordinates system using the planes positions. In the next step the points are combined to tracks. As the last step the tubes for the planes, which were not combined in triple planes, should be checked, whether they belong to the found tracks. During the last beam time only 13 of 15 planes were used, therefore one of them should be approximated.

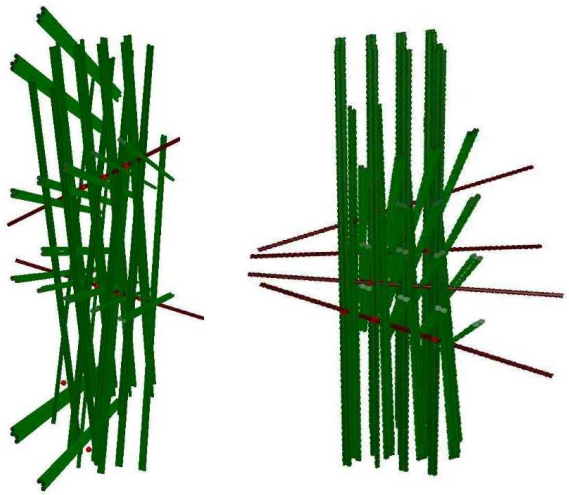

Fig. 3: Example of complicated (left) and clear (right) STT track reconstruction. The left picture has two of four tracks with large angles. For these angles there are not enough tubes on the tracks to get a good reconstruction.

The limitation for this reconstruction are angles larger than 50 degree (Fig. 3) and the events, tracks, which are too close to each other. In this case it is not possible using only the tubes positions, to distinguish, to which of the two neighboring tracks the hitted tubes belongs. But in contrast to the offline data analysis, in which it is important to reconstruct all the tracks and the time of reconstruction is not so essentially, in the online reconstruction at first the passing conditions are checked, and only the appropriate events are reconstructed.

The track reconstruction could be done as by using only STT values, as by calculating hit points also from other subdetectors. The very quickly to check the hits positions at the stop detectors Quirl, Ring, and Calorimeter. To provide most simple tracks examination only the elastic events could be selected for reconstruction. Such events are very convenient for check the SQT orientation, making the Barrel calibration etc.

5.) Results

The online control software was successfully used during the beam time in summer 2010. The event display, based on the earlier created complete 3D COSY-TOF experiment geometry, was developed. Routines to create the event display and check its visualization were tested with the online track reconstruction. For the convenient data control and selection were developed the GUI's for both data spectra and the event display.

Feasibility study of ^{3}H-η bound states production by means of the COSY-TOF facility

M. Skurzok[a], P. Moskal[a,b] for the COSY-TOF collaboration

Formation of η-mesic Tritium might be realized by quasi-free reactions as already successfully used at COSY to study meson production in quasi free proton-neutron collisions [1, 2]. Measurements of such reactions is possible for the external COSY-TOF detector, where the search for η-mesic Tritium can be carried out by the measurement of the excitation function of the $nd \to (^3\text{H-}\eta)_{bs} \to dp\pi^-$ reaction using a deuteron beam and tagging the nd reactions by measuring the spectator protons (p_{sp}) from the $dd \to p_{sp}nd \to p_{sp}(^3\text{H-}\eta)_{bs} \to p_{sp}dp\pi^-$ reaction, which is schematically schown in Fig. 1. The signal from $(^3\text{H-}\eta)_{bs}$ is expected below the threshold of the $nd \to {}^3\text{H-}\eta$ production [3].

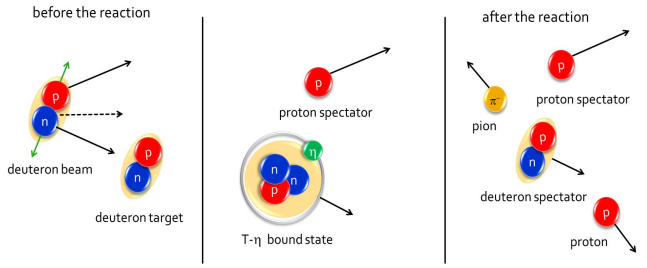

Fig. 1: Schematic picture of the quasi-free $dd \to p_{sp}nd \to p_{sp}(^3\text{H-}\eta)_{bs} \to p_{sp}dp\pi^-$ reaction. The Fermi momentum of the nucleons inside the deuteron is presented by the green arrows and the beam momentum by the dashed arrow. The figure is adapted from reference [4].

The systematic uncertainties in establishing the shape of the excitation functions are significantly reduced when using this method, because in the case of quasi-free reaction the energy scan (in the range of about 100 MeV) around the η meson production threshold can be achieved from the Fermi motion of the nucleons inside the deuteron beam at a fixed value of the beam momentum.

The feasibility of the measurement of the $(^3\text{H-}\eta)_{bs}$ bound states production via quasi-free reaction: $dd \to p_{sp}nd \to p_{sp}(^3\text{H-}\eta)_{bs} \to p_{sp}dp\pi^-$ with COSY-TOF detection setup is analised in Reference [4]. The effective detector acceptances as a function of the beam momentum were determined and are presented in Fig. 2 and Fig. 3. From the dependence shown in those figures it follows that the highest probability to register the quasi-free $dd \to p_{sp}(^3\text{H-}\eta)_{bs} \to p_{sp}dp\pi^-$ reaction is for the beam momentum p_{beam}=3.1 GeV/c corresponding to the $dd \to p_{sp}(p_F = 0)^3\text{H-}\eta$[1] reaction threshold whereas for beam momenta above and below the threshold the effective acceptance decreases. Thus, the measurement of quasi-free reaction products is the most efficient at the η meson production threshold.

[1] p_F−Fermi momentum of proton spectator inside beam deuteron.

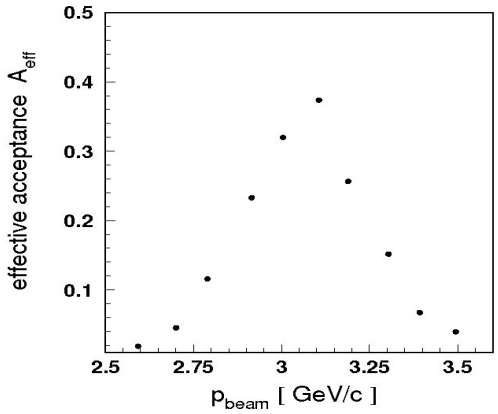

Fig. 2: Effective acceptance to register the quasi-free $dd \to p_{sp}(^3\text{H-}\eta)_{bs} \to p_{sp}dp\pi^-$ reaction near the η production threshold (Q∈(-60,20) MeV) as a function of the beam momentum.

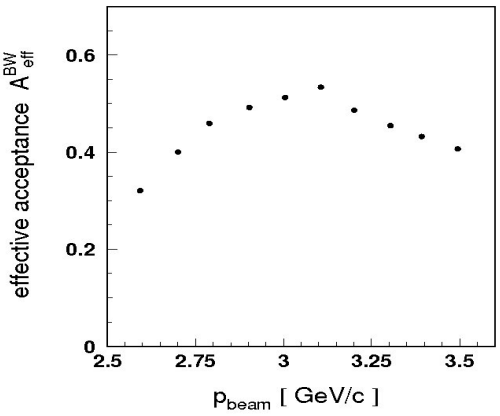

Fig. 3: Effective acceptance to register the quasi free $dd \to p_{sp}(^3\text{H-}\eta)_{bs} \to p_{sp}dp\pi^-$ reaction near the η production threshold (Q∈(-60,20) MeV) as a function of the beam momentum assuming a Breit-Wigner distribution of the squared invariant mass $\sqrt{s_{nd}}$ for the bound state width Γ=10MeV.

We acknowledge support by the Foundation for Polish Science - MPD program, co-financed by the European Union within the European Regional Development Fund and by the FFE grants of the Research Center Jülich.

References:

[1] P. Moskal *et al.*, *Phys. Rev.* **C79**, 015208 (2009).
[2] M. Abdel-Bary *et al.*, *Eur. Phys. J* **A29**, 353 (2006).
[3] P. Moskal, *arXiv:0909.3979* (2009).
[4] M. Skurzok, *Diploma Thesis, Jagiellonian University of Cracow* (2010), Berichte des FZ-Jülich, Jül-4332 (2010), *arXiv:1009.5503* (2010).

[a] M. Smoluchowski Institute of Physics, Jagiellonian University, 30-059 Cracow, Poland
[b] IKP, Forschungszentrum Jülich, D-52425 Jülich, Germany

Status of COSY Injector Cyclotron, Ion Sources and Polarimeter

R. Brings, O. Felden, R. Gebel, A. Kieven, N. Rotert

The operation of the COSY injector cyclotron showed a new record of availability in 2010. Only 48 hours contributed to the facility's unscheduled downtime. Table 1 lists all periods of unavailability. In order to keep the level of availability various activities have been pursued. The completed tasks in 2010 have been:

- Spare tuning element TE8
- Electrostatic septum deflector
- Test of refurbished amplifier tubes
- Refurbishment of cryo pumps and valves
- Additional temperature measurement for the cryopumps
- New cooling and target control for the INM-5 irradiation station
- New permanent dosimetry at the FhG irradiation station

Table 1: Downtime data of the injector cyclotron in 2010

cause of downtime	date	duration
Flowmeter RN3 defect	16.3.2010	4 h
Power drop, all systems off	20.4.2010	2 h
Injector cooling off	24.5.2010	28 h
RF system off	10.6.2010	6 h
Inflector power supply off	11.8.2010	6 h
Septum exchange (sparking)	23.11.2010	55 h
Compressor cooling off	1.12.2010	7 h
Sum of downtime	2010	108 h
Operational hours	2010	6871 h
Total as COSY injector	31.12.2010	136061 h

Besides the injector operation additional irradiation has been provided to internal (4) and external users (4).

Fig. 1: New external target set-up (INM-5)

The main activities at the ion sources concentrated on

- Improvement of the vacuum separation of sources from the source beam line
- Usability of the lambshift polarimeter
- Replacement and extension of scintillators at the low energy polarimeter in the transfer beam line to COSY

The vacuum system of the unpolarized ion sources had not sufficient capacity to allow parallel operation without significant losses of transmitted beam intensity. Also the performance of the unpolarized ion sources had been restricted due to the low gas flow. The availability of large chambers from the former EDDA polarized atomic beam target allowed an economic exchange of the existing chambers. Meanwhile both ion sources have been installed at these chambers and have been connected to the existing beam line. The four-way cross piece had been replaced in order to allow a larger angle. First tests approved the expected vacuum separation.

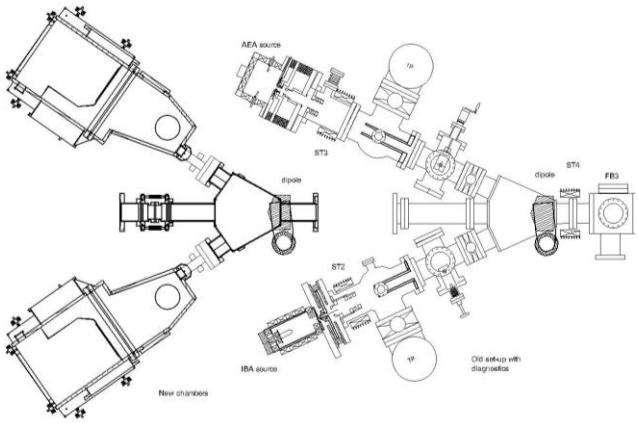

Fig. 2: New (left) and old set-up of the transfer beam line section with the two unpolarized ion sources.

With the delivery of polarized deuterons one misses the diagnosis of tensor polarization. For preparation purposes the lambshift polarimeter is still underway to be operated routinely. With exception of a damaged isolator at the double charge exchange gas target this polarimeter is in principle operational. In order to measure and to tune the polarization behind the cyclotron the detector set-up of the low energy polarimeter has been changed from 4 NaJ scintillators to 12 plastic ones (NE110A) with a separation of 10°, as shown in figure 3. The benefits are higher count rate capabilities in general and a possible kinematic correlation for background reduction, if a CH_2 target is used. Both points have been proved in January 2011. The detail analysis of the data is in progress.

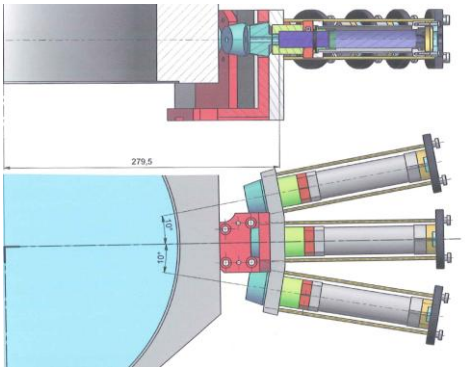

Fig. 3: Cross section and top view of one of four triple detector set-ups at the low energy polarimeter behind the cyclotron. One detector consists of a collimator, the scintillator and a compact multiplier. The detectors are separated by 10° and moveable to cover the range from 25° to 75° for left, right, up and down direction.

Progress with the Scintillation Profile Monitor at COSY

C. Böhme, J. Dietrich, V. Kamerdzhiev, F. Klehr, K. Reimers

The Scintillation Profile Monitor (SPM), being developed at COSY, is intended to measure profiles of the beam circulating in the machine [1]. To detect the light, a commercially available 32-channel Photomultiplier (PMT) equipped with a simple lens system is used. The size of each photocathode of the PMT is 0.8×7 mm with 1 mm spacing. All 32 PMT channels are read out by a 48-channel picoammeter module developed by iThemba Labs, South Africa [2]. The data acquisition and visualization software running on a PC in the COSY control room, uses an Ethernet connection to the picoammeter module. Besides the real-time beam profiles the software displays the beam current stored in the ring, residual gas pressure and their evolution over time. Up to now, the application of this method was difficult due to vacuum conditions in COSY [3]. The recently installed commercially available piezo-electric leak valve (fig. 1) allows injecting small amounts of nitrogen into the vacuum chamber in a controlled and reproducible way. The dedicated vacuum chamber is now equipped with two DN100 vacuum windows for horizontal and vertical profile measurements as well as two DN40 vacuum ports for vacuum measurement and gas inlet (fig. 1). The vacuum chamber is blackened inside to prevent light reflection. A local pressure bump of less than one order of magnitude is necessary to obtain clear beam profiles at nominal COSY conditions. Fig. 2 shows a preliminary beam profile measured during the first attempt to use the new SPM setup. The lens focusing needs to be verified before an accurate scaling in mm can be given.

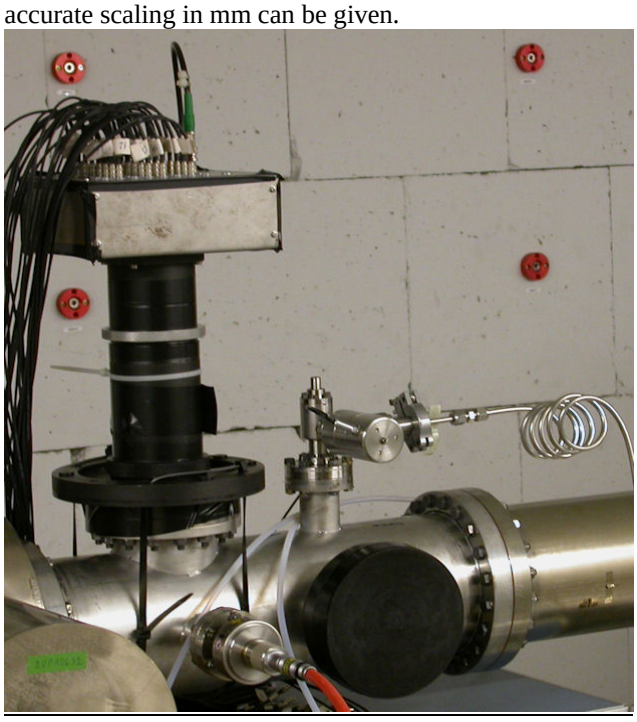

Fig. 1: The new SPM setup. Shown are the vacuum chamber, the piezo-electric leak valve with its nitrogen line and the light detection system consisting of the PMT and a lens.

Fig. 3 shows the vacuum reading during SPM operation. The voltage controlled leak valve allows continues control over the amount of gas injected.

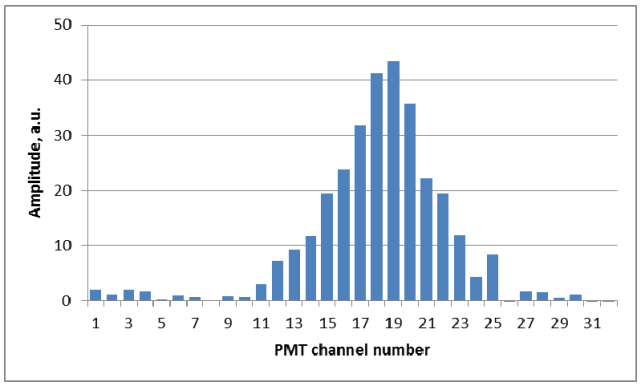

Fig. 2: An example of a horizontal beam profile measured with the SPM with $1.5 \cdot 10^{10}$ protons in the ring at 2.6 GeV/c. Temporary pressure bump at the SPM location amounted to $4 \cdot 10^{-8}$ mbar.

A power supply, controlled remotely via TCP/IP from the COSY control room, provides up to 1 kV to the piezo-electric valve.

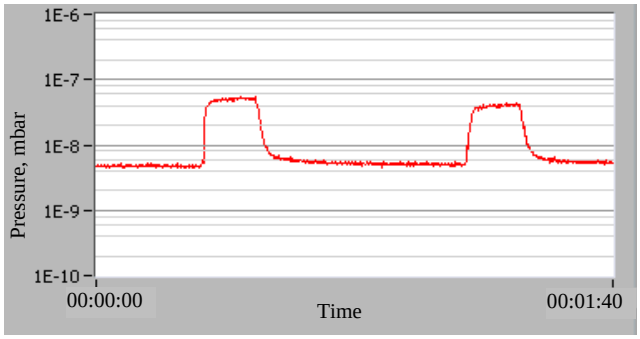

Fig. 3: Vacuum reading during the profile measurement. The pressure was intentionally increased from $5 \cdot 10^{-9}$ to $5 \cdot 10^{-8}$ mbar by injecting pure nitrogen.

The valve control software is written in LabView. For the first attempts a conservative valve driving procedure was chosen. The user defines voltage ramping speed, flat top voltage and flat top duration. The trapezoid curve is then displayed for verification. After the "Send" button is activated the valve is driven according to the predefined curve and is safely closed. Based on the latest experience one can summarize, that the profile measurement method based on residual gas scintillation excited by the beam particles is very promising and can be successfully applied at a circular machine like COSY.

Acknowledgement

The authors would like to thank L. Conradie, iThemba LABS and F. Becker, GSI for collaboration. We are very grateful for the support by the COSY vacuum group and the assistance by D. Ruhrig.

References:

[1] J. Dietrich et al., First Measurements of Light Emission of Atoms Excited by the Proton Beam at COSY, IKP Annual Report 2002.

[2] C. Böhme et al., Beam Profile Monitoring at COSY via Light Emitted by Residual Gas, Proceedings DIPAC09.

[3] C. Böhme et al., Beam Profile Monitor using Residual Gas Scintillation, IKP Annual Report 2009.

New PLC for Vacuum Bake Out System

F. Jordan[1], W. Schmitz[1], B. Dahmen[2], H. Zens[2], N. Bongers[2]

Vacuum components used in the COSY have to meet stringent requirements so that a good beam quality can be guaranteed. For this reason we run a vacuum test system since the construction phase of COSY. The components to be installed in COSY are not only analyzed for their vacuum performance, but also heated out to minimize out gassing.
After a lightning strike the original S5-PLC was unfortunately no longer functional. Hardware and software support for this family of controllers has run out by Siemens for some years. Only a complete replacement by a modern S7-PLC was possible.

Fig. 1: S7-PLC

The complete replacement of the S5 PLC with a S7 PLC offered the advantage of an advanced functionality, higher performance and availability of spare parts.

The current development environment (SIMATIC Manager STEP 7 Version 5.4) was used successfully in previous projects and was available for software development.

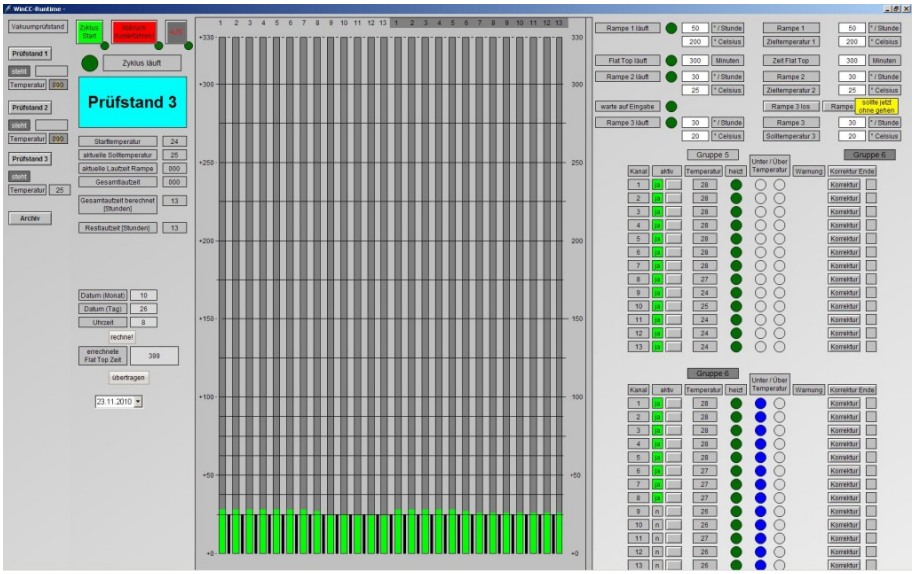

Fig. 2: Operation, Visualization of the Vacuum Bake System

The control system was realized with a S7-315 CPU. For the connection to the 3 independent subsystems (2 already equipped) of the test system digital and analog input as well as output cards are available. In this stage of extension 2x26 heating circuits can be operated in sync. The complex temperature-control is realized in software through standard controller from the S7 library. The connection to the HMI system is produced via Ethernet (TCP/IP).

The visualization system was implemented on the basis of Siemens / WinCC version 7. Each sub system of the test stand has its own user interface.
The new control has already been used successfully on several components that are already in use in our accelerator. New vacuum components have recently been installed mainly in connection with the PAX experiment.

[1] Zentralabteilung Technologie
[2] Institut für Kernphysik

Magnets, Alignment and New Installations

U. Bechstedt, G. Dolfus, R. Enge, G. Krol, M. Küven, G. Langenberg, H. Pütz,
B. Erkes, F. Scheiba

Magnets

Discussions with a possible manufacturer for HESR dipole and quadrupole magnets convinced us that the design of these magnets is feasible. The only change is that the laminations of the dipole magnet will be stacked parallel to each other.
The only design work in 2010 was for the HESR injection dipole magnets and the upstream and downstream dipole magnets of the PANDA chicane.

Installations

The main installation in 2010 was for the PAX experiment. During a five weeks long summer shutdown we installed the PAX target chamber with the atomic beam source and the Breit Rabi polarimeter.
At ANKE we changed back from the atomic beam source to the cluster target.
During the whole year 2010 we were busy with design work for the integration of the new 2 MeV electron cooler that will be installed in 2011. In preparation for the coming cooler we moved the rf cavity from its former position where the cooler will be installed to a place behind the EDDA detector. The wall current monitor was taken out of the ring and the beam current transformer was moved to a place between dipoles 10 and 11 where it replaced a resonant Schottky pickup.

Alignment

As in 2009 the main alignment activities were related to the PAX installation. The support frame of the target chamber and the atomic beam source as well as the target chamber itself had to be aligned with respect to the COSY beam axis.
A support structure to position the big flange which will later on carry the storage cell and the detector telescopes had to be aligned with respect to the target chamber.
Besides these activities like in all the past years we had to measure positions of detectors for the experiments as well internal as external.

Radiation Protection

H.Borsch, O.Felden, J.Göbbels

In 2010 about 190 persons from IKP staff, universities or other laboratories have been under radiation protection supervision at IKP. 150 of these colleges are under permanent survey because they are involved in long running experiments at COSY. In 2010 some new installations have been done at COSY, but here only short running experiments or test of detector components for use at the upcoming FAIR facility will be performed. The experimentalists only stay for a short while at COSY but need to have access to the COSY controlled areas (while the beam is down). In this case the surveillance will be done with officially certificated electronic personnel dose meters (EPD) from Type RADOS Rad 62-SE. The acceptable dose is restricted to 10µSv/day.
In 2010 around 40 persons had been surveyed by this method and the daily dose stays well below the 10µSv-treshold. Due to the fact, that the behavior of the EPDs in pulsed radiation fields is not yet clear, these dose meters must not be used for the persons who have access to the inner hall during beam on. The investigation about the suitability of the EPDs at COSY is still ongoing.

In 2009 first rough estimations of the expected doses produced by an electron beam loss at the wall of the vacuum pipe had been performed [1]. The results rely on the construction as known in 2009. The expected dose was in the range of some Gy. The estimations clearly proved the necessity of a shielding around the cooler. In 2010 more detailed informations about the construction became available. New estimations based on this knowledge will be carried out.

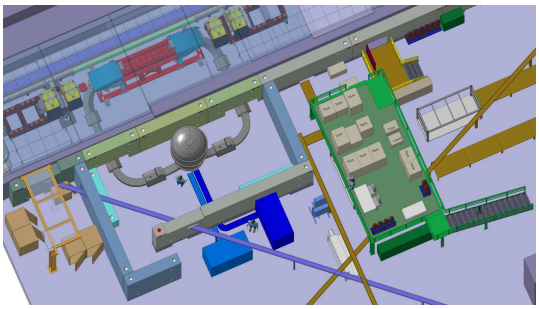

Fig 1: Artist´s view of the shielding and electron cooler installed inside the COSY-accelerator tunnel and inner hall.

Therefore the simulation geometry is enhanced with this more detailed data and a shielding concept is developed. Fig. 1 shows an artist's view onto the electron cooler installed in the COSY-accelerator as well as the concrete walls for shielding. A special task is the entrance door and the concrete roof which are not shown in this picture. Again we simulated the expected radiation field around the electron cooler. Different loss scenarios are looked at, e.g. point wise loss of the full electron beam as well as losses along the beam path. Inside the shielding the dose rate rises up to some Sv/h.

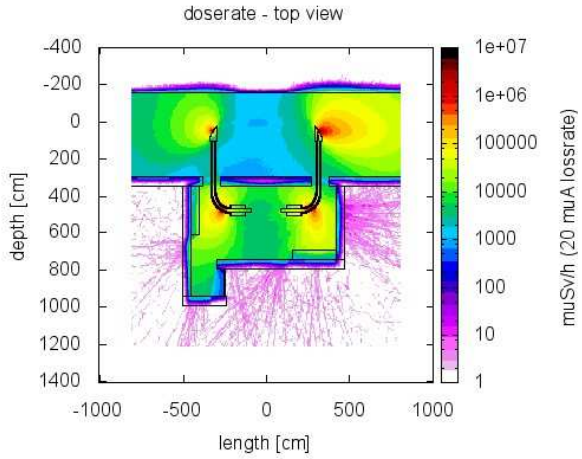

Fig 2: Dose rate around the electron cooler in case of 20µA-lossrate. The losses take place in the 90°-bendings.

Outside of the 50 cm concrete shielding walls the dose rate is reduced mainly to values below 3 µSv/h. Some small areas show dose rates up to 6 µSv/h.
In autumn 2010 the electron cooler was presented to the safety board of COSY (SAEB). Here, all aspects regarding safety e.g. electricity, pressure-tank, handling of the pressurized SF6-gas as well as radiation safety will be inspected. All presented measures to enhance the safety fulfill the requirements of the board. However the board pointed out the necessity of the roof shielding due to super positioned radiation fields from the different facilities of the Research Center. They result from dose rates outside the FZJ-Campus via sky shine which must not exceed 1mSv/year.

References

[1] Radiation Protection, IKP Annual report 2009
[2] FLUKA code: Description and benchmarking", G. Battistoni, S. Muraro, P.R. Sala, F. Cerutti, A. Ferrari, S. Roesler, A. Fasso`, J. Ranft, Proceedings of the Hadronic Shower Simulation Workshop 2006, Fermilab 6--8 September 2006, M. Albrow, R. Raja eds., AIP Conference Proceeding 896, 31-49, (2007)
[3] "FLUKA: a multi-particle transport code", A. Fasso`, A. Ferrari, J. Ranft, and P.R. Sala, CERN-2005-10 (2005),INFN/TC_05/11, SLAC-R-773
[4] Strahlenschutzverordnung vom 20.07.2001

Status of the 2 MeV Electron Cooler for COSY/HESR

J. Dietrich, V. Kamerdzhiev, V.V. Parkhomchuk[1], V.B. Reva[1]

The 2 MeV electron cooling system for COSY-Juelich was proposed to further boost the luminosity in presence of strong heating effects of high-density internal targets. The 2 MeV cooler is also well suited in the start up phase of the High Energy Storage Ring (HESR) at FAIR in Darmstadt. It can be used for beam cooling at injection energy and is intended to test new features of the high energy electron cooler for HESR. The design and construction of the cooler is accomplished in cooperation with the Budker Institute of Nuclear Physics in Novosibirsk, Russia.

The project is funded since mid 2009. Manufacturing of the 90% of the cooler components was completed by the end of 2010 at BINP. Figure 1 show the assembly of the cooling section solenoid and the toroids. The space required for the 2 MeV cooler was made available in the COSY ring. Beam instrumentation and the cavity were moved to another place in the COSY ring. Cabling and water cooling pipes were moved, to make space for the electron beam transport channel available.

The high voltage vessel, the oil cooling system vessel, the SF6 gas system and the main power supplies were ordered from German companies. The corrector power supplies designed and manufactured by BINP are being tested.

Fig. 1: Cooling section with toroid.

The requirement on straightness of the longitudinal magnetic field inside the cooling section is very high ($\Delta B / B \leq 10^{-5}$). To satisfy this requirement the solenoid of the cooling section is assembled from numerous short coils (pancakes). To achieve the required field straightness the angles of individual pancakes are adjusted mechanically. For better compensation of transverse components of magnetic field generated by current leads, two types of coils with opposite direction of winding are used in this cooler (in contrast to previous coolers EC-35, EX-300, LEIR). Such an arrangement allows cancelling out of some transverse components of magnetic field.

The core of the cascade transformer is made of amorphous iron with small power losses for 20 kHz (in iron and winding 180 W/cascade). The 33 cascades will be installed in a vertical column so that each core will correspond to high voltage section (shown in figure 2). Transformer oil circulated along transformer is used for cooling and isolation.

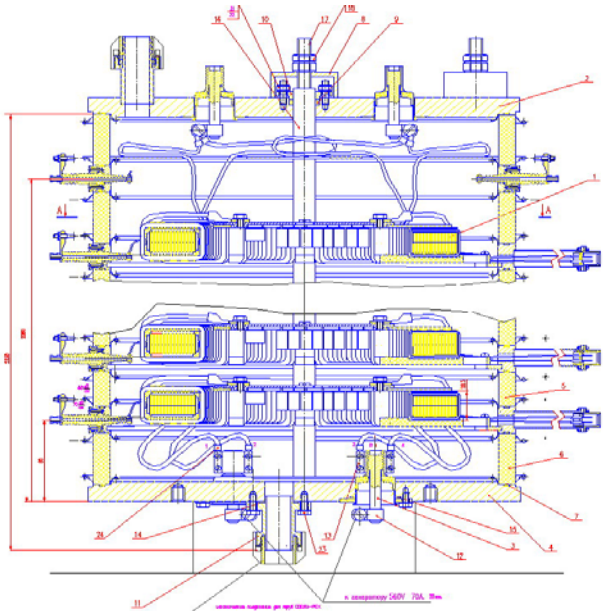

Fig. 2: High power cascade transformer.

Figure 3 shows the test bench which is being prepared at BINP for commissioning of the cooler with electron beam.

Fig. 3: High voltage vessel, preparation of the test bench.

The manufacturing of the cooler components is nearly complete. Electron beam commissioning is being prepared at BINP. The design of additional radiation shielding for the cooler is complete. The process of radiation shielding approval by the authorities is initiated.

Acknowledgements

The authors would like to thank the members of the project teams at BINP, Novosibirsk and at Forschungszentrum Jülich for their cooperation and extensive support of the project.

References:

[1] Conceptual Design Report, Novosibirsk 2009
[2] J. Dietrich et al., Progress with the 2MeV Electron Cooler for COSY Juelich/HESR, RuPAC 10, pp 147-150

[1] BINP Novosibirsk

BARRIER-BUCKET OPERATION AT COSY FOR HESR

R. Stassen, M. Böhnke, P. Brittner, F.J. Etzkorn, G. Schug, H. Singer

Abstract

The promising results of the first HESR barrier-bucket cavity installed at COSY lead to a routine operation of the cavity during several experiments to compensate for the mean energy loss. Meanwhile, one prototype of the FAIR 2kW solid-state amplifier has been installed and a lot of measurements have been carried out. An increase of the available barrier-bucket (BB) voltage seems feasible. A FAIR beam-time has been used to extract the beam with the BB cavity. First results show that the USE kicker can be substituted by the BB cavity and an additional HESR test place could become available.

2kW solid-state amplifier

Many RF driver amplifiers will be used at the FAIR project for different RF cavities. The GSI RF-group decided to use only one type of multipurpose amplifier to minimize the costs and number of different amplifiers. A prototype of this amplifier was installed at the barrier-bucket cavity and successfully tested during different machine runs where a barrier bucket was needed.

Table 1: Main parameters of the GSI driver amplifier

Frequency range	0,3...6MHz
Amplifier type	Solid state
Input impedance	50Ω
Output impedance	50Ω
VSWR @ output	Better than 2
RF power	2kW
Groupdelay variation vs. freq	+- 2ns (3°@5MHz)
Groupdelay variation vs. power	+- 3° (50W to max power)

The amplifier fulfils all requirements in the acceleration/decceleration mode and bunch rotation, but for the barrier-bucket operation the amplifier needs some modifications. Although the frequency range is not specified higher than 6MHz we operated the amplifier already up to 10MHz. This is essential for accumulation in the HESR because a 10% barrier bucket is needed built up by 20 harmonics. The amplifier had been optimized for a flat phase response over the whole frequency range and power range. This flat phase is not needed in any operation mode of the HESR. Thus an amplifier optimisation according to the power could help to increase the agreement with the HESR requirements. The cavity mismatch and the non-sinusoidal waveform of the BB signals lead to an early safety shutdown of one module. Nevertheless we reached already a BB voltage of +/-250V, which should be sufficient to compensate for the mean energy loss caused by gas- and cluster-targets. In the case of the new cavity design [2] the mismatch will be much smaller. So, we expect to get an accelerating tension of around 1kV using the 2 kW amplifier and a suitable scheme of power dividing.

USE-Kicker

The ultra-slow extraction system (USE) makes use of RF-noise pattern around one harmonic to shape the beam and to move it slowly into a betatron resonance. A ferrite loaded structure is used based on the CERN LEAR kicker with several modifications to reach the desired broadband behavior [1].

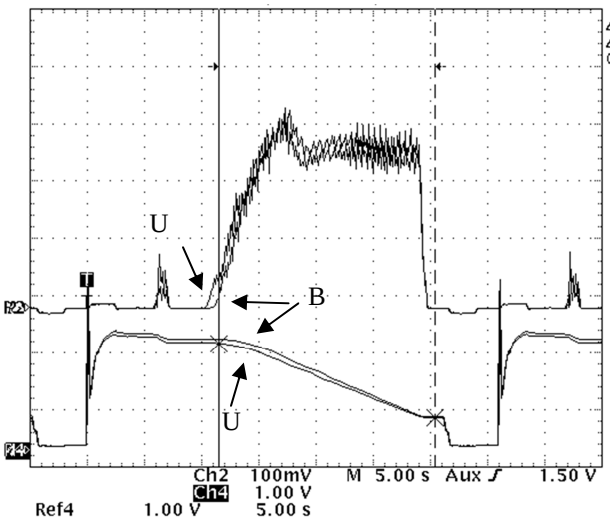

Fig. 1: Ultra-slow extraction in COSY: upper trace: extracted beam (signal of ionization chamber), lower trace: circulating beam (BCT signal), U: USE ferrite kicker, B: BB cavity as kicker

An extraction beam time (CBM) during one HESR week was used to test the BB cavity with the powerful 2kW amplifier as extraction kicker. We prepared COSY for spill measurement using both the standard USE kicker and the BB cavity with the same noise generation system, but different power amplifier: a 500W ENI at the USE and the above 2kW amplifier at the BB cavity. The spill analyses of the first ionisation-chamber in the extraction beam line show that the same extraction pattern was reached by the BB cavity with much lower RF power because of the higher cavity impedance. More particles per second can thus be extracted with noise at a higher harmonic avoiding the nonlinearities of the noise system often found due to the high driving power needed at the old USE kicker. We shall test the BB cavity at different energies, and if we meet the performance using the USE kicker, we shall remove that and gain a free space in COSY to install the new HESR cavity. So, we shall scrutinize the HESR cavity under real beam conditions both at acceleration and at BB operation.

References

[1] F.-J. Etzkorn, G. Heinrichs, S. Papureanu, A. Schnase, H. Stockhorst, Development of the USE System, IKP Ann. Rep. 1994, Jül-3035, pp. 219-220.

[2] R. Stassen, M. Böhnke, P. Brittner, F.-J. Etzkorn, G. Schug, H. Singer, Redesign of the HESR RF-system, this Annual Report

REDESIGN OF THE HESR RF-SYSTEM

R. Stassen, M. Böhnke, P. Brittner, F.J. Etzkorn, G. Schug, H. Singer

Abstract

The discontinuation of the RESR in the first construction phase of FAIR leads to the requirement to accumulate the anti-protons in the HESR. Different scenarios have been simulated and analyzed. The necessary complete redesign of the RF-system has been done, switching to forced air cooling, changing the coupling to use only solid state amplifiers and modification of the low-level RF (LLRF) to synchronize the CR with the HESR RF-system.

The Collector Ring CR delivers 1E7 antiprotons every 10 sec. The analysis of the beam-parameters, geometrical emittances and time structure shows as a possible solution the use of the barrier-bucket system together with the stochastic cooling to accumulate antiprotons in the HESR [1]. A moving barrier bucket will create a gap into the HESR beam, which is long enough for the kickers' rise-and-fall time plus the beam length of the CR beam. After injection of the new beam into the gap, the barrier-bucket system is switched off and the dissolved beam can be cooled by the stochastic-cooling system for about 9 sec before the next injection from the CR takes place. If the gain of the stochastic cooling system is adjusted according to the accumulated beam, the efficiency of the stacking can be hold very high till 1E10 antiprotons are reached after 1000 injections [2].

LLRF changes

The new accumulation scheme in the HESR requires a bunch synchronized operation. Thus the LLRF-system has been changed (Fig. 1).

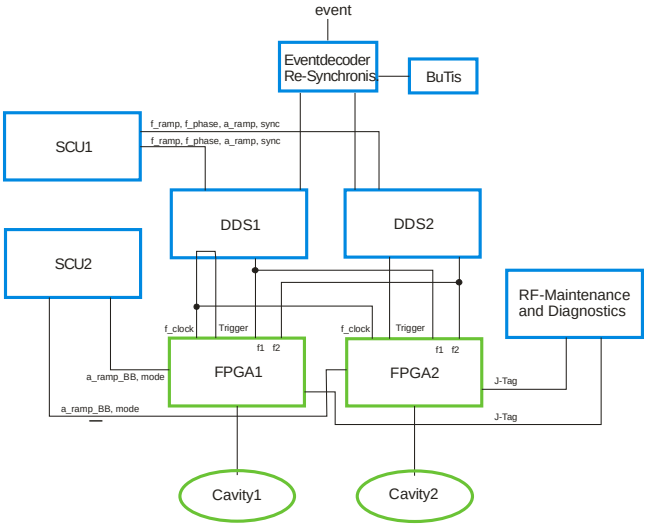

Fig. 1: LLRF for accumulation in the HESR: SCU1, SCU2 standard control unit; DDS1, DDS2 direct digital synthesizer, FPGA1, FPGA2: field programming gate array based system for BB-signal generation; BuTis: bunch phase timing system.

The two DDS (direct digital synthesizer) can be resynchronized by an event. This allows a precise phase adjustment according to the CR RF. The rectangular signal output will be used as clock for both FPGA systems. This clock will be internally phase-locked to generate the sampling rate for the pre-distorted BB-signals.

Each trigger at the trigger-inputs will start the pre-distorted BB signals saved in files. A phase ramp at the second DDS moves the BB signal of cavity 2 with respect to cavity 1 and creates the desired gap in the beam. Additional mode-switches allow both cavities used for acceleration and deceleration in single or dual harmonic operation. The design-work of the FPGA systems will start in 2011 in collaboration with the ZEL. These systems will be based on the FPGA solution done during the DIRAC phase [3].

Cavities

We increase the voltage at moderate RF power by changing the cavity cooling from water to forced air cooling.

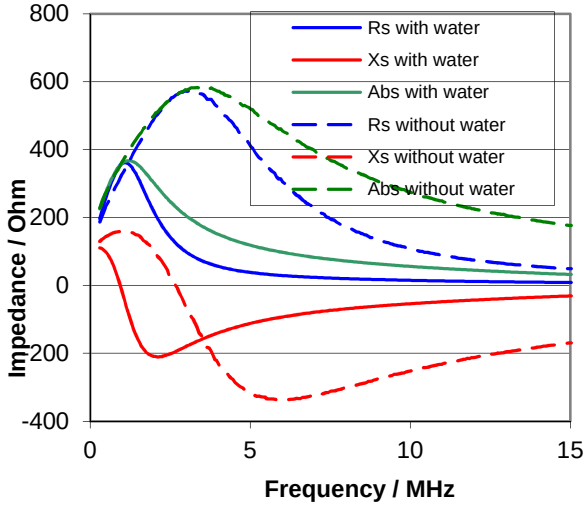

Fig. 2: Low-level impedance of prototype cavity before after filling with cooling water; magnetic core material: resin-impregnated Vitroperm, size of ring cores: ∅200x∅400x25mm, number of rings:6.

The advantage of using air cooling instead of water cooling is reflected in Fig. 2 [4]. The first prototype of the HESR accelerating cavity – designed and constructed under the DIRAC program – was measured before and after filling with cooling water. The impedance of the cavity decreased especially at higher frequencies that are important to create a high BB signal. The cores need a coating when the cavity is water-cooled. This coating influences the impedance of the cavity and will reduce the available voltage at a given RF power. Thus the uncoated material Vitroperm800F has been chosen. The pressurized air will be dried to prevent the material against humidity.

Both cavities will be identical now and driven by solid state amplifiers (Table 1). Each cavity consists of one gap and two tanks operating in push-pull mode. Each tank will house 6 ring cores of Vitroperm 800F. Each ring will be separately coupled and fed through the outer conductor. This coupling scheme shows the following advantages:

- The combination of two cores connected to one amplifier gives the best matching condition for all operation modes.
- The rings will only be selected in pairs.
- The influence of the parasitic elements of the rings is reduced. The individual compensation of the rings lead to a higher bandwidth compared to the usual gap coupling. Further, series compensation has the higher bandwidth.

This merits make allowance of more complex and somewhat longer tanks.
The impedance parameters shown in Table 2 have been estimated for the accelerating power level in opposition to the measured curves in Fig.2 which are at mW-level. The impedances at the operating conditions have been interpolated using curves given for low level and for B=0.1T ([5], [6], [7], [8]) with the aid of a frequency-dependent threshold B field. The nonlinearity of the permeability starts at that threshold and affects the real and imaginary parts in the same manner. Our phenological model nearly fits at cores that had been annealed in a transverse magnetic field and are not impregnated with a resin. This material has the lowest nonlinearity.
Fig. 3 shows the significant parts of the HESR cavity. The size of the ring cores has been chosen to be the same as the largest standard ferrite rings at the frequency range of 0.5 to 10MHz. Also, this size is favourable for winding the ring cores. The choice of 12 ring cores per cavity leads to a moderate dissipated power in the rings even at 2.5 kV. So the rings will be air cooled at only one of the front sides of them by air-jet disks. These disks contain radial 0.5mm slots as jet orifices. These slots are separated by 22.5° near the inner diameter because the largest power-loss density is located here. An air velocity of 50m/s causes a turbulent air flow instead of a laminar flow in order to reach a higher heat transfer rate. The boundary layer contributes the largest portion to the heat-transfer resistance between the power dissipation and removing. We have estimated this rate by scaling air jets measured and calculated in the literature of fluid dynamics and heat transfer, especially [9], [10], [11], [12] and papers cited herein. The temperature of each ring core will be surveyed at the inner diameter and will be kept well below 120°C. So, the pulsed operation at accelerating tensions over 2kV will be secured.

Table 1: HESR RF stations

No of cavities	2 (identical cavities with common LLRF to allow a moving barrier-bucket operation)
HESR revolution frequencies	440 kHz … 520 kHz
Frequency-range	1-20 harmonics (0.4 … 10 MHz)
Gap voltage: Accumulation Acceleration Experiment	 +/- 2500V Barrier-Bucket, f_{BB} ~ 5MHz, pulsed (1:10), moving barrier by second cavity +/- 1000V dual harmonic, CW +/- 1000V Barrier Bucket, f_{BB} ~ 2.5MHz, CW
Amplifier	12x 1 kW solid-state amplifiers

A first prototype is scheduled in 2011. The design allows an operation at the HESR as well as at COSY. Thus all operation modes can be tested with beam at COSY [13].

Table 2: Parameters of the HESR cavities

max. CW gap tension per cav. max. duty cycle at 2.5kV	2 kV 50%
Fitting length	approx. 1.2 m per cavity
No of gaps per cavity No of tank per cavity	1 2
No of ring cores per cavity Magnetic Material of ring cores size or cores	12 Vitroperm 800F, not impregnated ∅200x∅500x25mm
Series resistance per ring at accelerating level at h=1 at h=2 at BB level at h=1-2 at h=4-16 series compensation condenser at acc. level, h=1 h=2	 90 Ω 120 Ω ~ 150 Ω ~ 200 Ω 4.5 nF 2 nF
max. averaged loss per ring max. temperature of ring cores max. temp. spread within a core max. thermal time constant of cores	125 W 90°C 25K 2 min
Cooling of cores No of air jet disks per cavity Air velocity at jet outlets Air flow per cavity Air-pressure drop at parallel cooling	Forced air 6 50m/s 600l/s ~ 1 bar

References

[1] H. Stockhorst, HESR accumulation of antiprotons, 29th consortium meeting, 2010
[2] T.Katayama, Stacking of 3 GeV Pbar Beam in HESR with Use of Barrier Bucket and Stochastic Cooling, internal report, 2010
[3] G. Schardt, Entwicklung und Aufbau eines arbiträren Funktionsgenerators zur Ansteuerung einer Hohlraumresonanz, Diplomarbeit FH Jülich, 2008
[4] A. Schnase, M. Böhnke, F.-J. Etzkorn, U. Rindfleisch, H. Stockhorst, preparing a broadband cavity for installation at COSY, IKP Ann.Rep., Jül-3744, 1999
[5] G. Herzer, nanocrystalline soft magnetic alloys, Handbook of Magnetic Materials, Vol 10, pp.415-462, 1997 (Ed. K.H.J. Buschow)
[6] G. Herzer, softmagnetic materials – nanocrystalline alloy, Handbook of Magnetism and Advanced Magnetic Materials, Vol. 4, pp 1882-1908, 2007 (Ed. H. Kronmüller, S. Parkin)
[7] J.Petzold, Applications of nanocrystalline soft magnetic materials for modern electronic devices, Scr. Mat. 48, pp 895-901, 2003
[8] J. Petzold, Advances of soft magnetic nanocrystalline materials for modern electronic applications, JMMM 242-245, pp 84-89, 2002
[9] H. Schlichting, K. Gersten, Grenzschicht-Theorie, 10th Edition, Springer, 2006
[10] H. Recknagel, E. Sprenger, E.-R. Schramek, Taschenbuch für Heizung und Klimatechnik, 72th Edition, Oldenburg, 2005
[11] E. Truckenbrodt, Fluidmechanik, Vol I, II, Springer, 1992
[12] H. Gröber, S.Erk, U. Grigull, Die Grundgesetze der Wärmeübertragung, Springer, 1963
[13] R. Stassen, F.J. Etzkorn, R. Maier, D. Prasuhn, H. Stockhorst, L. Thorndahl, COSY as ideal test facility for HESR RF and stochastic cooling hardware, PAC09, Vancouver 2009.

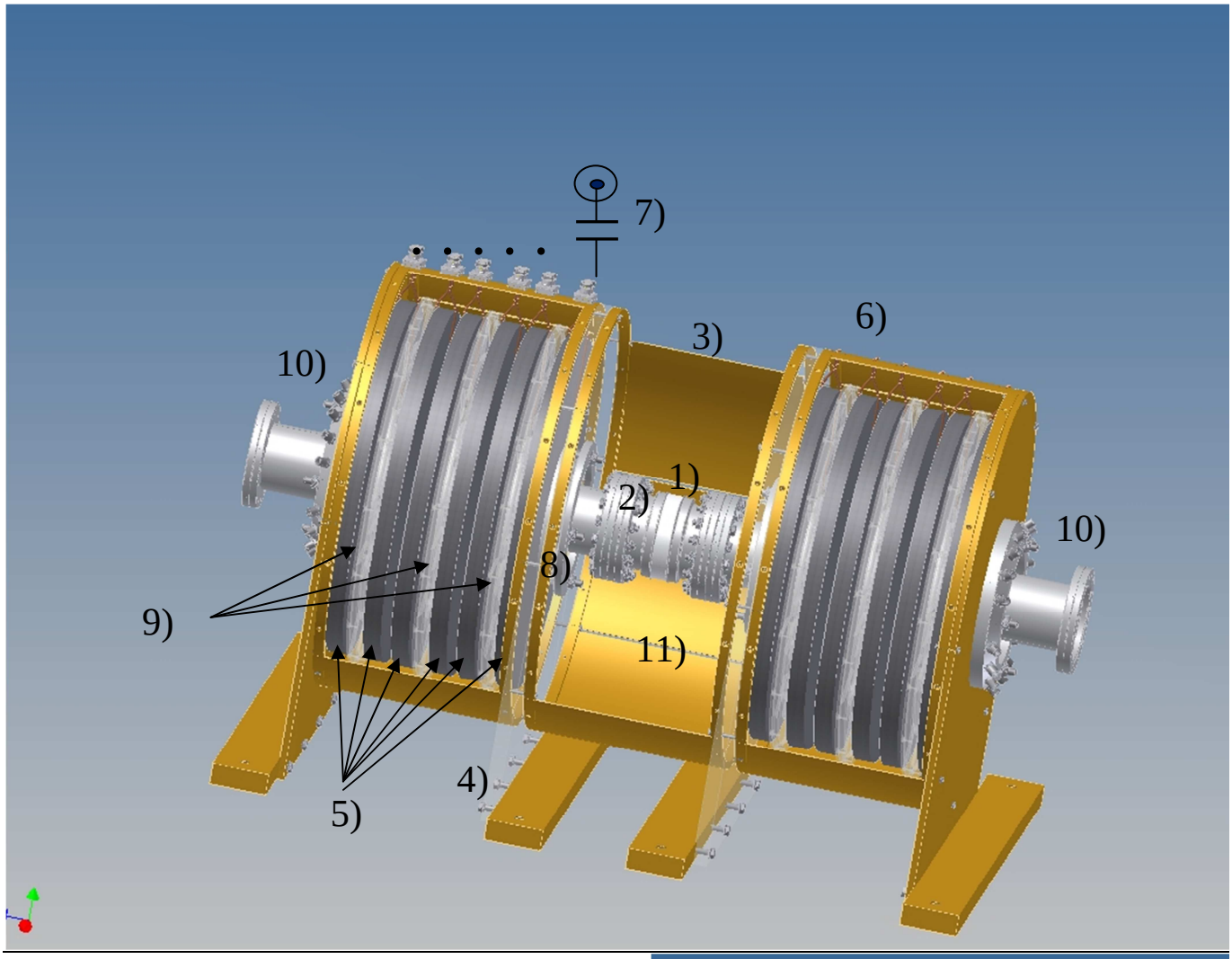

Fig. 3: redesigned HESR-cavity, housing partly removed:

1) Accelerating gap
2) Inner conductor and beam pipe
3) Outer conductor and housing
4) Support plate (PMMA)
5) Ring cores (Vitroperm 800F, uncoated)
6) Coupling loops
7) Series compensation condensers and signal ports
8) Core bearing (PMMA) including pressure-air channels
9) Air-jet disks containing air distribution and plane-jet orifices
10) Cooling air inputs
11) Cooling air outputs

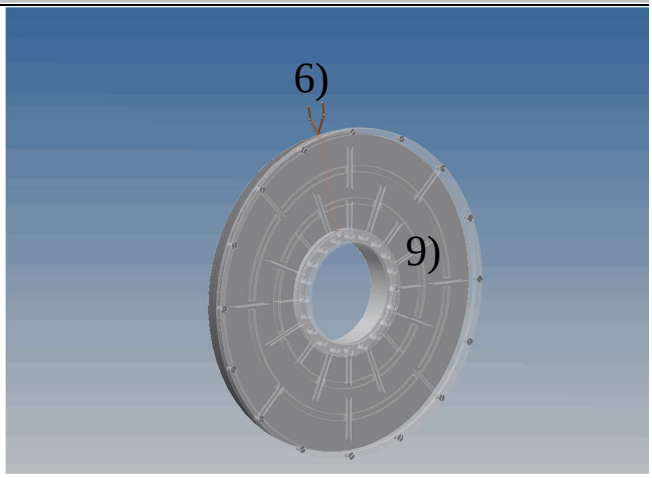

RECENT DEVELOPMENTS of the HESR STOCHASTIC COOLING SYSTEM

R. Stassen, M. Böhnke, P. Brittner, F.J. Etzkorn, G. Schug, H. Singer

Abstract

Besides the main 2-4GHz stochastic cooling system an additional system at 4-6GHz is needed to fulfill the experiment requirements. Simulations have shown that this system is only needed to support the longitudinal cooling. The higher frequencies required at least 12 electrodes instead of 8 used for the 2-4GHz system. 12 combiner-boards around the structure are no longer mountable. Thus the electrodes and the ring design have been changed that 2 electrodes will already be combined within the structures.
The longitudinal cooling systems need notch-filters with very high accuracies. Further improvements to compensate for the temperature behavior of the optical notch filter have been reached.

4-6GHz Structure

Based on the good results of the 2-4GHz system [1], a similar design for the 4-6GHz structure was chosen. Simulations have shown that the longitudinal coupling impedance of the 4-6GHz structure is much lower than that of the 2-4GHz one [2]. While the 2-4GHz structure has an impedance of $Z_k \sim 36\Omega$ constant over the whole frequency band, the impedance of the 4-6GHz structure decreases from about $Z_k \sim 27\Omega$ at 4 GHz down to $Z_k \sim 6.5\Omega$ at 6 GHz. A part is compensated by the smaller dimension in beam direction. 80 rings instead of 64 in the 2-4GHz system can be installed in the same tank. The lower sensitivity is tolerable because only the longitudinal cooling in the 4-6GHz range is needed [3]. Two electrodes are already combined within the structure to reduce the number of combiner-boards (Fig.1).

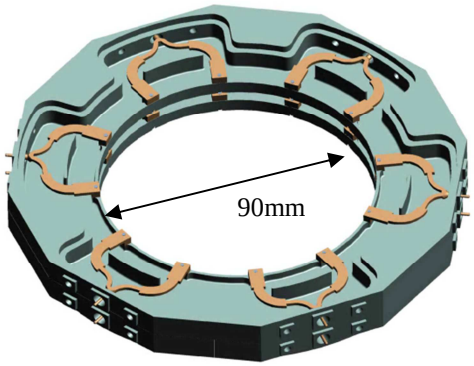

Fig. 1: 4-6GHz slot-ring structure with combined electrodes

Although this double electrode is a complicate 3d device, the fabrication was possible with moderate costs and adequate tolerances. The combination of the rings is similar to the 2-4GHz design. Each structure is closed by the next ring which gives the ground of the microstrip electrodes. Special mechanical tolerances guarantee the desired ground connections of the rings.
Wilkinson-combiner boards couple 16 double electrodes in beam direction (Fig.2). The higher frequencies and less space required the use of board-material with higher ε_r. A compromise was necessary for a correct phase combining at injection energy and a feasible fabrication of the combiner board. The remaining phase error is in the order of 10%.

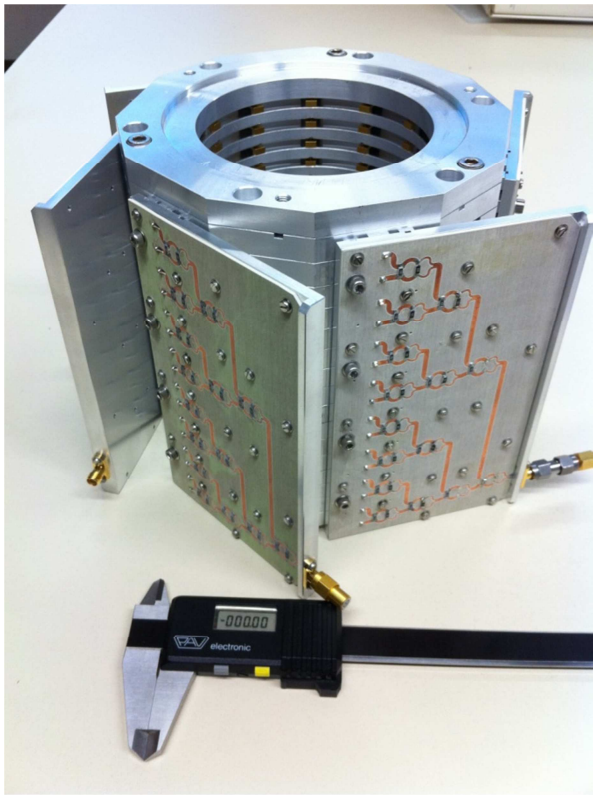

Fig. 2: Picture of 4-6GHz structure with installed combiner boards.

The first measurements show great resonances above 4.8GHz (Fig. 3). The 33mm inner conductor of a 31/8" RF transmission line has been used to measure the longitudinal sensitivity.

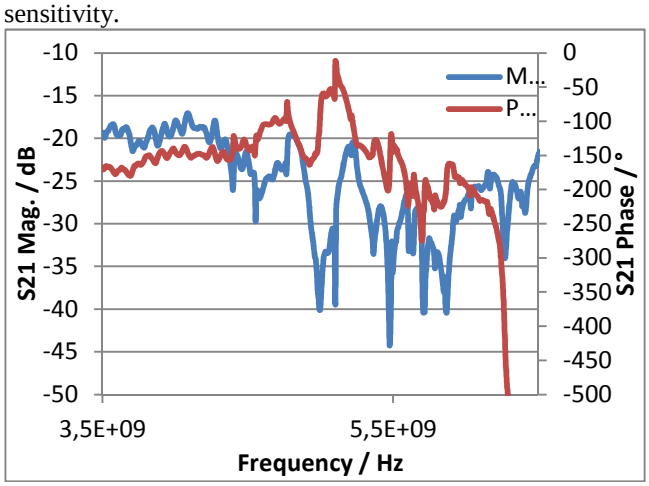

Fig. 3: Transmission from N-norm transition of beam simulating 33mm conductor to one combiner board.

We get a 60 Ohm coaxial system together with 90mm inner diameter of the structures. Both ends of this system are completed by commercial 3 1/8" to N-norm transitions. We performed the TEM measurement feeding one transition and terminating the other one.
An the moment, we are preparing different additional measurements to classify the reason for these resonances. Different sources are possible like the measurement setup with commercial transitions. These are nominally used for frequencies up to several hundreds of MHz. Additional

modes are propagable not only in the beam pipe but also within the structure. The beam aperture of the slot-ring structure resembles a corrugated waveguide in the beam direction. The multipole E modes particularly interact with the electrodes, and the cut-off frequencies are commensurably lower compared to an undisturbed pipe (4, 4.2 and 4,7GHz at the E11, E12 and E13 modes). In the nonevanescent state, this interactions weaken the coupling impedance (the effect of the H modes is scarcely pronounced). So, we are now developing measures against the propagation of these modes.

Optical Notch-Filter

The principle of the notch filter for the HESR is shown in fig. 5. Similarly to the COSY design, both signal paths will operate in the optical range. This eliminates phase noise and amplitude variation from the laser. The fluctuations of each notch frequency over the time must be within 0.5 Hz. The main source for such changes is the high temperature sensitivity of the fibre-optic delay line. An active temperature control of the coil can only minimize the temperature dependence, but not additional sources and is limited by the achievable precision of the temperature control. That's the reason why for the HESR the following control system has been chosen (Fig. 5):

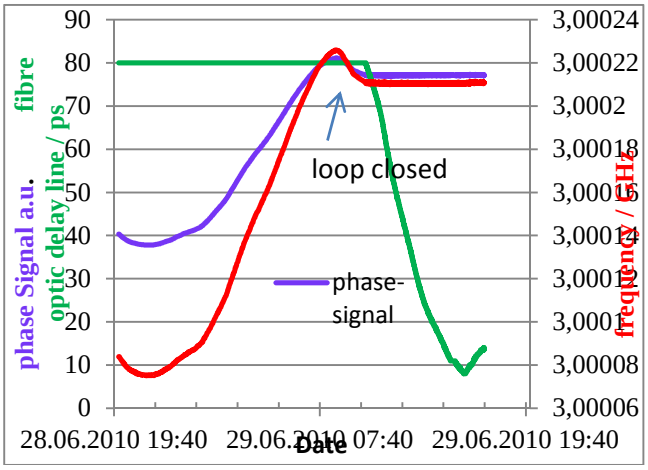

Fig. 4: Frequency change (red) of the 7100th harmonic of the first HESR notch-filter during one night (left part) and after closing the control loop.

Besides the signal from the pickup (In), a fixed frequency pilot signal will be added and transmitted through both optical paths. Directional couplers after the photo-detectors take band-pass-filtered parts of the transmitted signals to a phase detector. Any differences between the lengths of the two signal paths and thus any change of the notch frequencies will be detected by the phase detector. The controller closes this active loop by driving the fibre optic delay line according to the phase change of the pilot signal.

The drift of the 7100th notch frequency over one night is shown in the left part of Fig. 4. This corresponds to a change of the fundamental notch frequency of 25Hz during the night. This relates to a deviation of 5E-5, which is far too high for the required cooling. At 8:30 in the morning, the phase loop was closed and the frequency-change due to the day's warming up was completely compensated by the phase loop.

The length of the optic delay line (green curve in Fig.4) was changed by about 70ps (=21mm electrical length) during the day. The setting range of the used delay line is 560ps, thus one delay line gives enough margin for a full compensation.

A similar system can be used to control the optical fibre link from pickup to kicker either by sending a portion back via an additional fibre line or by using the BuTis (bunch phase timing) system to generate a phase stabile pilot signal at the kicker side.

Collaboration with ZEL and RWTH will start in 2011 to integrate the control loop into the photo-detectors and to optimize the amplitude and phase response of the receivers in the desired frequency range 2-4GHz and 4-6GHz. At least an amplitude accuracy of 0.5db and phase error of lower than 1° is needed over the whole frequency range to reach the desired notch depth of 35-40 dB.

Acknowledgements

We thank the ZAT for the aid at the design and fabrication of the slot-ring structure, especially Mr. R. Greven.

References

[1] R. Stassen, P. Brittner, R. Greven, H. Singer, H. Stockhorst, L. Thorndahl, Recent Developments for the HESR Stochastic Cooling System, IKP Ann. Rep, 2008.

[2] L. Thorndahl, 90mm Full-Aperture Structure with TM01-Mode Propagation for 4-6 GHz Stochastic Momentum Cooling in the HESR, internal report, 2010

[3] H. Stockhorst, T. Katayama, R. Maier, D. Prasuhn, R. Stassen, L. Thorndahl, Stochastic Cooling for the HESR at the FAIR Facility, PAC09, Vancouver, 2009

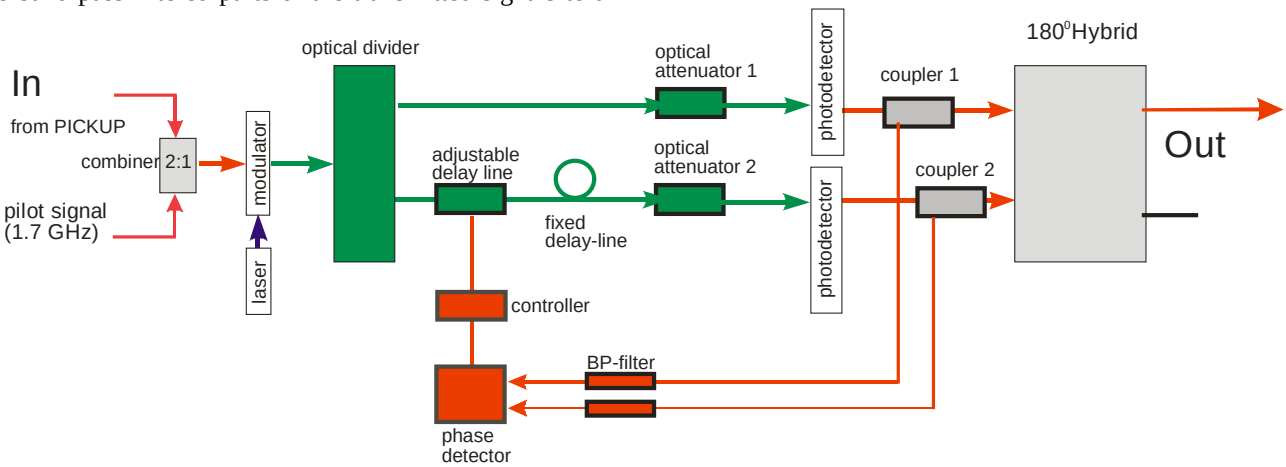

Fig. 5: Optical Notch filter with phase control loop.

An efficient threshold and noise extraction algorithm suitable for FPGAs

M. C. Mertens and J. Ritman

A silicon pixel detector's threshold and noise are typically characterized by recording the detection efficiency as a function of the signal amplitude. This data follows a characteristic S-curve and can be described by a Gauss error function. The common way to extract the threshold and noise is to fit the error function to the data, i.e. solving a nonlinear optimization problem. In the following, we present a novel method to determine the threshold and noise in a purely analytical way, suitable for an FPGA implementation.
The Gauss error function R which describes the detection efficiency as a function of the signal amplitude q is:

$$R\left(q\right) = \frac{A}{2} \cdot \left(1 + \mathrm{erf}\left(\frac{q-\mu}{\sqrt{2}\cdot\sigma}\right)\right) \tag{1}$$

with

- A the number of signal injections
- μ the threshold
- σ the noise

Fig. 1 shows a fit of this function to the response R recorded from an ATLAS FE-I3 frontend chip with μ and σ as free parameters (thick black line). The thin black line shows the binned data gathered from 200 charge injections per signal amplitude q. As can be seen, the data is indeed well described by Equation (1). The limits of the integral over the error function, used to derive the analytical parameter extraction method, are denoted by q_{min} and q_{max}.

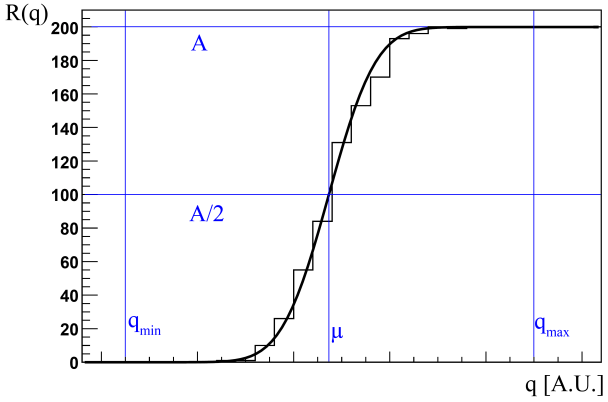

Fig. 1: Typical response function to repeated charge injection into a charge sensitive amplifier and discriminator as a function of signal amplitude.

A much more efficient approach is the direct calculation of μ and σ from the recorded data using Equations (2) and (3).

$$\mu = q_{\mathrm{max}} - \underbrace{\frac{q_{\mathrm{max}} - q_{\mathrm{min}}}{n}}_{=d=\frac{q_{n-1}-q_0}{n-1}} \cdot \frac{M}{A} \tag{2}$$

$$\sigma = \underbrace{\frac{q_{\mathrm{max}} - q_{\mathrm{min}}}{n}}_{=d=\frac{q_{n-1}-q_0}{n-1}} \cdot \frac{m_{\mu 1} + m_{\mu 2}}{A} \cdot \sqrt{\frac{\pi}{2}} \tag{3}$$

with

- q_0 the amplitude of the smallest signal injected
- q_{n-1} the amplitude of the largest signal injected
- n the total number of different signal amplitudes
- M the total number of responses
- $m_{\mu 1}$ the number of responses below threshold
- $m_{\mu 2}$ the number of missing responses above threshold

The derivation of Equations (2) and (3) is structured in two steps, which can only be sketched here. The full proof along with a detailed discussion of systematic errors is given in [1].
As the first step, the known definite integral over the error function is used to express the threshold and noise as functions of the integral with certain fixed limits between q_{min} and q_{max} (compare Fig. 1).
The next step is the expression of the integrals as sums over approximated step functions as done in Riemann's definition of the integral. Using this notation, the integral can be replaced by the sum over the individual bins.
Already a very simple test, carried out by implementing this method as a C++ macro within the ROOT framework, shows a speed advantage of a factor of more than 250 over the standard procedure of fitting the error function to the data.
At the same time, there is no drawback in accuracy compared to the fit method. Statistical errors on the input data affect both methods and are thus not discussed here. Given a not too large step size between the individual signal amplitudes (half of the noise to be measured or better, which is generally the case), the maximum relative systematic error on the threshold is less than 10^{-11}, thus neglegible. An equivalent discussion for the noise yields a maximum relative systematic error of less than 2%, which is well below the statistical errors which are typically achieved.
However, the main advantage of this method is that it is not only faster in software, but also feasible to be implemented in FPGAs. While the standard procedure would require the implementation of the whole nonlinear optimization problem, the method shown here only needs a small set of basic arithmetic operations. Such circuits can be implemented very efficiently and also allow online processing if the data is streamed through an FPGA-based readout system.

References:

[1] M. C. Mertens, Der PANDA Mikro Vertex Detektor, Dissertation, Ruhr-Universität Bochum (2010)

Characterization of a silicon pixel readout chip for the PANDA Micro Vertex Detector

D.-L. Pohl*, T. Stockmanns*, J. Ritman* for PANDA collaboration

The Micro Vertex Detector (MVD) is the innermost tracking subdetector of the future PANDA experiment and is necessary to detect secondary vertices marking the decay of open-charm particles. It consists of several barrel and disk layers of silicon sensors. The outer part is made of strip detectors and the inner part is made of pixel detectors. To cope with the requirements of a triggerless readout, a high data rate and a good spatial resolution, a new pixel readout chip is designed at the INFN in Torino named ToPiX.

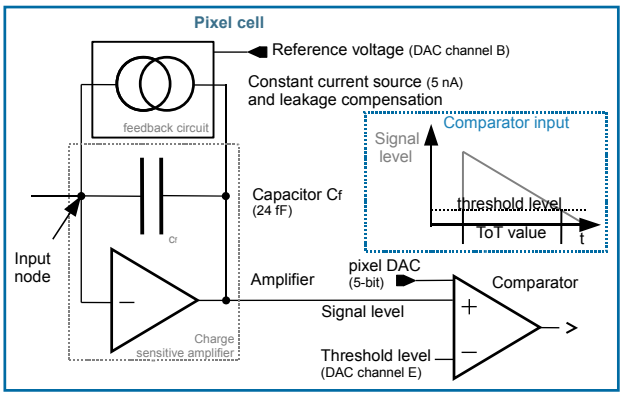

Fig. 1: Charge digitization circuit of one pixel cell.

Every pixel cell of the ToPiX has a charge sensitive preamplifier with a feedback capacitor that gets discharged by a constant current source leading to the signal shape shown in Figure 1. The amplifier is followed by a comparator that compares the charge signal with a fixed threshold voltage and changes its state when the signal level crosses the threshold level. The times when the comparator changes its state are stored into two 12-bit time stamp registers. The difference of these values is the so called Time-over-Threshold value (ToT) which is proportional to the charge deposited in the pixel. To decrease the threshold dispersion of the pixels, each pixel cell provides a 5-bit pixel DAC.

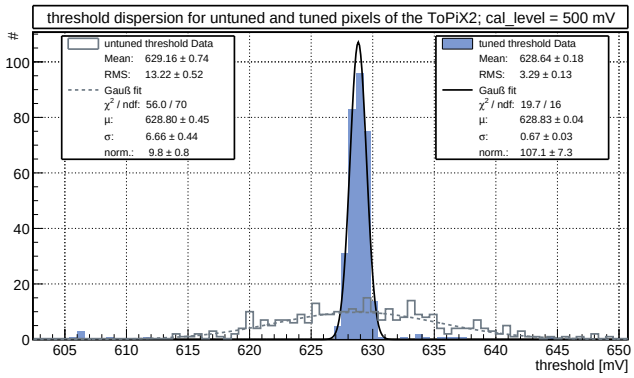

Fig. 2: Threshold distribution before (gray) and after (blue) threshold tuning for the 320 pixels of the ToPiX2.

In order to test readout chips for the MVD an FPGA based digital readout system was developed in Jülich and was used to characterize the second prototype of the ToPiX (ToPiX2). The noise of the 320 pixels of the ToPiX2 was measured. The result of an average noise value with 130 e is compatable with the requirements (< 200 e). The result for the threshold dispersion before and after threshold tuning can be found in Figure 2. The pixel DAC is able to reduce the threshold dispersion by a factor of 10 leading to a dispersion of the charge information to 100 e that is smaller than the noise of 130 e. Therefore the pixel DAC capabilities to match the threshold levels is sufficient.

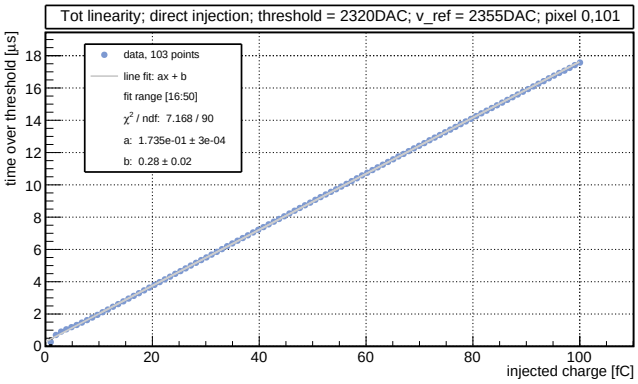

Fig. 3: Time-over-Treshold as a function of the deposited charge; linear behavior for charges > 5 fC.

Also the base line restoring, the Time-over-Threshold linearity, the amplifier gain and the discharging current were measured (Tab. 1). For the specified dynamic range up to a deposited charge of 100 fC the ToPiX2 showed a linear behavior except for charges below 5 fC (Fig. 3). There the discharging current is not constant leading to a nonlinear behavior between deposited charge and the ToT value. For the next prototype the gain will be doubled to increase the linear region down to lower charges.

parameter	**measured value**	**specification**
noise	130 e $\equiv^*$ 170 e	$<$ 200 e RMS
tuned threshold dispersion	0.67 mV $\equiv$100 e $\equiv^*$ 130 e	$<$ 200 e RMS
ToT linearity	$ToT = 173\frac{\text{ns}}{\text{fC}} Q_{\text{in}} + 300$ ns for $Q_{\text{in}} = 5 \ldots 100$ fC	linearity for $Q_{\text{in}} < 100$ fC
discharging current	5.7 nA *only one pixel measured*	5 nA
rising time ($t_{10\%,90\%}$)	$80-100$ ns const. for $Q_{\text{in}} > 5$ fC	100 ns const.
gain	$(32 \pm 3)\frac{\text{mV}}{\text{fC}}$	$41.5\frac{\text{mV}}{\text{fC}}$

*: left with specified gain / right with measured gain

Tab. 1: Measurement results for the ToPiX2.

All measured parameters of the ToPiX2 match the requirements for a deposited charge above 5 fC despite the gain that is about 25% lower than expected.
The new prototype ToPiX3 will be available in the second quarter of 2011. During the production process the next version of the digital readout system is being developed in Jülich and will also be used to characterize the ToPiX3.

* Institut für Kernphysik I, FZ Jülich GmbH, Germany.

Progress in the dE/dx particle identification method with the PANDA-type straw tube tracker

S. Costanza[1], W. Erven[2], P. Kulessa[2,3], R. Nellen[2], H. Ohm[2], D. Prasuhn[2], K. Pysz[2,3], J. Ritman[2], V. Serdyuk[2,4], P. Wintz[2], P. Wuestner[2]

The feasibility of the PANDA STT for the particle identification by the measurement of the specific energy losses was checked. The experimental investigation of the optimal detection conditions and parameters of the readout electronics were performed with the use of Sr-90 ß-source as well as with the mono-energetic proton beam of COSY.

In order to permit the off-line processing of the individual signals from the straw tubes and selection of the optimal analysis method the analog output signal from the straws have been recorded by means of fast (160 MHz and 240 MHz) flash ADCs.

The analysis shows that the best energy resolution is achieved when the so called truncated mean correction of the energy distribution is applied. With the truncation of 30 - 40 % of the highest energy losses composing the particle track the natural Landau distribution is replaced by a symmetric Gaussian and the obtainable sigma to mean ratio of the distribution approaches 10 % when all 16 straws fired (see fig.1).

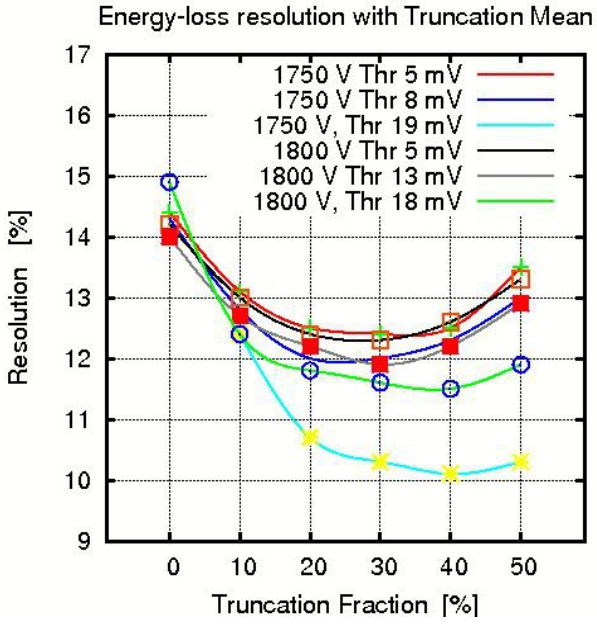

Fig. 1: Energy loss resolution obtained for various detection conditions and for the different truncation fractions of the energy spectrum.

Fast and straightforward analysis method, which tries to deduce the particle energy loss from the length of the output signals (so called time over threshold) occurred insufficient with the use of the applied readout electronics.

The tests were continued with the proton beam at the former area of the GEM experiment at BigKarl spectrometer, which was adapted as a universal place for testing of the experimental equipment.

The experimental setup, presented in fig. 2, consists of 128 straw tubes, 1500 mm long and of diameter equal to 10 mm, organized in 8 layers. 4 layers are readout by 240 MHz flash ADC whereas remaining signals are fed via CMP16 discriminator into the fast TDCs. External, precise tracking is done by a set of drift chambers and a small size (4 mm diameter) straw tube planar detector. Coarse tracking as well as the triggering is done by means of ensemble of scintillating detectors. A set of scintillators and position sensitive silicon strip detectors installed upstream serves as beam diagnostic.

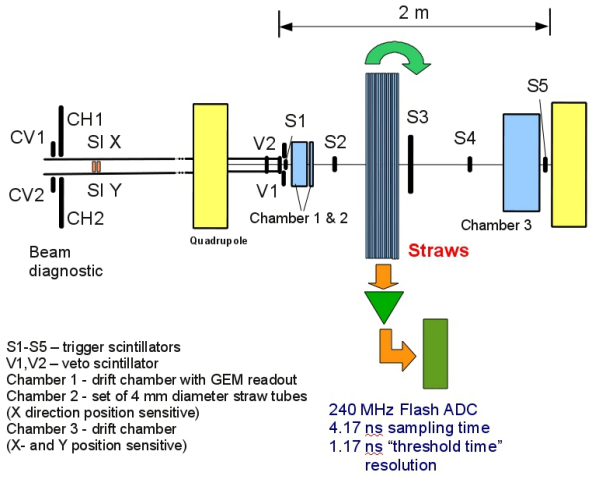

Fig. 2: Experimental setup for the test of the energy loss resolution of the PANDA STT prototype in the BigKarl area.

Beam of protons at momentum of 2.95 GeV/c was extracted and shot onto the detectors with up to 6000 particles per second. The beam was defocused in vertical direction in order to cover a broader region of the straw tracker. Sampled output signal waveforms of the STT were used both for building the truncated energy loss distributions as well as for the evaluation of the drift times. Despite of a limited precision of drift times measured in this way (4.17 ns), the full tracking based only at the response of STT was possible and the path lengths of the particles have been reconstructed. This allowed for the further correction of the measured energy loss distribution by normalization to the actual ionization distance of the traversing particles resulting in the obtained experimental resolution of dE/dx equal to 9 % for events when 16 tubes contributed to the reconstructed track. This result is very promising for the planned final PANDA STT, which will consist of 26 layers.

[1] INFN Pavia, [2] IKP-Juelich, [3] IFJ-Kraków, [4] JINR-Dubna

Supported by the FFE program of ICHP-FZJ.

Measurements at COSY with the Bonn beam telescope

S. Bianco[1], M. Becker[1], K.-Th. Brinkmann[1], R. Kliemt[1], K. Koop[1], R. Schnell[1], T. Würschig[1], H. G. Zaunick[1]

The Bonn PANDA MVD group has built a tracking station equipped with silicon strip sensors as a prototype for the future MVD realization. The tracking station consists of four layers of double-sided silicon strip sensors with an active area of 1.92 cm · 1.92 cm, a thickness of 300 µm, a pitch of 50 µm and 90 degrees stereo angle.
The tracking station is aimed for the characterization of detector prototypes and for the measurement of multiple scattering in material samples. It allows using different setups changing the longitudinal position of the sensors as well as the incident angle of the beam. A holding tool is foreseen in the center of the station as a support for scattering volumes.

Fig. 1: The Bonn tracking station set up at the COSY accelerator (Jülich).

Measurements at COSY were performed with two different beam momenta: 2.95 GeV/c and 800 MeV/c protons. Three volumes of carbon-based construction materials were placed on the trajectories of the particles:

- a 2 cm thick carbon scatterer with a density of ~ 1.70 g/cm^3;
- a 1 cm thick carbon scatterer with a density of ~ 1.79 g/cm^3;
- a carbon foil with a thickness of (0.65 ± 0.05) mm.

The scattering angle distribution was measured for all three scatterers as well as without using the high momentum proton beam.
These blocks of material were placed in the center of the tracking station so that it was possible to measure two hits in front of them and two downstream (see Fig. 2).

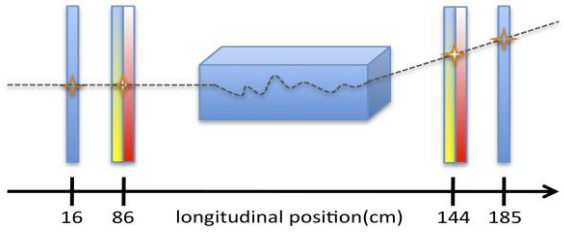

Fig. 2: The setup used to measure the scattering in the carbon volumes. One double-sided strip sensor and two single-sided ones were used both before and behind the volumes.

Results are summarized in Fig. 3, where the distributions of the projected scattering angles obtained at COSY are shown. The measurements are in good agreement with simulations of the setup performed with GEANT3.

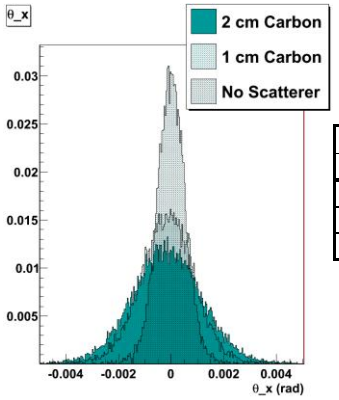

Scatterer	Data $\sigma(\theta_x)$ mrad	Sim $\sigma(\theta_x)$ mrad
None	0.532	0.000541
1 cm C	1.021	1.011
2 cm C	1.334	1.334

Fig. 3: Distributions of the projected scattering angles obtained with 2.95 GeV/c protons and different scattering volumes. The table shows a comparison with simulations.

A second test performed during this beam time regarded the effect of the rotation of one sensor. Changing the incident angle of the beam, the effective length of the track within a sensor becomes longer, so one expects that the energy loss increases with bigger rotations. This is what was measured in the range [5,45] deg, as shown in Fig. 4. The absolute energy loss values are obtained with a calibration based on MIP hypothesis.

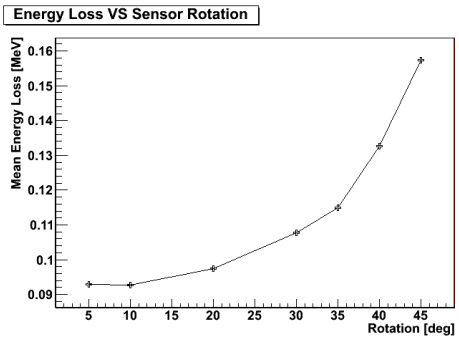

Fig. 4: The peak value of the energy loss distribution obtained in one sensor plotted as a function of the rotation angle of the sensor. These data were obtained with a 2.95 GeV/c proton beam.

Future measurements will complement the recorded data with the usage of lower momentum beams and with measurements of scattering in volumes of light carbon foam foreseen to be used for the MVD support structure.
Supported by BMBF(06BN9005I), JCHP FFE(41877498) and BCGS.

References:

[1] PANDA at the future GSI facility, K.-Th. Brinkmann, Nuclear Instr. Meth. A, 549 (2005)146-152.
[2] M. Becker et al 2011 JINST 6 C01008, doi: 10.1088/1748-0221/6/01/C01008
[3] The FAIR simulation and analysis framework, doi:10.1088/1742-6596/119/3/032011

[1] Helmholtz-Institut für Strahlen- und Kernphysik, Universität Bonn, Nussallee 14-16, 53115 Bonn, Germany

Antiproton-proton elastic scattering as a day-one experiment at HESR

H. Xu, J. Ritman, T. Stockmanns and T. Randriamalala for PANDA collaboration

PANDA will achieve more than an order of magnitude higher mass resolution than available at the B-factories by performing resonance and threshold scans with the phase space cooled antiproton beams. The cross section will be analyzed as a function of the nominal beam momentum, therefore the integrated luminosity must be determined with high precision. In order to determine the integrated luminosity with even higher precision than available from Schottky measurements of the HESR beam, a concept for a luminosity monitor based on measuring elastic scattering in the Coulomb-strong interference region has been developed. The detector will be located at about 10 m downstream of the target and will measure forward outgoing antiprotons which are emitted at an angle of 3-8 mrad with respect to the beam axis. The angle of the scattered antiproton will be reconstructed by measuring the track with 4 planes of silicon strip detectors. Figure 1 shows the layout of luminosity monitor of PANDA.

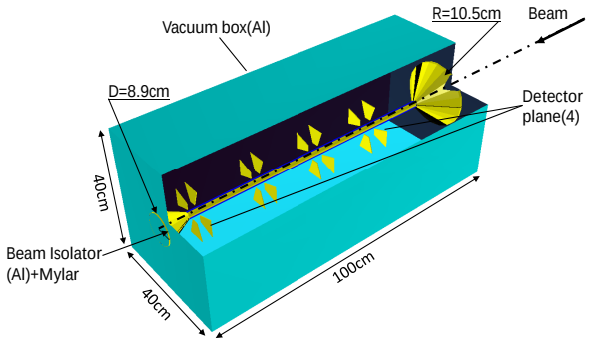

Fig. 1: Layout of PANDA luminosity monitor detector.

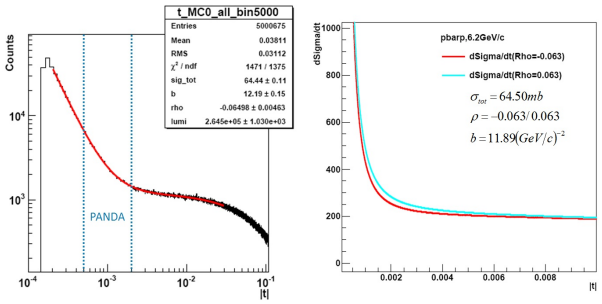

Fig. 2: Left: A large t-spectrum reconstructed using Monte Carlo information with ideal fitting; Right: Differential cross section as a function of t with different values of ρ.

With the conceptual design, a simulation to study the precision of the absolute integrated luminosity determination using DPM (Dual Parton Model) generator within PANDARoot framework has been performed. The 4-momentum transfer t distribution of antiproton-proton elastic scattering at momentum of 6.2 GeV/c has been plotted by using Monte Carlo information. By analyzing a large range of the t-spectrum not only the absolute luminosity, but also the relevant parameters (σ_{tot}, ρ and b) could be determined with good precision. The reconstructed t-spectrum with ideal fitting has been plotted in Figure 2 (left).

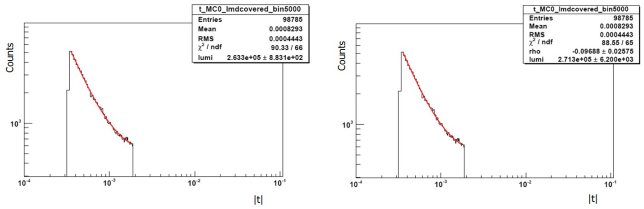

Fig. 3: Luminosity precision of 0.34% and 2.29% by fitting the t-spectrum with only the luminosity, and both the luminosity and ρ as free have been plotted in the left and right, respectively.

As marked by the dash lines in the left of Figure 2 the real luminosity monitor detector covers only a small part of the t-spectrum, therefore the absolute luminosity can not be determined with sufficient precision due to the strong correlation between parameters which shown in Figure 2 (right). It is expected to fix the parameters (σ_{tot}, ρ and b) when determining the luminosity. The comparison of the test fitting with only the luminosity and both the luminosity and ρ as free parameters has been plotted in Figure 3.

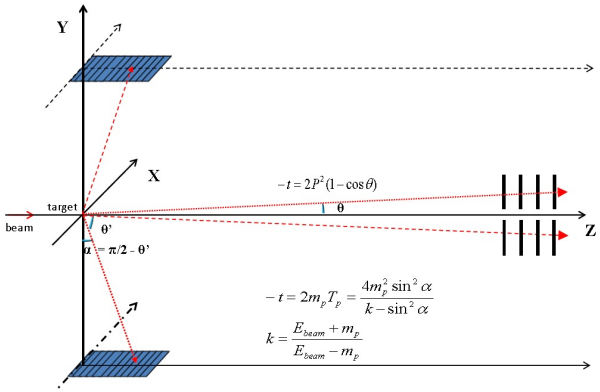

Fig. 4: One sketch of the day-one experiment with two arms.

In order to alleviate the lack of existing data on this system in the relevant momentum region, a "day-one" experiment at HESR dedicated to antiproton-proton elastic scattering has been proposed. Figure 4 shows a sketch of the general design of the "day-one" experiment. The goal of this experiment is to measure a wide range of t ($0.0008\text{-}0.1 GeV^2$) so that the contribution of the physical differential distributions to the absolute luminosity uncertainty will be less than 1%. The polar angle of the scattered antiprotons and the energy of the recoil protons will be measured at forward angles by tracking detectors and by thick energy detectors near 90°, respectively. The complete "day-one" experiment will be performed at HESR in its early running phase. The commissioning of the experiment equipment will take place with proton beams at COSY in the next couple of years.

Electronics Laboratory

C.Berchem, N.Dolfus, H.Metz-Nellen, R.Nellen, J.Sarkadi, H.Schiffer, T.Sefzick

The activities of the IKP Electronics Laboratory can be assigned to mainly the following three topics:

Electronics and Data Acquisition for experiments

In the course of development for the PANDA experiment which will be carried out at the upcoming HESR accelerator at GSI, front end modules for the MSGCROC based readout were built. For the STRAW detector several power supply and signal PCB concepts based on Kapton and FR4 were designed to meet the special requirements of this detector component as the central tracker of the experimental setup, at this novel contact systems were developed because nothing appropriate is available on the commercial market. First prototypes were tested successfully. The mechanical retaining system was modified. Support was given during assembly of the detector.

For the discriminators and preamplifiers of FPC setup at WASA power distribution printed circuit boards were built.

The control system of the atomic beam source at ANKE was checked for the next beam time and the process visualisation was modified. The new low voltage power supply system for the RAL electronics of the stop chamber has been built. Various adapter boards were designed, ordered, fitted with components, and tested.

At PAX the process visualisation program based on WinCC was updated. Control software for a DC motor rotational speed control was designed. The motor is used for moving the chopper device with adjustable speed, the action can be triggered by the COSY timing signal. This feature is needed to measure background and recombination. The atomic beam source (ABS), the Breit-Rabi polarimeter, and the target cell which had individual control systems have been integrated into a Profibus-DP based field bus system. The production of the new ADC modules for data acquisition—including material procurement, placement of order und receiving inspection—was undertaken.

New devices and vacuum pumps were integrated into the interlock system of the TOF experiment. A new process visualisation based on WinCC together with a new PLC based interlock has been programmed. The whole slow control system has been tested after these modifications and prepared for beam time. Multicoaxial signal cables were built.

A new crystal mount for the crystal spectrometer was designed and built. Control and visualisation of the rotating and tilting actuators were integrated into the existing system, tested, and calibrated.

At the ATRAP-II experiment the electronic lab assisted in maintenance and repair of the data acquisition system.

Furthermore, support was given for the WASA Simatic S5 PLC based slow control system and a slow control Simatic S7 PLC system in an IKP-2 laboratory.

COSY

New power supplies needed for steerer magnets at the beamline between source and Cyclotron were ordered and tested. A special requirement was that these units should be exact reproductions of already existing ones.

Computer network

At several locations the fiber based and wireless networks were extended. The latter now allows access to the secure, world-wide roaming access service ‘eduroam’ developed for the international research and education community. At the PAX experiment the network was setup. Frequent support was granted to ensure continuous operation of the existing networks.

Miscellaneous

Like every year substantial support was given with regard to short term maintenance and repair or replacement of electronics. In some cases the urgent demand didn’t allow a time consuming outside repair procedure, in other cases the manufacturer doesn’t even exists anymore, but the electronics can not be replaced easily, or the manufacturer was unable to perform the repair.

The standard data acquisition systems at several COSY experiments were taken care of to assure stable operation during several beamtimes. Moreover, the extension of the server system at the WASA experiment was supported.

The collaboration with the ZEL was coordinated for several experiments.

Regarding S5 and S7 systems continuous support was given to the experiments TOF and WASA, the radiation safety division, and to the cyclotron group.

Part time supervision of BSc and MSc students of the FH Aachen was provided in the fields of process automation and measurement.

In the context of the german-egypt collaboration two staff members travelled to Cairo to supervise and help setting the Simatic S7-300 PLC system used to control the Kepco power supplies of the cyclotrons magnetic coils into operation. Moreover, a second S7-300 system was setup in a laboratory as a platform for software development and training.

Maintenance of the existing IKP webpages and their transfer into the new ‘Government Site Builder’ based content management system is ongoing.

Administrative activities for the safety inside the institute were carried out. This included the organisation of safety walkabouts and the supervision that the resultant requirements are met. Maintenance and upgrading of the 100V-based public address system was cancelled, instead a new system will be installed. The mandatory electrical safety inspection of movable electrical devices done by an external service provider was coordinated and monitored.

How to solder Temperature Diodes

C.Berchem, N.Paul, H.Schiffer, T.Sefzick, J.Uehlemann

Silicon diode temperature sensors like these[1] used at the liquid hydrogen target at TOF and soon at PANDA are precise measurement devices but extremely sensitive to over temperature. Soldering must be done well below 200°C, otherwise one risks damage of the diode. Consequently, in addition to the choice of the appropriate soldering metal—the diode manufacturer recommends indium, which has its melting point at 156°C—a continuous monitoring of the soldering temperature is essential.

The diodes are soldered either to small copper plates which are then fastened to a cooled part at the cold head or to the surface of the target finger which consists of thin electroplated copper (TOF) or thin stainless steel (PANDA). The metal surface and the bottom side of the diode–which is insulated from the diode itself—need to be tinned with indium, after final cleaning both are soldered together. The problem is that the target finger surface leads to a large heat dissipation and so the heat source (soldering iron and/or hot air pencil) must produce much more heat at higher temperature than is needed for the soldering process which works best around 165°C. Thus a temperature monitoring is needed.

The best measuring device for this purpose is—the diode itself.

The voltage drop across the diode as a function of the temperature behaves according to the well-known 'Standard Curve 10', a non-linear curve which can be described by Chebychev polynomials.

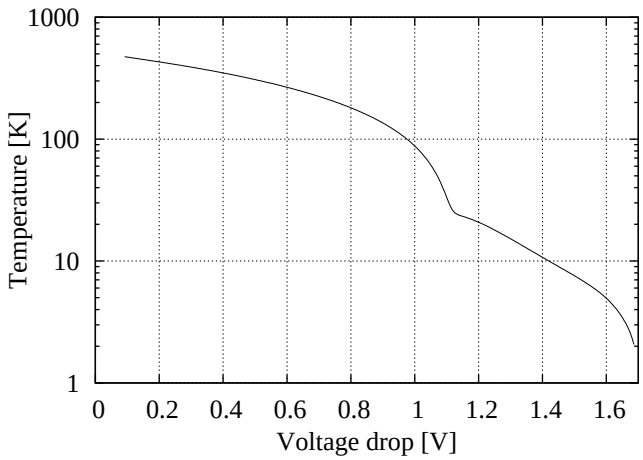

Fig. 1: Standard Curve 10: the relation between voltage drop accross a temperature measuring diode and the diodes temperature at 10μA measurement current.

Providing 10μA of measurement current is not difficult to do, a simple integrated current source[2] in standard application will do the job—in addition two resistors, a diode, and a 9V battery are needed only.

For measuring the voltage drop over the temperature diode a simple multimeter would be sufficient. But this would mean that the voltage reading must be interpreted according to the 'Curve 10' data table—a methode which is error-prone and wouldn't make soldering more reliable.

A multimeter[3] with RS-232 interface connected to a PC is a better solution of the problem. A simple program—reading the serial data in, calculating and displaying the temperature, giving an audible alarm when the maximum allowed temperature is approached—assures a reliable und reproducible soldering process.

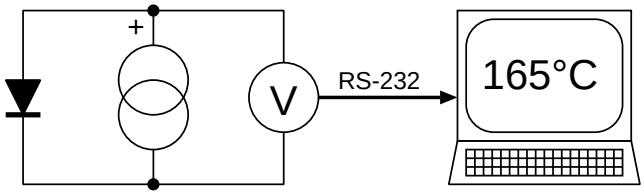

Fig. 2: Connection diagram of the soldering temperature setup consisting of temperature diode, constant current source, multimeter, and PC.

The fact that the temperature is monitored permits a very slow soldering process producing unstressed and reliable soldering joints which don't need to be secured with glue anymore.

As an example figure 3 shows a temperature diode soldered to a stainless steel target finger, this type of target finger is intended to be used in the PANDA experiment.

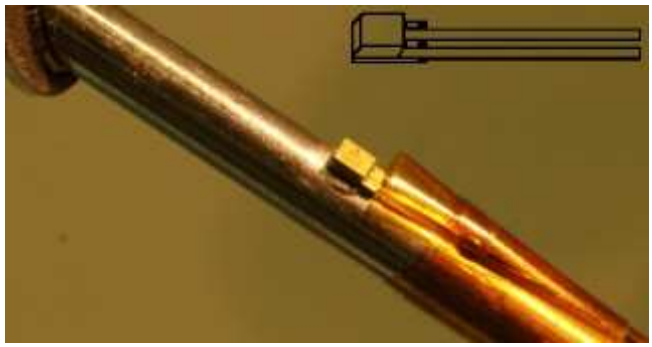

Fig. 3: Temperature diode soldered on a stainless steel target finger, superimposed is the mechanical layout of the diode.

[1] LakeShore DT-470-SD

[2] National Semiconductor LM334

[3] Amprobe 38XR-A